UNIVERSITY OF ALBERTA

Kinetic Parameters from Statistical Analysis of TREF Profiles and the Preparation of $MgCl_2$ as Supports for Polymerization Catalysts

by

Robert Andrew Butts

A thesis submitted to the Faculty of Graduate Studies and Research in partial fulfillment of the requirements for the degree of

Master of Science in Chemical Engineering

DEPARTMENT OF CHEMICAL AND MATERIALS ENGINEERING

EDMONTON, ALBERTA

Spring, 2000

National Library of Canada

Acquisitions and Bibliographic Services

395 Wellington Street
Ottawa ON K1A 0N4
Canada

Bibliothèque nationale du Canada

Acquisitions et services bibliographiques

395, rue Wellington
Ottawa ON K1A 0N4
Canada

Your file Votre référence

Our file Notre référence

The author has granted a non-exclusive licence allowing the National Library of Canada to reproduce, loan, distribute or sell copies of this thesis in microform, paper or electronic formats.

The author retains ownership of the copyright in this thesis. Neither the thesis nor substantial extracts from it may be printed or otherwise reproduced without the author's permission.

L'auteur a accordé une licence non exclusive permettant à la Bibliothèque nationale du Canada de reproduire, prêter, distribuer ou vendre des copies de cette thèse sous la forme de microfiche/film, de reproduction sur papier ou sur format électronique.

L'auteur conserve la propriété du droit d'auteur qui protège cette thèse. Ni la thèse ni des extraits substantiels de celle-ci ne doivent être imprimés ou autrement reproduits sans son autorisation.

0-612-60106-4

Canada

UNIVERSITY OF ALBERTA

LIBRARY RELEASE FORM

NAME OF AUTHOR: Robert Andrew Butts

TITLE OF THESIS: Kinetic Parameters from Statistical Analysis of TREF Profiles and the Preparation of $MgCl_2$ as Supports for Polymerization Catalysts

Degree: Master of Science

Year this Degree Granted: 2000

Permission is hereby granted to the University of Alberta Library to reproduce single copies of this thesis and to lend or sell such copies for private, scholarly or scientific research purposes only.

The author reserves all other publication and other rights in association with the copyright in the thesis, and except as herein before provided, neither the thesis nor any substantial portion thereof may be printed or otherwise reproduced in any material form whatever without the author's prior written permission.

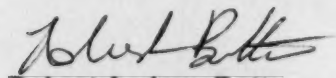

Robert Andrew Butts

154 Regency Drive
Sherwood Park, AB, Canada
T8A 5R9

Date: April 14, 2000

UNIVERSITY OF ALBERTA

Faculty of Graduate Studies and Research

The undersigned certify that they have read, and recommend to the Faculty of Graduate Studies and Research for acceptance, a thesis entitled **Kinetic Parameters from Statistical Analysis of TREF Profiles and the Preparation of $MgCl_2$ as Supports for Polymerization Catalysts** submitted **by Robert Andrew Butts** in partial fulfillment of the requirements for the degree of **Master of Science in Chemical Engineering**.

Sieghard E. Wanke (co-supervisor)

David . T. Lynch (co-supervisor)

Michael .L. Wayman

Jeffrey Stryker

April 13, 2000

ABSTRACT

Temperature Rising Elution Fractionation (TREF) profiles of polyethylenes, containing different amounts of 1-butene, were analyzed to obtain information about the catalytic sites in the Ziegler-Natta catalyst used to produce the polyethylenes. A good fit of molar mass distributions and analytic TREF profiles was obtained with four catalytic sites. The modeling results showed that each site had a different 1-butene incorporation rate, and that each site produced polyethylene with a different average molar mass but the molar mass was independent of 1-butene concentration. The fraction of polyethylene produced by each site was a strong function of 1-butene concentration.

$MgCl_2$ particles were precipitated in heptane by reacting *tert*-butyl chloride with di-*n*-butyl magnesium. The crystal structure of the $MgCl_2$, as determined by x-ray diffraction, was affected by reagent addition rate, stirring conditions and reactor geometry. Very active catalysts, >5.5 kg PE/(mol Ti · kPa C_2H_4 · min), were made using $MgCl_2$ with high degree of disorder as supports for $TiCl_4$.

ACKNOWLEDGEMENTS

I wish to express my gratitude to my supervisors Dr. Sieghard Wanke and Dr. David Lynch for their guidance and support during the course of my research. I am especially grateful for the tremendous effort that Dr. Wanke provided in guiding my writing of this thesis.

I would also like to thank the many people within the Department of Chemical and Materials Engineering that helped make my research experience pleasant. I with to specifically thank Ms. Naiyu Bu and Long Wu for their assistance in the polymerization laboratory and for demonstrating how the equipment works. I also thank Tina Barker for preparing the SEM pictures and Nikhil Rao for his assistance with particle size measurements. I am grateful to Ah-Dong Leu for the BET measurements and explaining the XRD equipment. Thanks also to Keith Faulder, Bob Scott and Ron Van den Heuvel for building great equipment to work with.

I wish to thank NOVA Chemicals Corporation and the Natural Science and Engineering Research Council of Canada for the financial support that was provided to the Polymerization and Characterization Laboratory and to myself.

I would like to thank my parents for their support and encouragement in both my University career and my life. Lastly, I would like to thank my wife, Amy, for her overwhelming patience, love and support over the long process of obtaining this degree.

TABLE OF CONTENTS

1.0 - Part I: Introduction 1

2.0 - Literature Survey – TREF Studies 3

3.0 - Numerical Model for Analysis of TREF Results 6
- 3.1 - Stockmayer Distribution Function 6
- 3.2 - Conversion of scales 10
- 3.3 - Curve Fitting Procedure 12
- 3.4 - Statistical Calculations 13
- 3.5 - Calculation of Preparative TREF Fractions 13

4.0 - Results for Fitting of TREF and SEC Profiles 15
- 4.1 - Description of Data Analyzed 15
- 4.2 - Fitting of SEC Results 16
- 4.3 - Fitting of Analytical TREF Results 25
- 4.4 - Prediction of Preparative TREF for fitted model 36
- 4.5 - Models with 5 and 6 active sites 51

5.0 - Summary and Conclusions on Modeling 65

6.0 - Part II: Synthesis of Spherical Magnesium Chloride 67

7.0 - Literature Survey - Catalyst Studies 69

8.0 - Experimental Procedures 71
- 8.1 - Preparation of Magnesium Chloride Support 71
- 8.2 - Preparation of catalyst 74
- 8.3 - Polyethylene polymerization 78
- 8.4 - Scanning Electron Microscopy (SEM) 80
- 8.5 - BET Measurements 81
- 8.6 - X-ray diffraction 82
- 8.7 - Optical microscope 85

9.0 - Results 87
- 9.1 - Surface Areas and Shapes of $MgCl_2$ Particles 87
- 9.2 - XRD Results 90
- 9.3 - Polymerization Results 99
- 9.4 - Scanning Electron Microscopy Results 101

10.0 - Summary and Conclusions 116

11.0 - References 118

APPENDIX A: FORTRAN Programs for TREF and Molar Mass Analysis 121

APPENDIX B: Equations and Nomenclature for Statistical Analysis 147

APPENDIX C: Results of Polymerization Experiments 149

LIST OF TABLES

Table 1	Results from the testing of linear independence.	9
Table 2	Reaction conditions used to produce the polymers (Huang, 1995).	15
Table 3	Comparison of measured and calculated molar masses.	17
Table 4	Mass Fraction results for SEC fitting for each active site.	19
Table 5	Comparison of mass distributions for Sample 3.	21
Table 6	Comparison of calculated mass distributions for 4, 5 and 6 active sites for Sample 2.	54
Table 7	Comparison of statisitcal information for the analytical TREF profiles for Sample 2.	57
Table 8	Comparison of mass distributions for 4, 5 and 6 active sites for Sample 3.	57
Table 9	Comparison of statisitcal information for the analytical TREF profiles for Sample 3.	60
Table 10	Numerical results of fitting TREF profiles using 5 and 6 sites.	63
Table 11	Reactor conditions for the catalyst support formation and the BET surface area measurement.	88
Table 12	Support particles mean diameters.	89
Table 13	Catalyst support crystal structure parameters.	97
Table 14	Measured Titanium content and catalyst activity.	100
Table 15	Summary of SEM results.	114

LIST OF FIGURES

Figure 1	Comparison between the measured mass distribution and calculated mass distribution using four sites for Sample 2.	18
Figure 2	Initial mass distribution fit for Sample 3 allowing Site 4 mass fraction to vary.	20
Figure 3	TREF profile for Sample 3 using the initial mass distribution.	22
Figure 4	Final mass distribution fit for Sample 3 fixing Site 4 mass fraction.	23
Figure 5	TREF profile for Sample 3 using the second mass distribution.	24
Figure 6	TREF profile for Sample 1 using four active sites.	26
Figure 7	TREF profile for Sample 2 using four active sites.	27
Figure 8	TREF profile for Sample 4 using four active sites.	28
Figure 9	Variation of the average ethylene concentration for the polymer produced at each active site with initial 1-butene charge.	29
Figure 10	Variation of number average molar mass with initial 1-butene charge.	31
Figure 11	Variation of mass fraction with initial 1-butene charge.	33
Figure 12	Variation of the r_1r_2 parameter with initial 1-butene charge.	35
Figure 13	Comparison of the measured preparative TREF number average molar mass for Sample 1 with model predictions.	37
Figure 14	Comparison of the measured preparative TREF weight average fraction molar mass for Sample 1 with model predictions.	38
Figure 15	Comparison of the measured preparative TREF fraction polydispersity for Sample 1 with model predictions.	39
Figure 16	Comparison of the measured preparative TREF number average fraction molar mass for Sample 2 with model predictions.	40

Figure 17	Comparision of the measured preparative TREF weight average fraction molar mass for Sample 2 with model predictions.	41
Figure 18	Comparison of the measured preparative TREF fraction polydispersity for Sample 2 with model predictions.	43
Figure 19	Comparison of the measured preparative TREF number average fraction molar mass for Sample 3 with model predictions.	44
Figure 20	Comparison of the measured preparative TREF weight average fraction molar mass for Sample 3 with model predictions.	45
Figure 21	Comparison of the measured preparative TREF fraction polydispersity for Sample 3 with model predictions.	46
Figure 22	Comparison of the measured preparative TREF number average molar mass for Sample 4 with model predictions.	47
Figure 23	Comparison of the measured preparative TREF weight average molar mass for Sample 4 with model predictions.	48
Figure 24	Comparison of the measured preparative TREF fraction polydispersity for Sample 4 with model predictions.	49
Figure 25	Comparison between the measured mass distribution and the calculated mass distribution using five sites for Sample 2.	52
Figure 26	Comparison between the measured mass distribution and the calculated mass distribution using six site for Sample 2.	53
Figure 27	TREF profile for Sample 2 using five sites.	55
Figure 28	TREF profile for Sample 2 using six sites.	56
Figure 29	Comparison between the measured mass distribution and the calculated mass distribution for Sample 3 using five sites.	58
Figure 30	Comparison btween the measured mass distribution and the calculated mass distribution for Sample 3 using six sites.	59
Figure 31	TREF profile for Sample 3 using five sites.	61
Figure 32	TREF profile for Sample 3 using six sites.	62

Figure 33	Schematic diagram of the one litre glass reactor.	72
Figure 34	Schematic diagram of the support collection bottles.	75
Figure 35	Schematic diagram of the catalyst preparation equipment.	76
Figure 36	Schematic diagram of the stainless steel reactor.	79
Figure 37	Schematic diagram of air tight XRD sample holder.	83
Figure 38	X-ray diffraction patterns for supports RBSP2 through RBSP5.	92
Figure 39	X-ray diffraction patterns for supports RBSP8 through RBSP11.	93
Figure 40	Comparison of the X-ray diffraction patterns of the catalyst supports with anhydrous magnesium chloride.	95
Figure 41	SEM picture of $MgCl_2$ support RBSP1. (85.7 μm)	102
Figure 42	SEM picture of $MgCl_2$ support RBSP1. (15.0 μm)	102
Figure 43	SEM picture of $MgCl_2$ support RBSP2. (30.0 μm)	103
Figure 44	SEM picture of $MgCl_2$ support RBSP2. (3.00 μm)	103
Figure 45	SEM picture of $MgCl_2$ support RBSP3. (20.0 μm)	104
Figure 46	SEM picture of $MgCl_2$ support RBSP3. (3.00 μm)	104
Figure 47	SEM picture of $MgCl_2$ support RBSP4. (20.0 μm)	105
Figure 48	SEM picture of $MgCl_2$ support RBSP4. (3.00 μm)	105
Figure 49	SEM picture of $MgCl_2$ support RBSP8. (75.0 μm)	106
Figure 50	SEM picture of $MgCl_2$ support RBSP8. (8.57 μm)	106
Figure 51	SEM picture of $MgCl_2$ support RBSP9. (30.0 μm)	107
Figure 52	SEM picture of $MgCl_2$ support RBSP9. (6.00 μm)	107
Figure 53	SEM picture of $MgCl_2$ support RBSP10. (20.0 μm)	108
Figure 54	SEM picture of $MgCl_2$ support RBSP10. (3.00 μm)	108

Figure 55 SEM picture of $MgCl_2$ support RBSP11. (10.0 μm) 109

Figure 56 SEM picture of $MgCl_2$ support RBSP11. (3.00 μm) 109

Figure 57 SEM picture of the catalyst RBCT3. (20.0 μm) 110

Figure 58 SEM picture of the catalyst RBCT3. (3.00 μm) 110

Figure 59 SEM picture of the catalyst RBCT4. (30.0 μm) 111

Figure 60 SEM picture of the catalyst RBCT4. (3.00 μm) 111

Figure 61 SEM picture of the catalyst RBCT5. (10.0 μm) 112

Figure 62 SEM picture of the catalyst RBCT5. (3.00 μm) 112

Figure 63 SEM picture of the catalyst RBCT6. (75.0 μm) 113

Figure 64 SEM picture of the catalyst RBCT6. (8.57 μm) 113

NOMENCLATURE

α	probability of crystal termination along appropriate directions within the layers
χ^2	residuals
γ	probability of crystal termination across the layers
τ	ratio of the total rate of transfer to the total rate of propagation
$\psi_k(j)$	mass fraction of polymer produced on site j within a TREF fraction in relation to the total amount of polymer made on site j.
ζ	fraction of ethylene in the polymer
a	length of the unit crystal of $MgCl_2$
c	depth of the unit crystal of $MgCl_2$
DSC	differential scanning calorimetry
F	F statistic
F_1	average comonomer concentration in the polymer produced
$\overline{F_1}$	average mole fraction of monomer type 1 in copolymer
$[H_2]$	hydrogen concentration
j	catalytic active site
k_β	β-hydride elimination rate constant
k_{aa}	activity of adding an ethylene molecule to a polymer with an ethylene terminal group adjacent to the active site
k_{ab}	activity of adding an 1-butene molecule to a polymer with an ethylene terminal group adjacent to the active site
k_{ba}	activity of adding an ethylene molecule to a polymer with a 1-butene terminal group adjacent to the active site
k_{bb}	activity of adding a 1-butene molecule to a polymer with a 1-butene terminal group adjacent to the active site

k_p	propagation rate constant
k_{tH2}	transfer to hydrogen rate constant
k_{tm}	transfer to monomer rate constant
$<L_{av}>$	length of the crystal domain in the a direction
$<L_{cv}>$	length of the crystal domain in the c direction
LLDPE	linear low density polyethylene
m	mass fraction of polymer produced
[M]	monomer concentration
M_1	molecular weight of monomer 1
M_2	molecular weight of monomer 2
M_n	number average molar mass
M_w	weight average molar mass
p_{cub}	probability of a cubic-like shift between two adjacent layers
Pd	polydispersity
p_{hex}	probability of a hexagonal-like shift between layers
p_{rot}	probability of two layers mutually rotated 60°
r	polymer chain length
r_1, r_2	reactivity ratios of the living polymer end
r^2	correlation coefficient
SEC	size exclusion chromatography
SEM	scanning electron microscopy
T	elution temperature in °C

TREF	temperature rising elution fractionation
w	distribution for each catalytic active site with respect to polymer chain length and deviation from polymer average comonomer concentration
x	degrees two theta
XRD	x-ray diffraction
y	deviation from polymer average comonomer concentration
z	intensity of the background for XRD

1.0 – Part 1: Introduction

The production of polymers is growing rapidly as their importance is growing in our society. For every industrial application of polymers the physical and chemical properties of the polymer resin are different. The properties of the polymer depend on many factors. These factors include the catalyst, reactor conditions, co-catalyst, monomer, post reaction processing, co-monomer, blending and many others. In order to produce polymers for a specific application the effect of these factors on the physical properties must be understood. An important polymer today is linear low density polyethylene (LLDPE). The production of LLDPE in Canada has grown from 186 000 tonnes in 1983 to 865 000 tonnes in 1994. The projected production world capacity for 1999 is 21 266 000 tonnes with 1 090 000 being produced in Alberta (SRI, 1996). What distinguishes LLDPE from other forms of polyethylene is the short chain branching. The degree of short chain branching affects the physical properties of the polyethylene. An analytical technique used to study short chain branching is temperature rising elution fractionation (TREF).

TREF does not directly measure the degree of short chain branching. Rather, TREF measures the degree of crystallinity from the elution temperature. From this information the average degree of branching can be inferred. To gain more information the TREF equipment can be run in a preparative mode. In this mode, polymer fractions are collected between two sets of elution temperatures.

The fraction can then be analyzed using size exclusion chromatography (SEC) to generate the molar mass distribution of each fraction.

At present, the information derived from analytical TREF and preparative TREF is limited to the breadth of the analytical TREF profile peaks that indicate the co-monomer incorporation. Soares and Hamielec (1995) developed a kinetic model that predicts analytical TREF profiles. The basis of the model is that a Ziegler-Natta heterogeneous catalyst has multiple types of active catalytic sites. Each type of active site produces a polymer that has Flory's most probable distribution. By varying the kinetic parameters in the model for each active site, the effects of catalyst kinetics on the overall polymer properties can be explored. One of the objectives of the current study was to determine whether kinetic information, e.g. activities of catalytic sites, could be extracted from measured TREF profiles using the model of Soares and Hamielec (1995).

The literature relating to the de-convoluting of TREF profiles is reviewed in Chapter 2. A detailed description of the model and the numerical procedures is presented in Chapter 3. The results from the analysis of LLDPE with varying 1-butene concentrations are presented in Chapter 4.

A second objective of the current work was to investigate the preparation of $MgCl_2$ supported Ziegler-Natta catalysts. This work is described in the second part of this thesis in Chapters 6 to 10.

2.0 - Literature Survey – TREF Studies

In this chapter the various TREF techniques and the information that is derived from them are introduced. Other methods that are being used to obtain short chain branching information are also described.

The analytical method of temperature rising elution fractionation has been described in many publications (e.g., Wild et al. 1982; Soares and Hamielec, 1995; Kelusky, 1987; Chakravarty, 1993; Huang, 1995). The TREF method consists of the following steps: 1. The polymer is dissolved in a solvent at an elevated temperature; 2. The solution is slowly cooled causing the polymer to precipitate; 3. The precipitated polymer is then dissolved by a solvent which is flowed through the column containing the precipitated polymer as the temperature is slowly increased (an infrared detector is usually used to measure the concentration of the eluted polymer). Analytical TREF is used to measure short chain branching distributions.

TREF has also been used in a preparative method in conjunction with size exclusion chromatography (SEC) (Chakravarty, 1993; Wild et al., 1982; Soares and Hamielec, 1995). This method is also referred to as "TREF-SEC cross-fractionation". The polymer sample is prepared in the same manner as the analytical TREF method. However, during the elution phase the temperature is increased in a step-wise manner and the polymer is collected for each step. The collected fractions are then analyzed by SEC to determine the molar mass distribution of the polymer collected between the two temperatures. This method

in conjunction with analytical TREF supplies information about how the molar mass is distributed with respect to the short chain branching.

There are several methods that are being examined to derive more information from TREF results. Also, other methods are being examined to extract information on short chain branching. One method being explored is differential scanning calorimetry (DSC) (Starck, 1996). Starck (1996) was able to obtain qualitative results of branch distribution similar to that obtained by TREF. The advantage is that the DSC method requires a shorter time and smaller implementation costs to obtain similar results. When calibration curves are used the short chain branching distribution can be obtained using DSC. Karoglanian and Harrison (1996) used calibration curves of known short chain branching to convert a TREF profile into a DSC curve and thus confirmed the similarity in the information available from the two methods.

The former literature dealt with the information about the polymer that may be derived from TREF and DSC. Other research has explored the mechanics of TREF from a thermodynamic perspective. Borrajo et al. (1995) developed a thermodynamic model that describes the fractionation process. Eliçabe et al. (1996a) in a continuation of the previous paper completed a "rigorous mathematical analysis of the solution of the fractionation model." This analysis was used to obtain "the distribution of crystallizable lengths" which can be related to the distribution of short chain branching. Eliçabe et al. (1996b), in a third part to this series, used low molecular weight polymers to validate the

previously developed model. The model shows that "chain folding may set a resolution limit" for the analysis of polymers by TREF.

3.0 - Numerical Model for Analysis of TREF Results

In this study, the TREF results obtained by Huang (1995) for four 1-butene –ethylene LLDPE samples synthesized over a supported Ziegler-Natta catalyst were analyzed. The Stockmayer bivariate distribution function was used to model the compositional and chain length distribution of the polymers produced with a Ziegler-Natta catalyst. The distribution function, the numerical method used to fit a TREF profile and the calculation of the preparative TREF fractions are described in this chapter.

3.1 - Stockmayer Distribution Function

Soares and Hamielec (1995) used the Stockmayer distribution function to model the active sites on a Ziegler-Natta catalyst. The distribution function is a function of polymer chain length and the deviation from average composition. The full differential form of the function is shown below.

$$w(r,y,j)drdy = \left[1 + y(j)\delta(j)\right]\tau^2(j)r\exp\left(-\tau(j)r\right)dr \cdot \frac{1}{\sqrt{2\pi\beta(j)\,r}}\exp\left(-y^2(j)r/\left(2\beta(j)\right)\right)dy \quad (1)$$

where

$$\beta(j) = \overline{F}_1(j)\left(1-\overline{F}_1(j)\right)K \quad (2)$$

$$K = \left[1 + 4\overline{F}_1(j)\left(1-\overline{F}_1(j)\right)\left(r_1(j)r_2(j)-1\right)\right]^{0.5} \quad (3)$$

$$\delta(j) = \frac{(1 - M_2\ M_1)}{M_2\ M_1 + \overline{F_1}(j)(1 - M_2\ M_1)} \tag{4}$$

$$\tau(j) = \frac{k_{tm}(j)}{k_p(j)} + \frac{k_\beta(j)}{k_p(j)[\mathrm{M}]} + \frac{k_{H_2}(j)[\mathrm{H}_2]}{k_p(j)[\mathrm{M}]} \tag{5}$$

where w is the distribution for each catalytic active site j with respect to polymer chain length r and deviation from polymer average comonomer concentration y. Stockmayer developed this function to describe the instantaneous distribution of long copolymer molecules (Stockmayer, 1945). His work, the continuation of work by Simha and Branson (1944), used "further approximations" to derive a distribution that is in a useful form (Stockmayer, 1945). Tacx et al. (1988) extended the distribution function to account for comonomers with different molecular weights.

In the work of Soares and Hamielec (1995), each type of active site j of a Ziegler-Natta catalyst is modelled by a Stockmayer distribution function. Each type of site is assigned a unique set of parameters. The superposition of the properties produced on the different active sites should give the properties of polymer produced by the whole catalyst. By this procedure Soares and Hamielec (1995) 'predicted' a TREF profile for a catalyst with an assigned number of different types of catalytic sites and assigned kinetic parameters for each site. The assumptions as detailed in their studies were that the "separation mechanism to be controlled only by copolymer composition of stereoregularity, free of cocrystallisation effects, molecular weight influence and peak broadening due to axial dispersion and crystallization kinetics."

The current study uses the same model and assumptions as those used by Soares and Hamielec (1995); however, the objective is not to predict TREF profiles but the objective is to obtain kinetic parameters for a Ziegler-Natta catalyst from measured analytical TREF profiles and molar mass distributions. The parameters to be estimated for each type of catalytic site are the parameters in the Stockmayer distribution. The dependence of those parameters on changes in 1-butene concentration during 1-butene – ethylene copolymerization was analyzed.

The parameters that were fitted for each type of catalytic site are the following:

1. $\tau(j)$ which is the ratio of termination rates to propagation rate. This parameter gives a measure of the activity of each active site.
2. $F_1(j)$ is the average comonomer concentration in the polymer produced at each site.
3. $m(j)$ is the mass fraction of polymer produced at each site.
4. $r_1(j)$ and $r_2(j)$ are the reactivity ratios of the living polymer end.

The distribution function in Equation 1 describes a surface. Equation 1 must be integrated over all chain lengths from zero to infinity to obtain an equation that can be used to model an analytical TREF profile, i.e.

$$w(y,j) = \int_0^\infty w(r,y,j)dr = \frac{3\left[1+\delta(j)y(j)\right]}{4\sqrt{2\beta(j)\tau(j)}\left(1+y^2(j)\ \left(2\beta(j)\tau(j)\right)\right)^{5/2}} \qquad (6)$$

Equation 6 is a function of mole fraction deviation from average composition. Equation 6 is not linearly independent in the parameters $\tau(j)$, $F(j)$, $m(j)$ and $r_1r_2(j)$. A distribution for $w(y,j)$ was produced using the parameters in the 'Actual' column of Table 1. Using the program described in Section 3.3, the parameters $\tau(j)$, $F(j)$, $m(j)$ and $r_1r_2(j)$ were fitted to the produced distribution with different initial conditions for each trial. For Trials 4 and 5 the $\tau(j)$ parameter was held constant at 0.00391.

Table 1. Results from the testing of linear independence.

Trial	Actual	1	2	3	4 τ constant	5 τ constant
Initial $F_1(j)$		0.78	0.65	0.95	0.78	.95
Final $F_1(j)$	0.821	0.821	0.821	0.821	0.821	0.821
Initial $\tau(j)$		0.000591	0.0086	0.0086	0.000391	0.000391
Final $\tau(j)$	0.000391	0.00115	0.00134	0.0365	0.000391	0.000391
Initial $r_1r_2(j)$		106	10600	1.06	106	1.06
Final $r_1r_2(j)$	1243	143	105	-0.561	1243	1243
Initial m(j)		0.222	0.4	0.4	0.222	0.0215
Final m(j)	0.122	0.122	0.122	0.122	0.122	0.122
χ^2 residuals		0	2×10^{-30}	4×10^{-30}	0	0
r^2 correlation coefficient		1.0	1.0	1.0	1.0	1.0

Table 1 shows that depending on the initial conditions the parameters $\tau(j)$ and $r_1r_2(j)$ will vary but still produce the distribution. In order to obtain unique

solutions for $\tau(j)$ and $r_1r_2(j)$ one parameter must be fixed from another independent data set.

When Equation 1 is integrated for all deviations from negative infinity to infinity the resulting Equation 7 has the parameters m(j) and $\tau(j)$ only.

$$w(r,j) = \int_{-\infty}^{\infty} w(r,y,j)dy = \tau^2(j)r\exp(-\tau(j)r) \tag{7}$$

Equation 7 describes the molar mass distribution produced by active Site j. Data on the overall molar mass distributions can be obtained by SEC measurements. Equations 8 and 9 show the calculation of the number average molar mass and the mass average molar mass for Site j.

$$M_n(j) = \left\{\int_0^{\infty} \frac{w(r,j)}{r}\,dr\right\}^{-1} = \frac{1}{\tau(j)} \tag{8}$$

$$M_w(j) = \int_0^{\infty} rw(r,j)\,dr = \frac{2}{\tau(j)} \tag{9}$$

These results show that the polymer produced at each active site produces a polymer with a polydispersity of 2. Therefore, the superposition of the multiple active sites is needed to produce polymers with a polydispersity greater than 2.

3.2 - Conversion of scales

Equation 6 is a function of deviation from the average comonomer concentration and was used to fit an analytical TREF profile which is a function of temperature. Data that were collected by Huang et al. (1997) give a

relationship between the number of methyl groups a polymer chain has and the elution temperature from the TREF column. These data were fit by the fifth order polynomial shown in Equation 10.

$$\frac{\#CH_3}{1000C} = 91.739097 - 1.7364486T + 0.01221566T^2 - 5.0736226\times10^{-5}T^3 \qquad (10)$$

$$+ 8.7451892\times10^{-10}T^4 + 9.985789\times10^{-16}T^5$$

where T is the elution temperature in °C. The total number of methyl groups is found by Equation 11.

$$\#CH_3 = \left(\frac{\#CH_3}{1000C}\right)\frac{M_n}{14}\frac{1}{1000} \qquad (11)$$

It is assumed that each methyl group was the result of the incorporation of a 1-butene molecule. The mass of 1-butene in the polymer is then given by the number of methyl groups multiplied by the molar mass of 1-butene. Therefore, the fraction of ethylene in the polymer is

$$\zeta = \frac{M_n - mass\ of\ butene}{M_n} = 1 - \left(\frac{\#CH_3\ 1000C}{1000}\right)\left(\frac{48}{14}\right) \qquad (12)$$

The above equations were used to transform the TREF temperature scale to a fraction ethylene scale. However, this conversion has two problems. The first problem is that non-ideal TREF elution occurred at high temperatures which results in negative #CH_3/1000C according to Equation 10. This causes problems for Equation 6 because it is only valid for fractions between 0 and 1. The second problem with this method is that the conversion changes the shape of the analytical TREF profile. The transformation spreads out the data points at low temperatures (low ethylene fraction) and compresses the data points at high

temperatures (high ethylene fraction). This changes the area under each section of the analytical TREF profile and the area under the original TREF curve is proportional to the mass of polyethylene that elutes. An additional conversion is required to correct for the distortion of the area-mass relationship. In order to avoid the problem of changing the weighting of the mass distribution the distribution is normalised with the logarithm of molar mass and not molar mass. Therefore, Equation 6 becomes (Soares, 1997)

$$w[\log_{10}(r)] = \frac{r^2\tau^2(j)\exp(-\tau(j)r)}{\log_{10}(e)} \tag{13}$$

3.3 - Curve Fitting Procedure

Two FORTRAN 77 programs were written. One program was used to fit the molar mass distributions and the second to fit the analytical TREF profiles. Two programs were used to ensure that the results from the mass distribution were consistent with the SEC results and to save computing time by only solving the mass distribution once and using the output file for several TREF trials. The program and output files are double precision to minimize round off error. The Marquardt-Levenberg method of minimization was used. The code used was taken from Press et al. (1992) in the subroutines MRQMIN, GAUSSJ, COVSRT, and MRQCOF. The subroutines were used with minor modifications to suit the main program. The Marquardt-Levenberg method requires the derivative of the function with respect to each parameter. These derivatives were calculated

analytically using Mathematica. The programs have the flexibility to allow certain parameters to be held constant during a fitting. The full code for each program is given in Appendix A. The programs also calculated statistics for the parameter fitting.

3.4 - Statistical Calculations

The statistical relevance of the parameters was tracked to ensure that any additional parameters were statistically significant. The programs determined the over-all goodness of fit and the error associated with each fitted parameter. This allowed seeing which parameters are fit well and which have greater uncertainty. A complete list of statistical equations used is given in Appendix B. The most important statistic calculated was the F statistic. The F statistic tracks the significance of added parameters. If the addition of parameters is significant, then the F parameter increases. If the additional parameters are not significant, then the F statistic will either remain almost constant or decrease.

3.5 - Calculation of Preparative TREF Fractions

As a check on the validity of the fitted parameters the properties of the preparative TREF fractions were compared to the measured preparative TREF fractions. To calculate the preparative TREF fraction the chain length

distribution function was calculated over the fraction limits (Soares, Hamielec, 1995).

$$w_k(r,j) = \frac{\int_{y(j)}^{y(j)+\Delta y_k} w(r,y,j)\,dy}{\int_{y(j)}^{y(j)+\Delta y_k} \int_0^{\infty} w(r,y,j)\,dr\,dy} \tag{14}$$

In Equation 14, y(j) is the start of the fraction and $y(j)+\Delta y_k$ is the end of the fraction for each active site. The denominator of Equation 14 is the mass fraction of the polymer produced on Site j in the fraction in relation to the total polymer produced by Site j (Soares, Hamielec, 1995). The mass distribution of the TREF fraction for the total polymer is given by

$$w_k(r) = \frac{\sum_{j=1}^{n} m(j)\psi_k(j)w(r,j)}{\sum_{j=1}^{n} m(j)\psi_k(j)} \tag{15}$$

Using Equations 14 and 15 the molar mass averages for each fraction can be calculated using the following equations.

$$M_{n_k} = \left(\int_0^{\infty} \frac{w_k(r)}{r}\,dr \right)^{-1} \tag{16}$$

$$M_{w_k} = \int_0^{\infty} r w_k(r)\,dr \tag{17}$$

Analytical solutions are not available for the above integrals. Maple V was used to numerically solve for all solutions.

4.0 - Results for Fitting of TREF and SEC Profiles

4.1 - Description of Data Analyzed

The molar mass distribution, analytical TREF and preparative TREF profiles for four polymer samples synthesized by Huang (1995) were analyzed in the current study. The conditions used for the synthesis of the polymers are listed in Table 2.

Table 2. Reaction conditions used to produce the polymers (Huang, 1995).

Sample	Run #	Mass of catalyst (mg)	Initial 1-butene (mL)
1	49	60	5
2	40	30	10
3	50	60	20
4	47	60	30

The four polymers synthesized had the following common conditions:

1. The hydrogen partial pressure was 100 psi.
2. The ethylene partial pressure was 200 psi.
3. The reactor temperature was maintained at 70°C.
4. 1 mL of tri-n-hexyl aluminum alkyl cocatalyst was added.
5. The length of each polymerization run was 2 hours.

Huang (1995) reported the characteristics for the whole polymer samples and Lacombe (1995) reported the preparative TREF and TREF-SEC cross-fractionation results.

4.2 - Fitting of SEC Results

The curve fitting programs were run on an IBM RISC 6000 mainframe computer system. The two programs, described in Section 3.3, were compiled to run using the UNIX operating system. The procedure used to fit the measured molar mass distributions and analytical TREF profiles was as follows:

1. An initialization file was created with initial estimates for $\tau(j)$ and m(j).
2. The "mass" program was executed using the initialization file and the mass distribution data file.
3. An initialization file was created with initial estimates for $F_1(j)$ and $r_1r_2(j)$. This file also allowed for m(j) and $\tau(j)$ to be fixed or a variable.
4. The "tref" program was executed using the initialization file, the analytical TREF profile data file and the output file from the SEC fitting.
5. The results of the TREF fitting were checked to ensure that the sites were in the correct sequence and to ensure that the homopolymer peak was fit.
6. If the homopolymer peak was not represented, the "tref" program was rerun allowing the m(j) to vary while using the $\tau(j)$ from Step 5.
7. The m(j) for the site with the lowest $\tau(j)$ was fixed from the previous step and the "mass" program was executed allowing $\tau(j)$ to be variables and m(j) to vary except for the one site.

8. The 'tref' program was executed with the new $\tau(j)$ and m(j).
9. If the sites were out of the prescribed order, the $F_1(j)$ initial estimates were changed to encourage the site to be in the proper sequence.

For each polymer sample the mass distribution function was initially fitted using four active sites. Active Site 1 corresponded to the active site that incorporated the most 1-butene. Active Site 4 corresponded to the site that incorporated the least 1-butene in the polymer. In Table 3 the measured number average molar mass and weight averaged molar mass are compared with the calculated values. The correlation coefficient for each fit is also shown in Table 3.

Table 3. Comparison of measured and calculated molar masses.

Sample #	Measured M_n	Calculated M_n	Measured M_w	Calculated M_w	Correlation Coefficient r^2
1	22220	20574	78054	75208	0.9992
2	17781	17260	65763	64118	0.9996
3	11545	13495	51317	52046	0.9986
4	10435	10770	51880	46480	0.9961

In Figure 1 a comparison is shown between the measured mass distribution and the calculated mass distribution for Sample 2. Even using just four active sites there is a very good correlation between the measured mass distribution and the calculated distribution. The prescribed order described in the SEC fitting procedure means that the active site that incorporates the most comonomer (in this case 1-butene) produces a polymer with the lowest molar

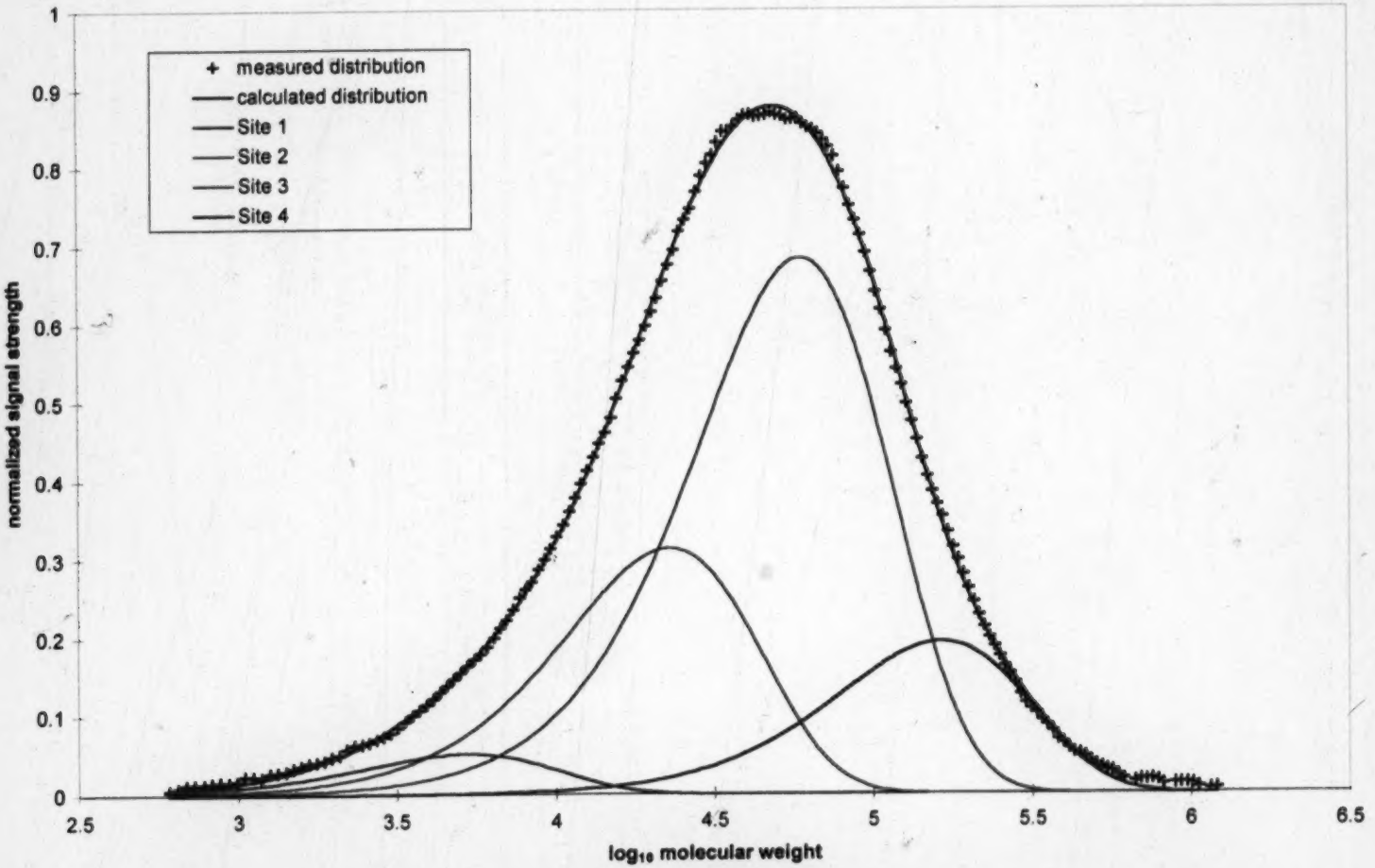

Figure 1. Comparison between the measured mass distribution and calculated mass distribution using four sites for Sample 2.

mass. The site that incorporates the least amount of comonomer produces a polymer with the highest molar mass. Keeping this order is important otherwise there would be a large number of combinations to examine. The initial conditions for the fitting of the TREF profile are set so that the site with the lowest molar mass is associated with an $F_1(j)$ with the lowest fraction ethylene, or greatest comonomer incorporation. Step 6 of the above procedure was required for Samples 3 and 4 that have the high initial 1-butene concentration. The mass fraction values calculated from the mass distribution could not be used for the analytical TREF profile.

The SEC fitting results for polymer Samples 1 through 4 are summarized in Table 4. The mass fraction correction used for Samples 3 and 4 are also shown in Table 4.

Table 4. Mass fraction results for SEC fitting for each active site.

Sample #		Site 1	Site 2	Site 3	Site 4
1		0.0300	0.255	0.559	0.163
2		0.0482	0.284	0.537	0.131
3	Initial	0.065	0.263	0.554	0.110
	Final	0.0847	0.343	0.493	0.0673
4	Initial	0.0890	0.264	0.510	0.124
	Final	0.121	0.401	0.449	0.00368

Sample 3 will be used to illustrate the need to use an iterative approach in extracting parameters from the SEC measurements. Figure 2 shows the results of the initial mass distribution fit, the mass fraction for Site 4 was 0.110. The fit of the analytical TREF profile is very poor when the parameters of the first mass

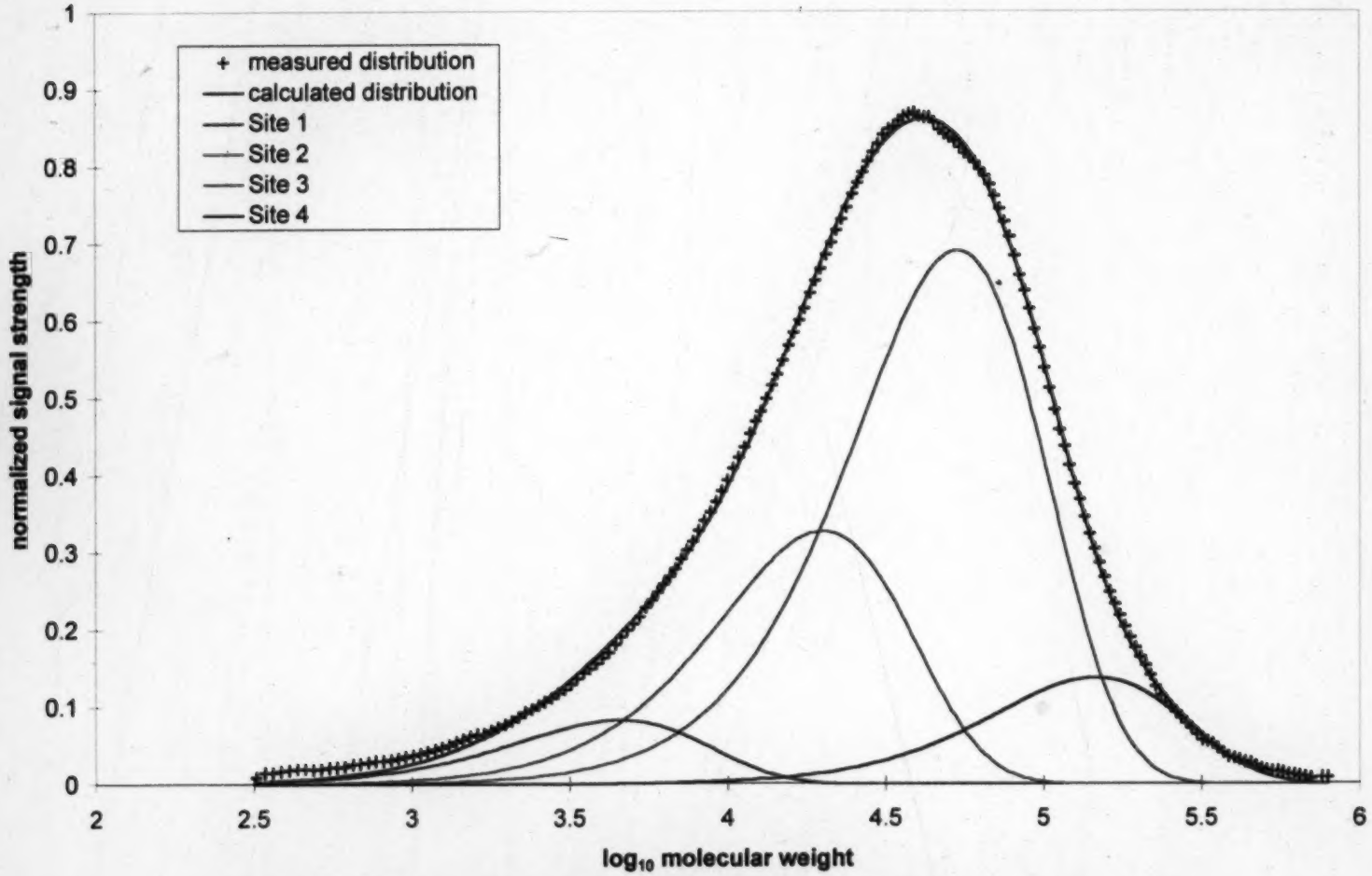

Figure 2. Initial mass distribution fit for Sample 3 allowing Site 4 mass fraction to vary.

distribution are used. Figure 3 shows that Site 4, which is associated with the least 1-butene incorporation, was not fitted well. There is large error produced and a poor correlation coefficient because Site 4 was not fitted well. Using Step 6 of the procedure to fit the TREF profile, the mass fraction of Site 4 was calculated at 0.0349. This means that only 3.5 percent of the total polymer was produced on Site 4. This is a significant reduction from the 11 percent from the original mass distribution fitting. The mass fraction from the second fitting of the analytical TREF profile is now put back into the initial conditions for fitting the mass distribution and is held constant. The new fit of the mass distribution is shown in Figure 4. Even though the fourth mass fraction was held constant a very good fit is achieved. Table 5 compares the two mass distributions with the measured mass distribution.

Table 5. Comparison of mass distributions for Sample 3.

	Measured mass distribution	First fitted mass distribution	Second fitted mass distribution
M_n	11545	12860	13495
M_w	51317	51313	52046
r^2	---	0.99950	0.9986
χ^2	---	0.00853	0.0231
F	---	48924	21178

Figure 5 shows a much-improved fit over the initial attempt with the first set of $\tau(j)$ values and mass fractions. The residuals were reduced from 1041 to 526.

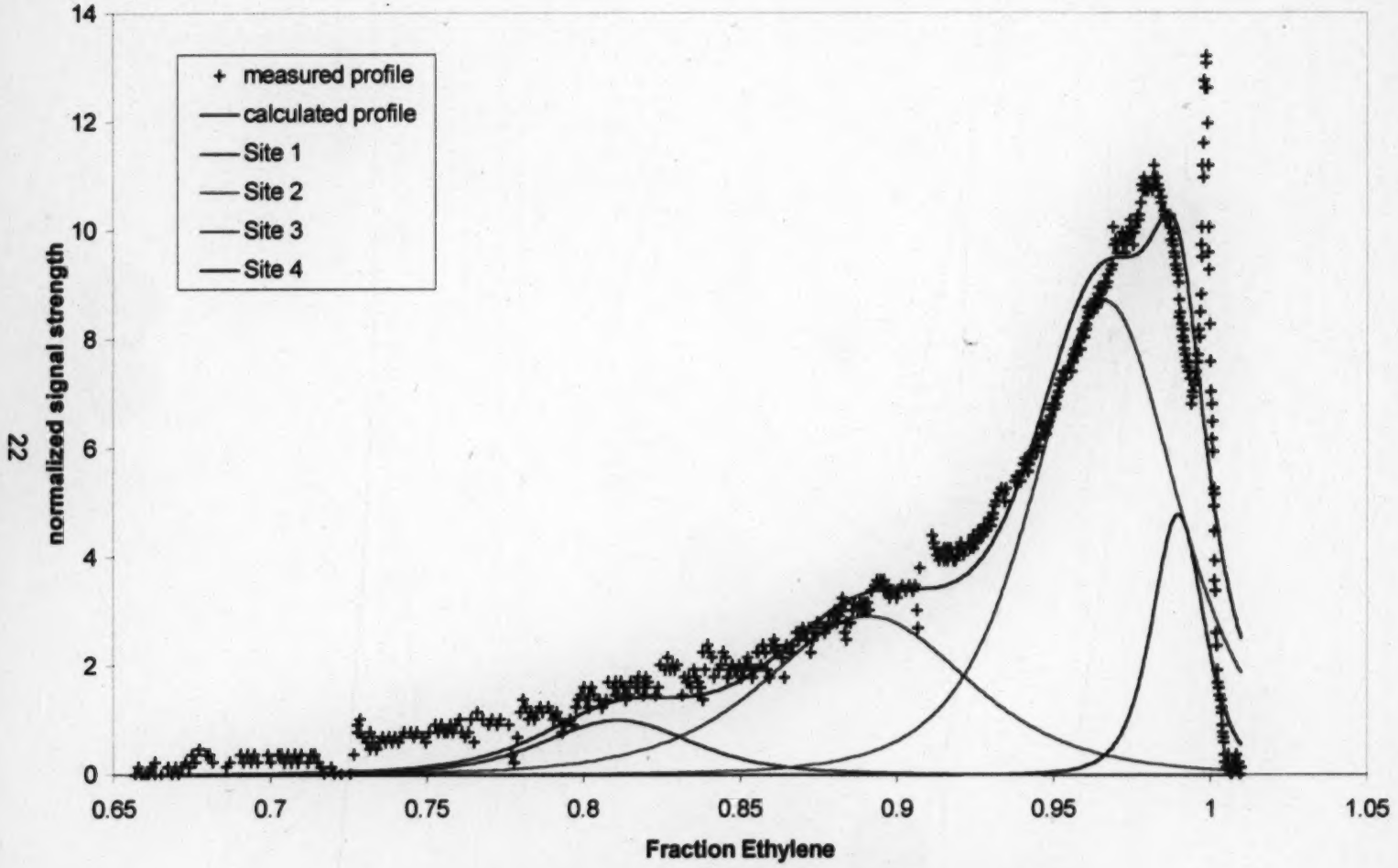

Figure 3. TREF profile for Sample 3 using the initial mass distribution.

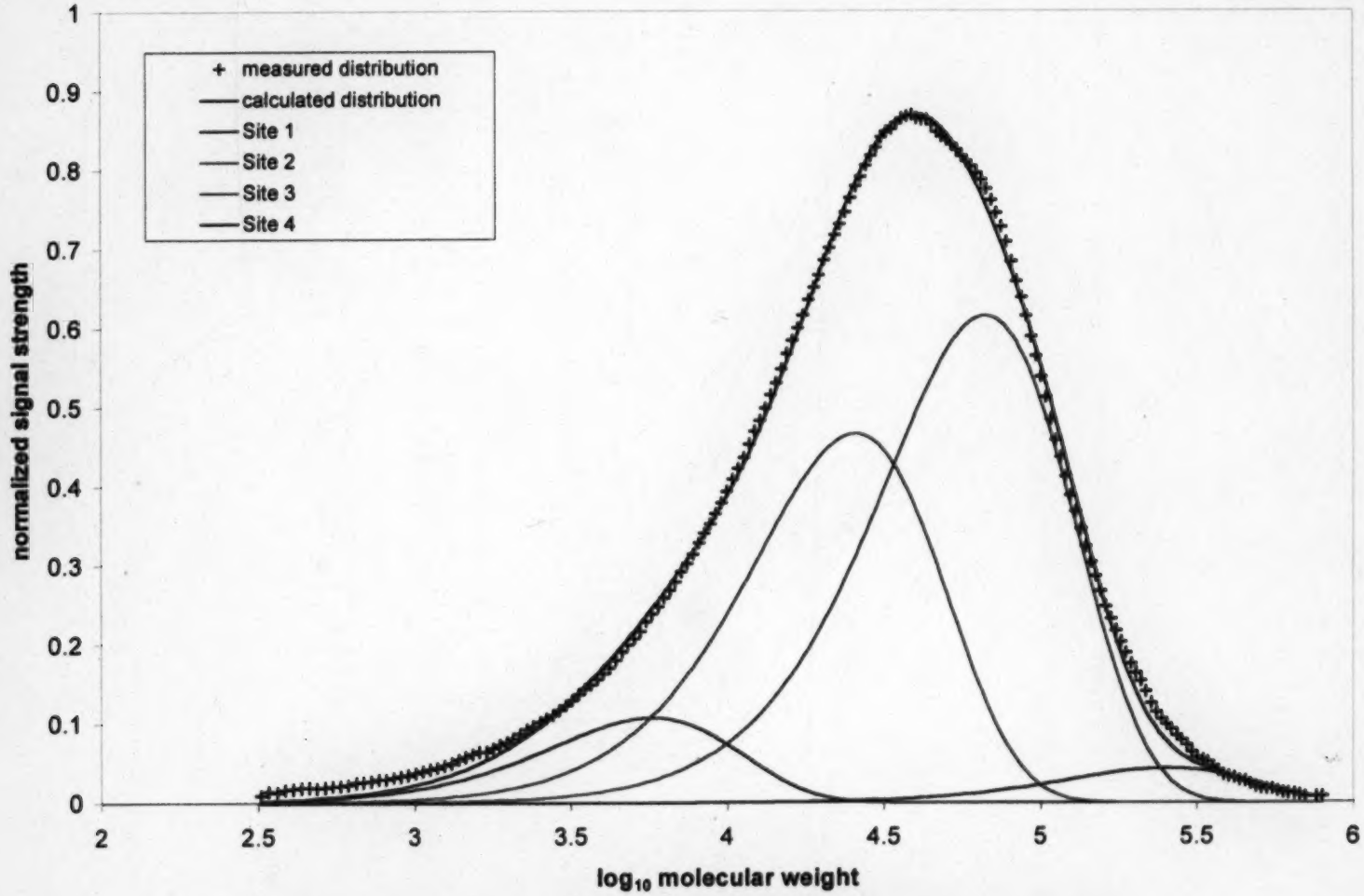

Figure 4. Final mass distribution fit for Sample 3 fixing Site 4 mass fraction.

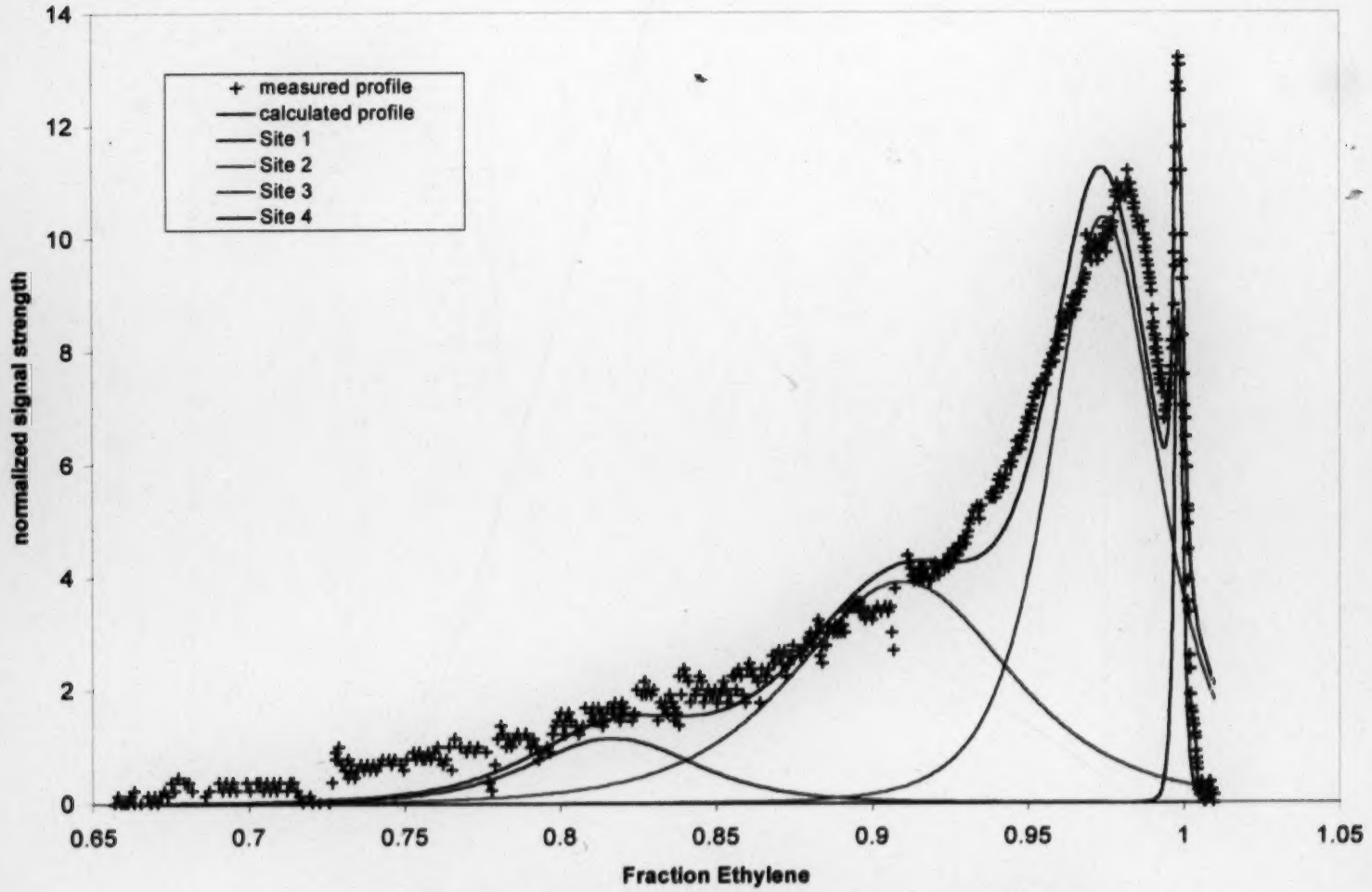

Figure 5. TREF profile for Sample 3 using the second mass distribution.

4.3 - Fitting of Analytical TREF Results

The analytical TREF profiles were well fitted with all four TREF profiles having a correlation coefficient greater than 0.9. Figures 6 through 8 show the remaining TREF profiles and the best fit distributions. For all four samples, the largest deviations in the fits are at the high and low ethylene fraction tails. At the high 1-butene incorporation (low ethylene fraction) the fitted distribution does not fit the measured distribution. Another catalytic site may be needed to fit this part of the profile. At high ethylene fraction the measured distribution ends abruptly, at 1, while the calculated distribution extends past an ethylene fraction of 1 (a physical impossibility).

Although there are problems with the fitted TREF distribution functions it is still worthwhile to examine how the parameters change with 1-butene concentration. In the next 4 figures it is shown how each parameter and each active site behaved with changes in 1-butene concentration. In Figure 9 it is shown how the $F_1(j)$ parameter (average fraction ethylene) varies with 1-butene concentration for each active site. For active Site 4, $F_1(4)$ was essentially independent of 1-butene concentration at a value slightly less than 1. The polymer produced at this site is essentially an ethylene homopolymer and changes in concentration of 1-butene do not have an effect on the degree of 1-butene incorporation. For Site 1 through Site 3 the 1-butene incorporation increased with increasing 1-butene concentration for each site. For example, for Site 2 when the initial 1-butene charged to the reactor was 5 mL the polymer

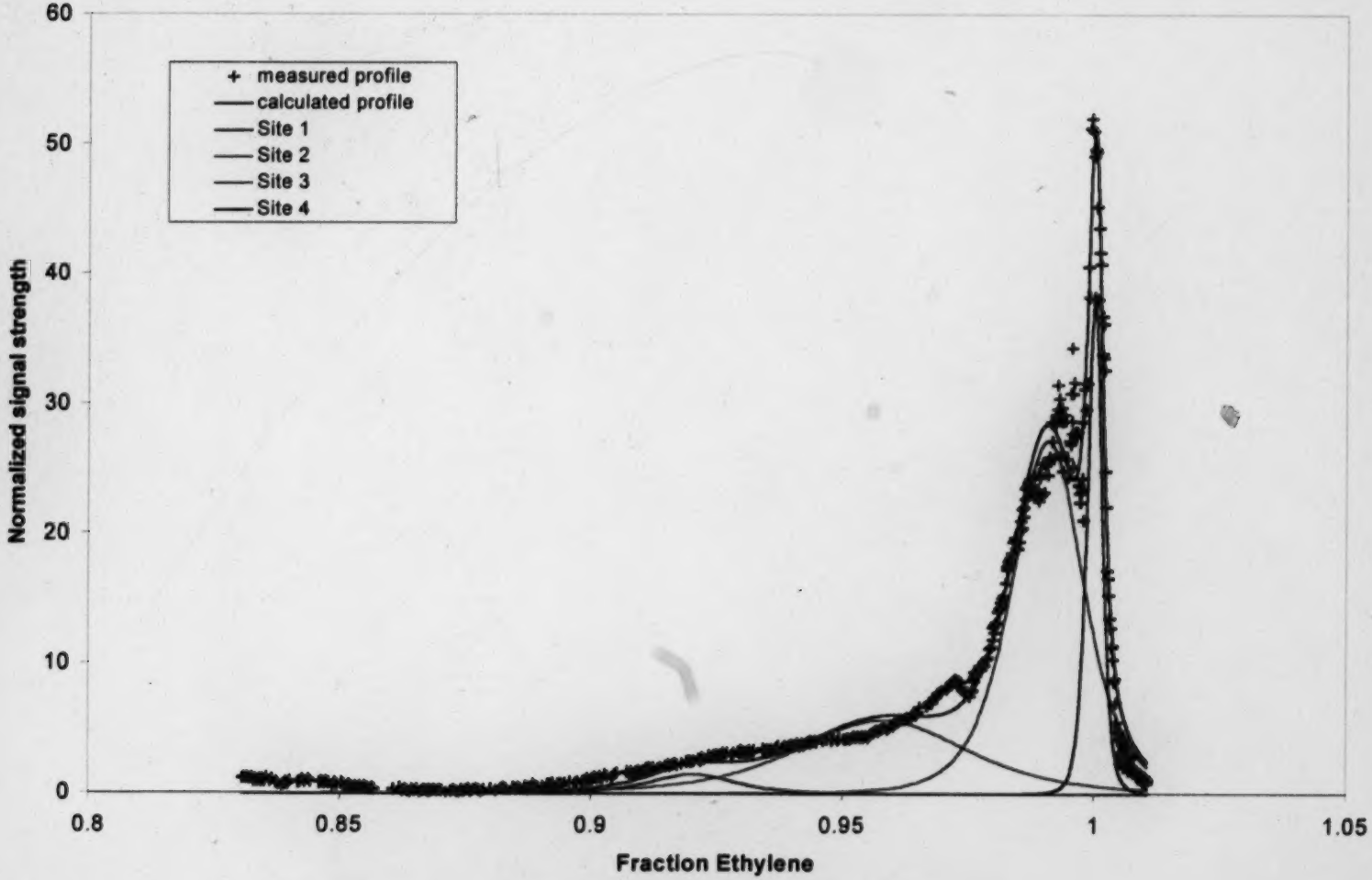

Figure 6. TREF profile for Sample 1 using four active sites.

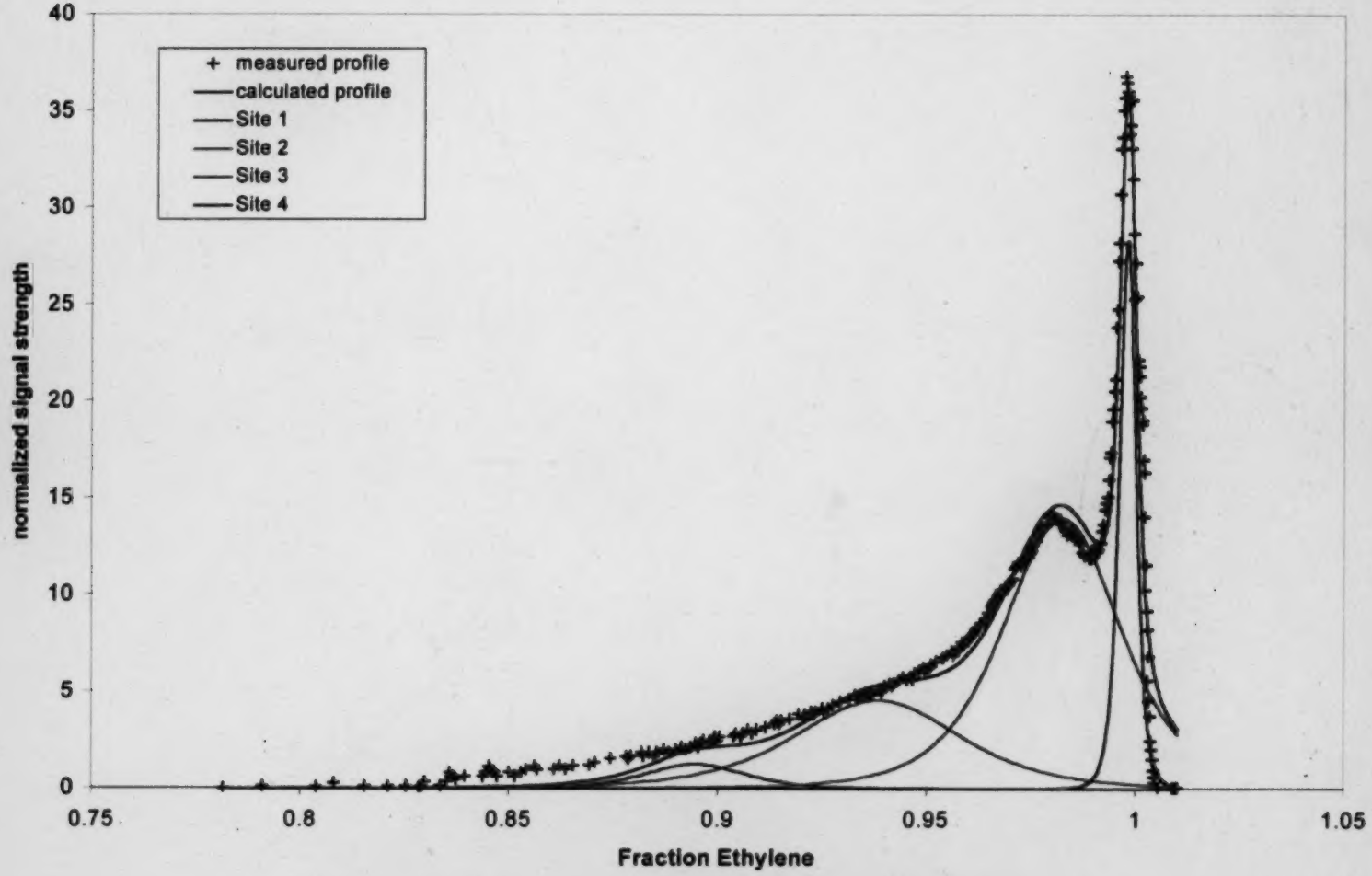

Figure 7. TREF profile for Sample 2 using four active sites.

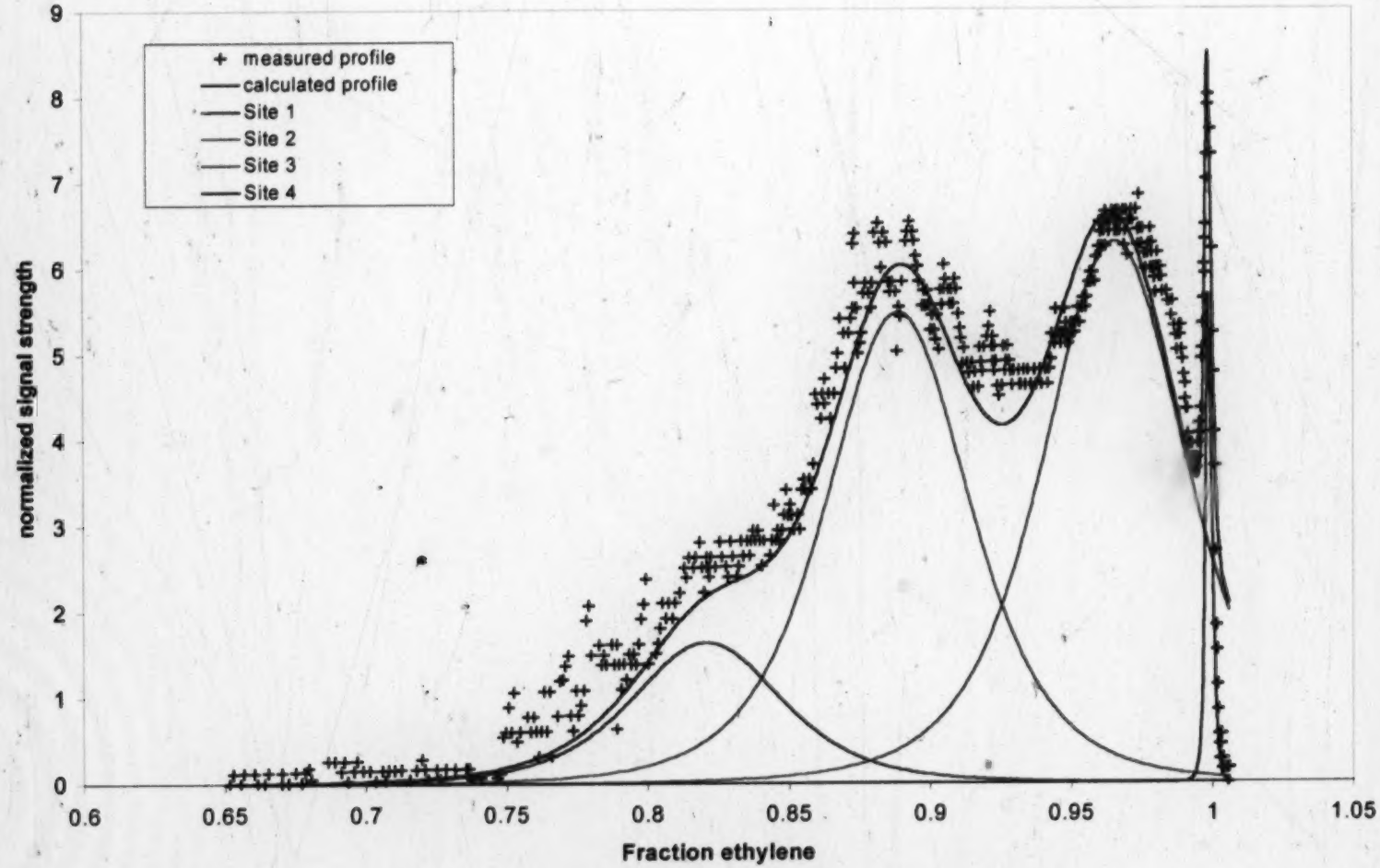

Figure 8. TREF profile for Sample 4 using four active sites.

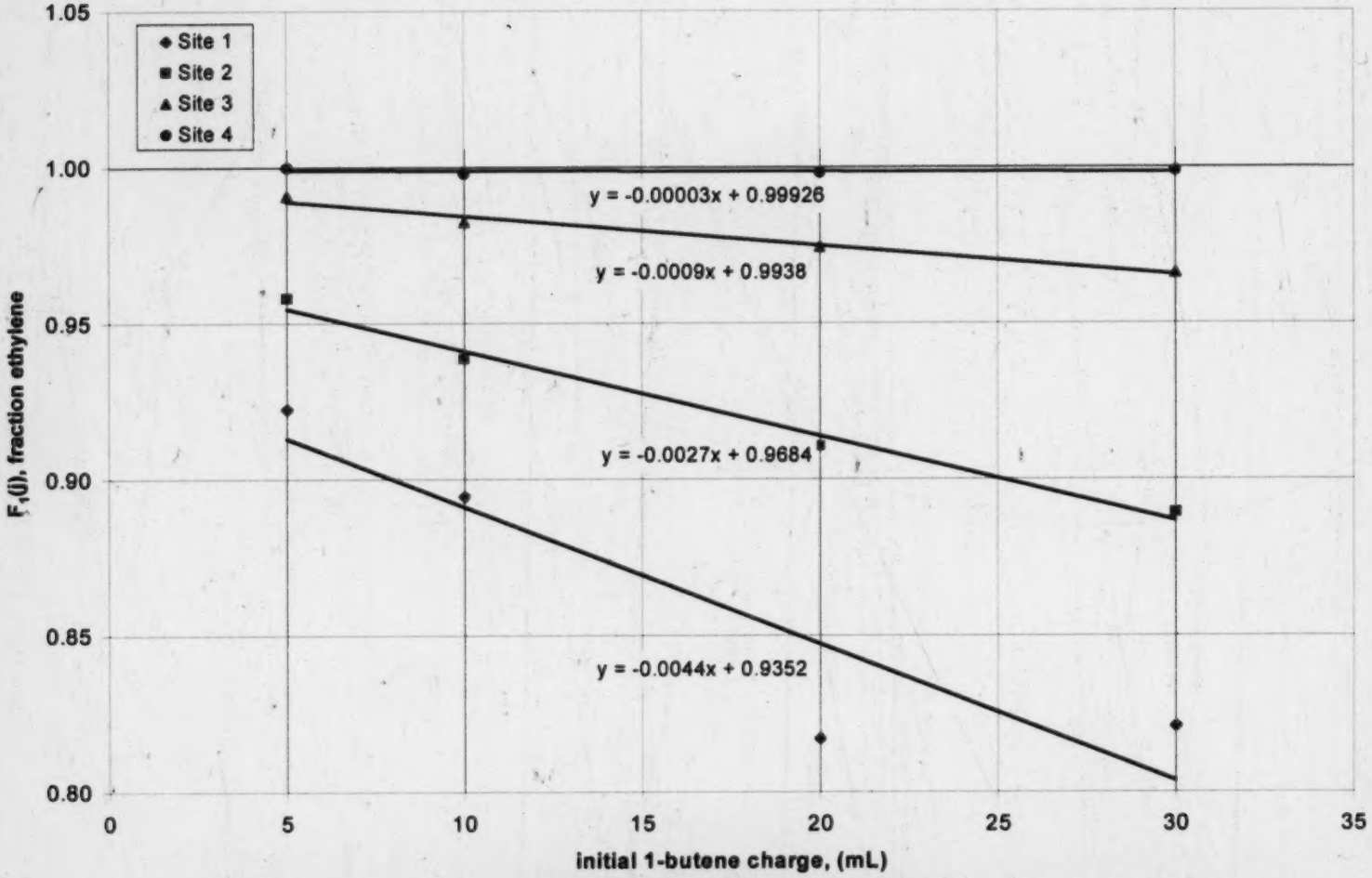

Figure 9. Variation of the average ethylene concentration for the polymer produced at each active site with initial 1-butene charge.

produced had an average 1-butene content of 4%. When the initial 1-butene charged to the reactor was 30 mL the average 1-butene content was 11%. The sequence of amount of 1–butene incorporated by the various types of catalytic sites was for Site 1 > Site 2 > Site 3 > Site 4 (see Figure 9). The slopes of the lines in Figure 9 indicate that the sensitivity of 1-butene incorporation to 1-butene was highest for Site 1, and sequentially decreased for Sites 2, 3 and 4. This is the trend for the fitted lines, but this trend is not followed for the 30 mL 1-butene point for Site 1 (see Figure 9). The average ethylene concentration at 30 mL was almost the same as at 20 mL 1-butene. This may indicate a saturation effect for this active site, but it is difficult to draw such a conclusion with any certainty on the basis of two data points.

Equation 8 showed that the number average molar mass of the polymer produced on a site is the reciprocal of the $\tau(j)$ parameter. This relationship was used to convert $\tau(j)$ to M_n, and the results, showing the effect of 1-butene concentration, are shown in Figure 10. The lines in Figure 10 are the linear least squares regression for each site. The results in Table 3 showed that the molar mass for the whole polymer decreased with increasing 1-butene concentration. However, results in Figure 10 show that the molar masses of the polymer produced for Sites 1, 2 and 3 were essentially independent of 1-butene concentration. The molar mass of the polymer produced at Site 4 increased with increasing 1-butene concentration, but this increase is relatively small. Hence, it appears that the molar mass of the polymer produced at each catalytic site is relatively independent of 1-butene concentration; i.e. termination by 1-butene is

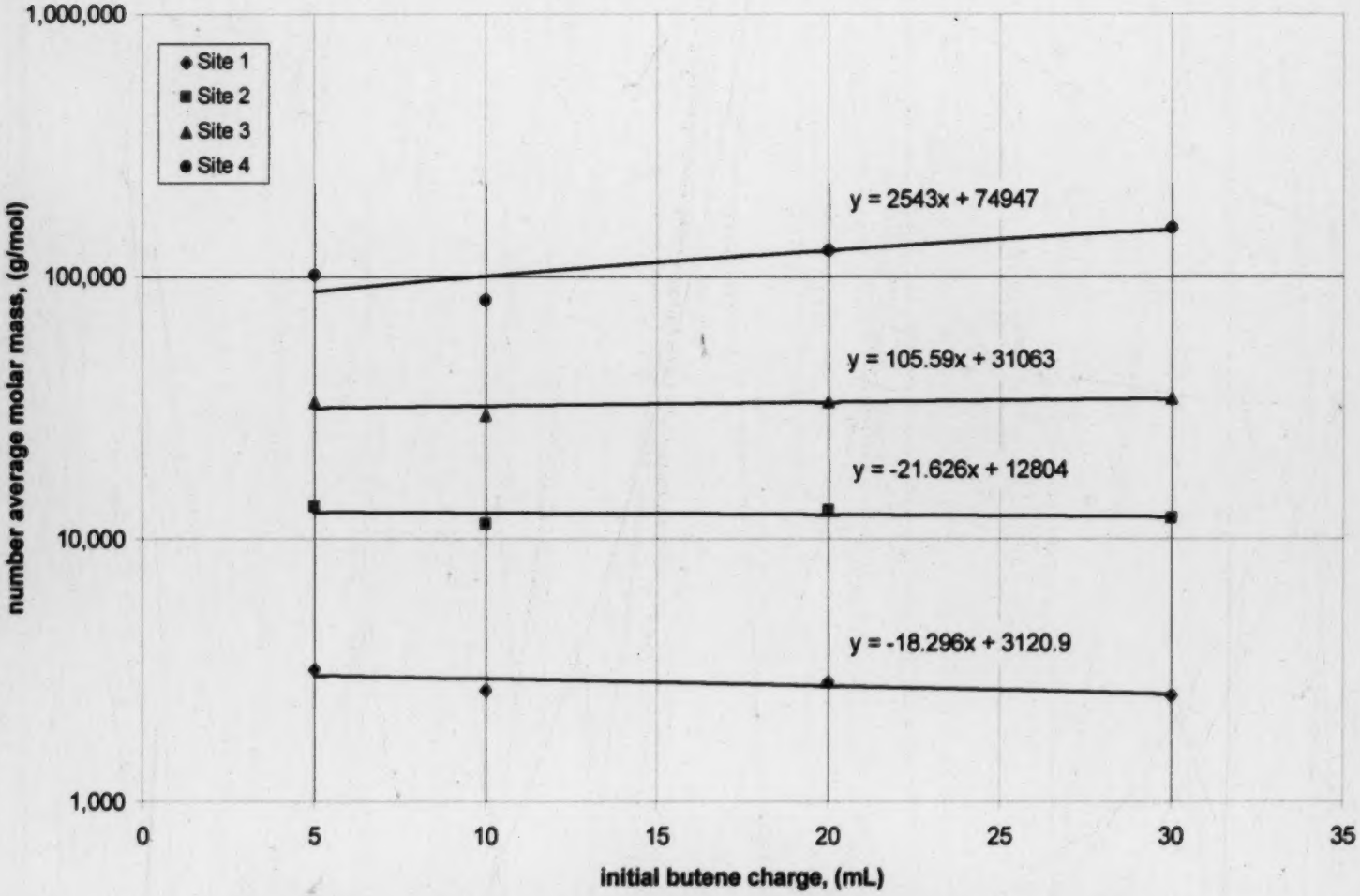

Figure 10. Variation of number average molar mass with initial 1-butene charge.

not significant for any of the sites. However, as stated earlier, the measured molar masses of the whole polymer deceased markedly with increasing 1-butene concentration.

The change in average molar masses of the whole polymer is brought about by changes in the mass fraction that was produced at the different sites. The changes in the mass fraction of the polymer produced by each of the sites as a function of the initial 1-butene concentration is shown in Figure 11. The results in Figure 11 show that as the 1-butene concentration increased, Sites 3 and 4 produced less of the total polymer; Sites 3 and 4 produced the higher molar masses. Figure 10 showed that each site produced polymer essentially of the same molar mass. The decrease in the molar mass of the whole polymer was caused by the shifting of production of polymer from Sites 3 and 4, which produced high molar mass polymer, to Sites 1 and 2, which produced low molar mass polymer.

The most difficult parameter to assess is the r_1r_2 parameter. It is difficult to interpret because the distribution function has the product of the individual reactivity ratios r_1 and r_2. The reactivity ratios are represented by Equations 18 and 19.

$$r_1 = k_{aa}/k_{ab} \tag{18}$$

$$r_2 = k_{bb}/k_{ba} \tag{19}$$

where k_{aa} is the activity of adding an ethylene molecule to a polymer with an ethylene terminal group; k_{ab} is the activity of adding an 1-butene molecule to a polymer with an ethylene terminal group; k_{bb} is the activity of adding a 1-butene

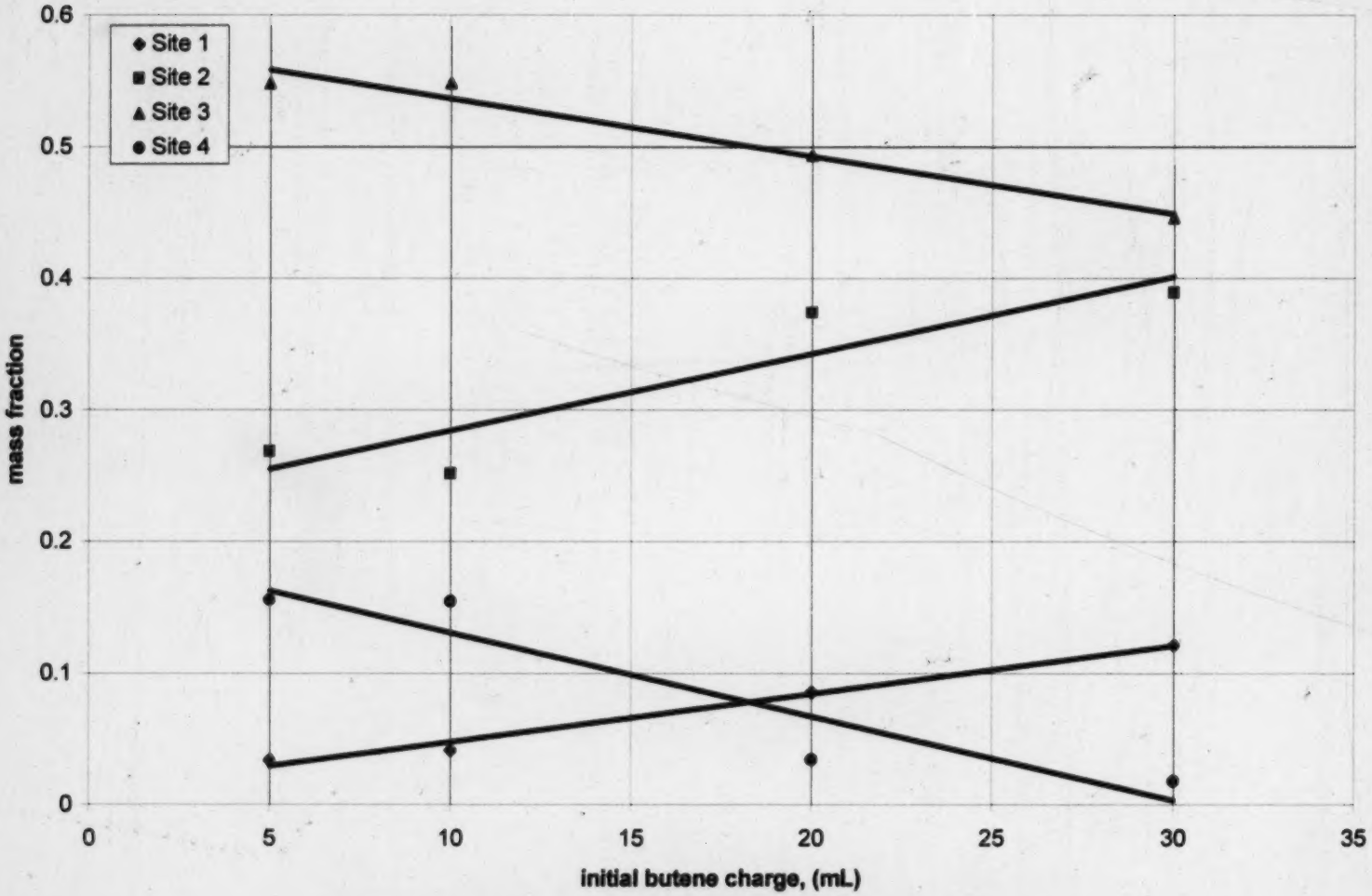

Figure 11. Variation of mass fraction with initial 1-butene charge.

molecule to a polymer with a 1-butene terminal group; and k_{ba} is the activity of adding an ethylene molecule to a polymer with a 1-butene terminal group.

Hamielec and Soares (1995) used the assumption that the r_1 parameter increases for each site as elution temperature increases. However, for each site they also assumed that the r_2 parameter is the reciprocal of r_1. These two assumptions mean that the r_1r_2 parameter is constant at a value of one for each site. An r_1r_2 of one also means that the catalytic site is as reactive when adding monomer or comonomer. It is clearly shown in Figure 12 that this assumption is not valid, i.e. each site has a unique r_1r_2 value. The value of the site r_1r_2 does reflect the nature of the polymer produced at the site, i.e. Site 4 produced homopolymer almost exclusively and the r_1r_2 parameter is in order of 100,000,000, whereas Site 1 incorporates the most comonomer of the four sites and has a r_1r_2 parameter in the order of 1000. From Figure 12 it appears that a linear fit on a semilog plot results in a reasonable fit. However, the variances associated with the calculated values the slopes of the lines indicate little statistical significance can be assigned to the values of the slopes; i.e. it cannot be ruled out from these fits that the r_1r_2 values could be independent of the 1-butene concentration for each site (a value of zero for all the slopes). The r_1r_2 value for Sample 1 for Site 4 has been omitted because the standard error of the calculated parameter was 4 orders of magnitude larger than the parameter value.

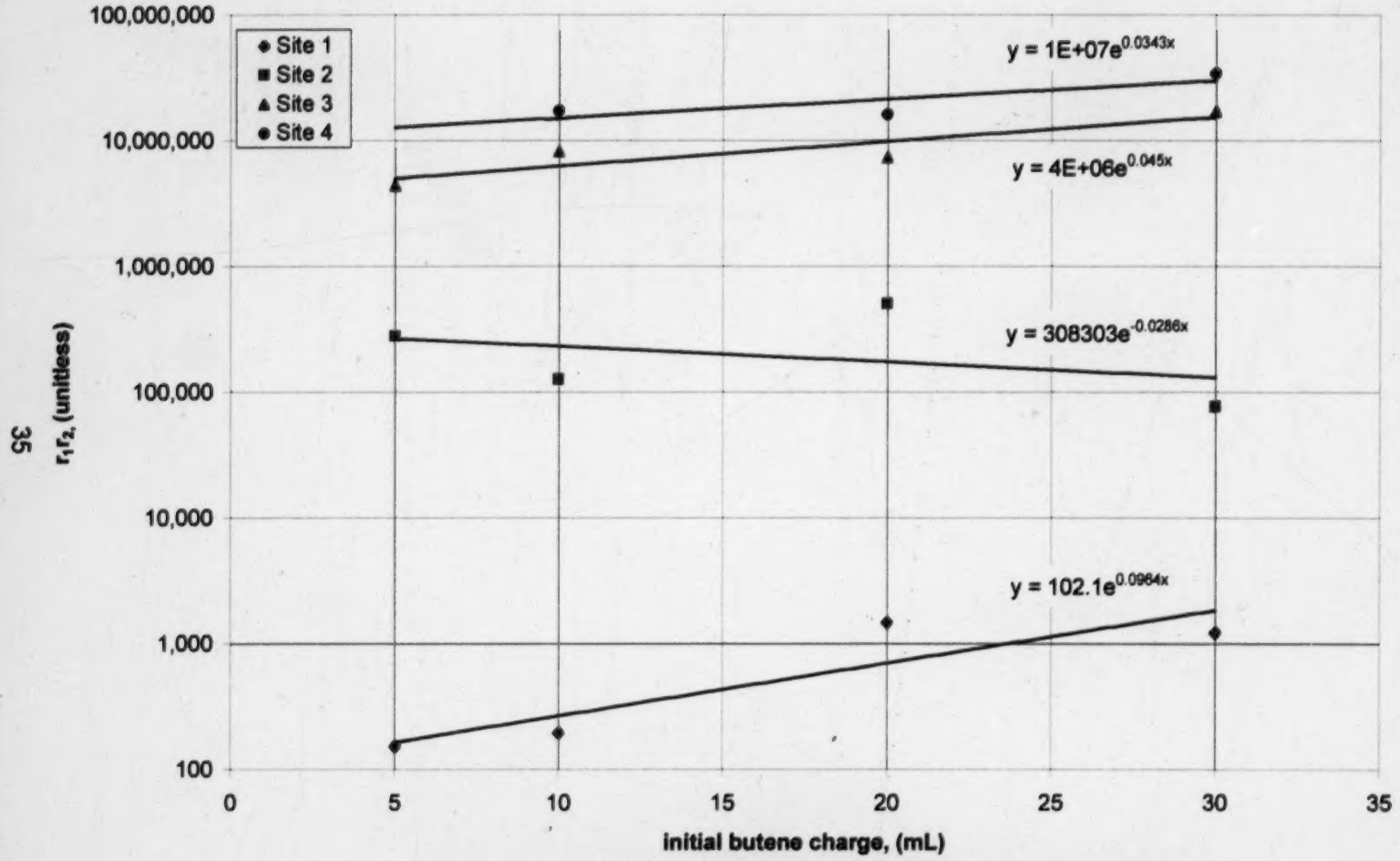

Figure 12. Variation of the r_1r_2 parameter with initial 1-butene charge.

4.4 - Prediction of Preparative TREF for fitted model

The last area examined was how well the model can predict preparative TREF fractions. Using Equations 10 through 12, the end point temperatures of the measured TREF fractions were converted into mass fraction ethylene. Equations 14 through 17 were next used to calculate the molar masses for each fraction. In Figure 13 it is shown how the preparative TREF fraction number average molar masses (M_n) vary with fraction temperature for Sample 1 (the overlapping model is described below). The weight average molar mass (M_w) for Sample 1 is shown in Figure 14. Both, the measured and calculated M_n and M_w, generally follow the same trends. However, Figure 15 shows that the calculated polydispersity remains at around 2 for all fractions whereas the measured polydispersity starts at about 6.5 at the lowest temperature fraction and then decreases to about 2.5 for the highest temperature fractions. The high experimental polydispersity may be caused by the fractions overlapping one another during the preparative TREF elution. A calculation was completed in which the fractions were overlapped by 5°C. Figure 15 shows that the polydispersity was higher for most fractions but the increase was only marginal. It is interesting to note that the highest measured polydispersity was higher than the polydispersity of the total polymer.

The results for Sample 2 in Figure 16 show that the measured and calculated M_n of the fractions follow generally the same trend. However, Figure 17 shows that the fraction M_w calculated values are lower than the measured

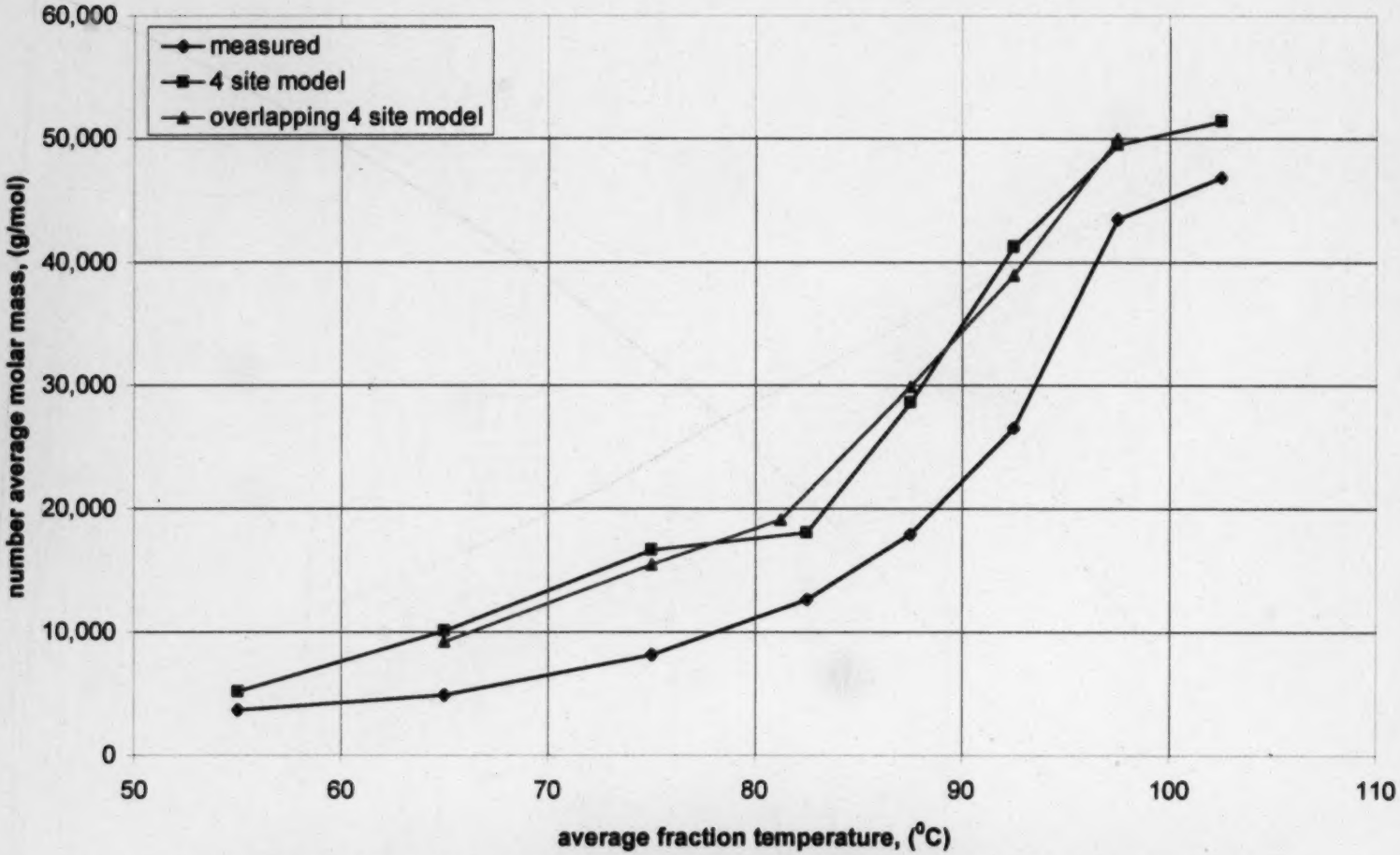

Figure 13. Comparison of the measured preparative TREF number average molar mass for Sample 1 with model predictions.

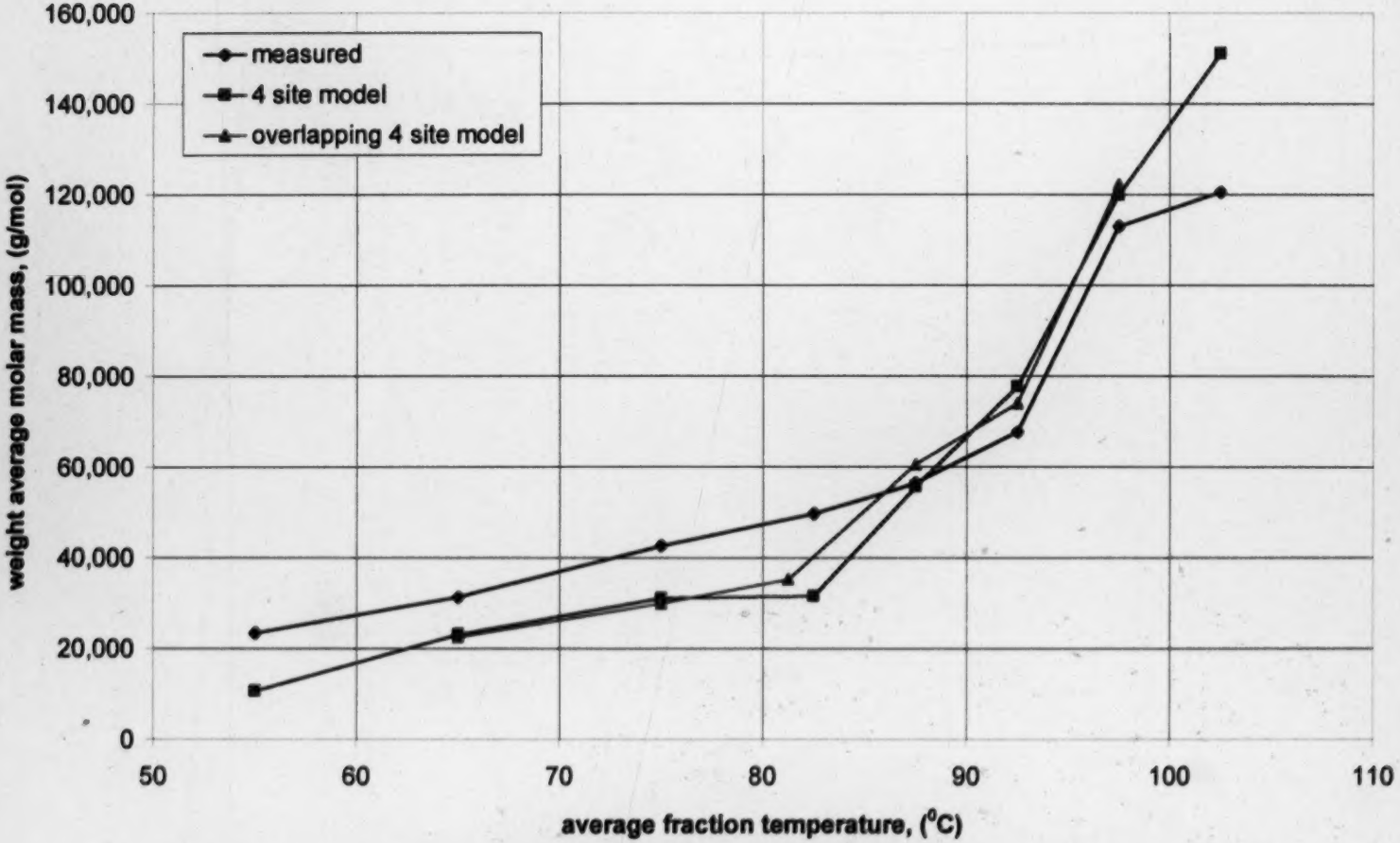

Figure 14. Comparison of the measured preparative TREF weight average fraction molar mass for Sample 1 with model predictions.

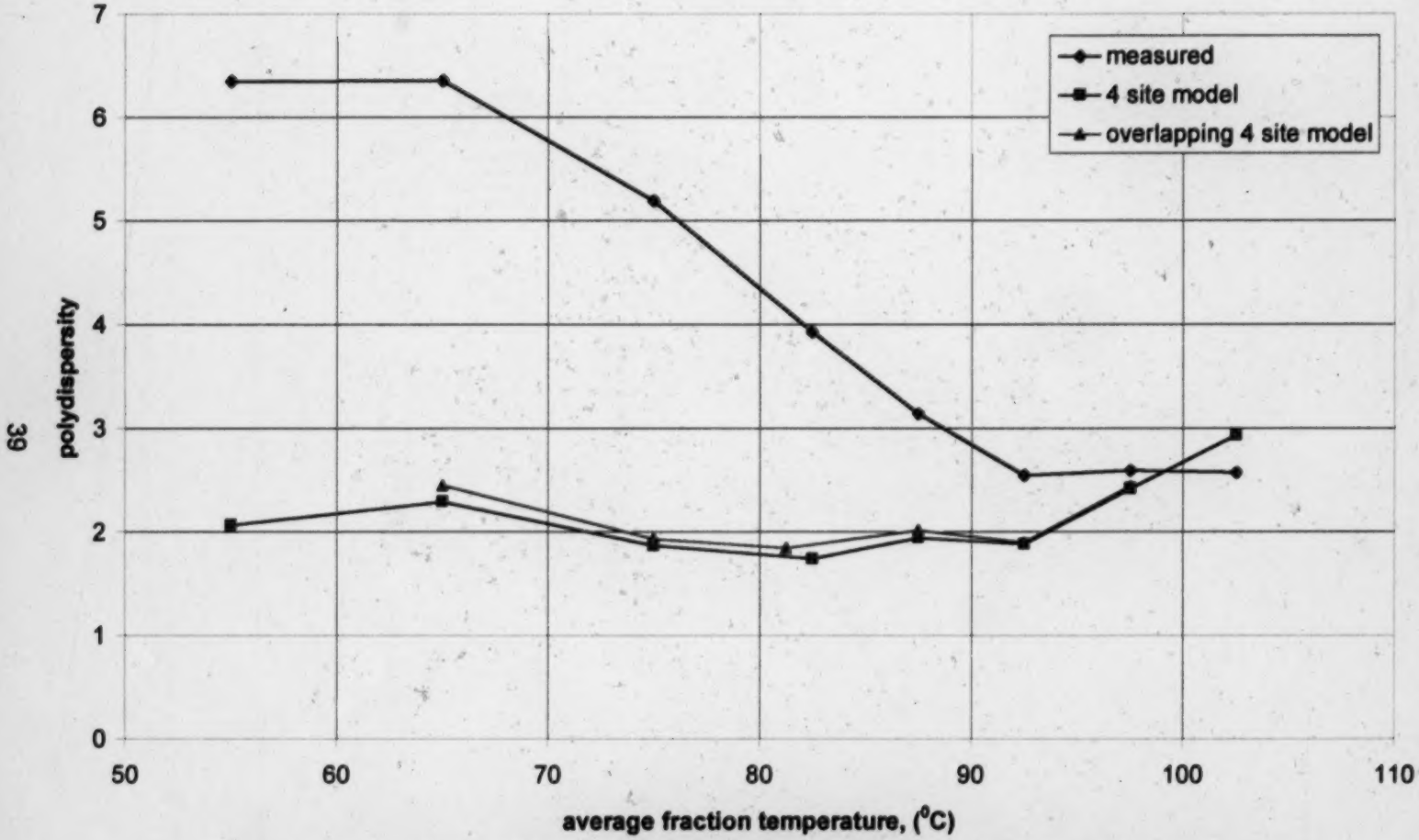

Figure 15. Comparison of the measured preparative TREF fraction polydispersity for Sample 1 with model predictions.

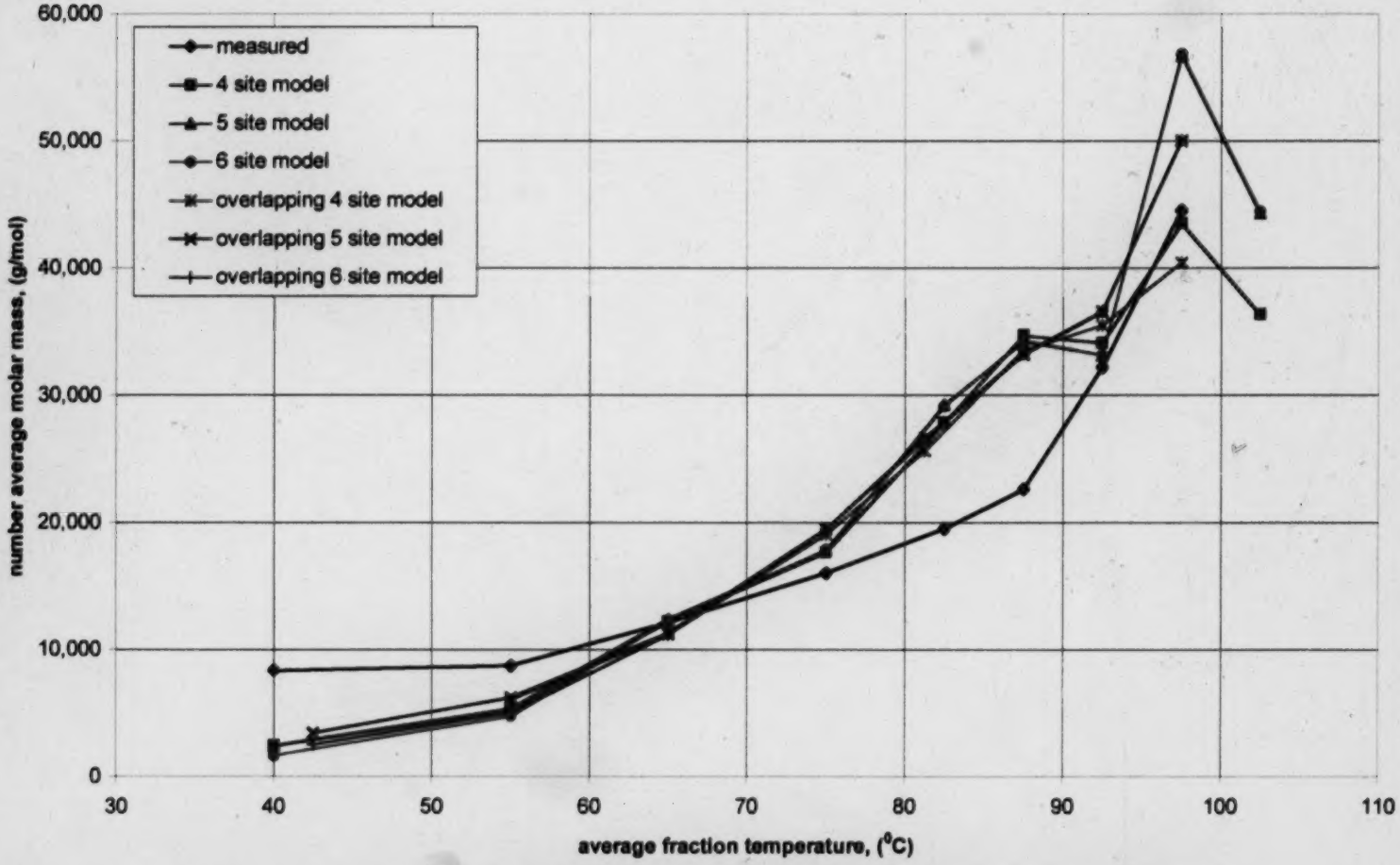

Figure 16. Comparison of the measured preparative TREF number average fraction molar mass for Sample 2 with model predictions.

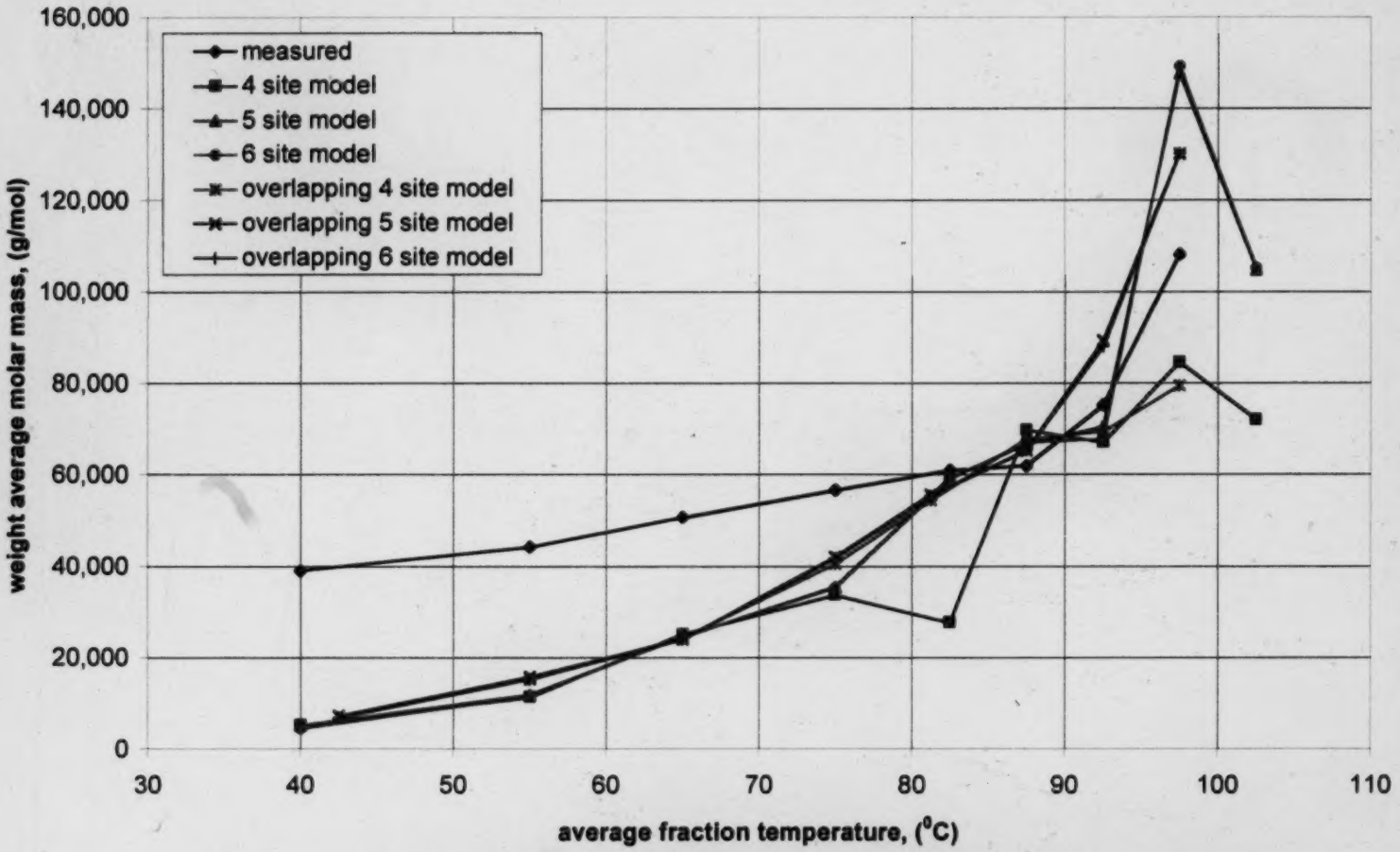

Figure 17. Comparison of the measured preparative TREF weight average fraction molar mass for Sample 2 with model predictions.

ones for all but one fraction. Figure 18 shows the same trends as in Figure 15, the measured polydispersity is higher than the calculated polydispersity for all fractions, and the calculated polydispersity is around 2 for all fractions.

For Sample 3, the measured M_n and M_w in Figures 19 and 20 show a dramatic difference from those predicted by the four-site model. The measured M_n and M_w show very little change as the fraction temperatures increase. The M_n goes from 5,000 g/mol at the low temperature fraction to a maximum of 17,000 g/mol at the high temperature fraction. The results in Figure 21 show that the measured polydispersity decreases from a high polydispersity to a low polydispersity of around 3 and the predicted polydispersity for the 4-site model stays around 2 for all fractions.

The results for Sample 4 in Figures 22 and 23 show that the measured number average and weight average molar masses varied from the molar mass trends predicted from the model based on the analytic TREF results. The measured molar masses, both M_n and M_w, were fairly constant for all preparative TREF fractions from 10°C to 80°C and then increased sharply for higher temperature fractions. However, in this case, as shown in Figure 24, a very different behavior was observed for the measured polydispersity. In this case, the measured polydispersity started at a maximum of 2.5 for the low temperature fractions and decreased to 2 at the high temperatures.

The differences between the measured and predicted preparative TREF results can be attributed to two general causes. Firstly, the model used to describe the analytical TREF profiles could be wrong and must be modified to

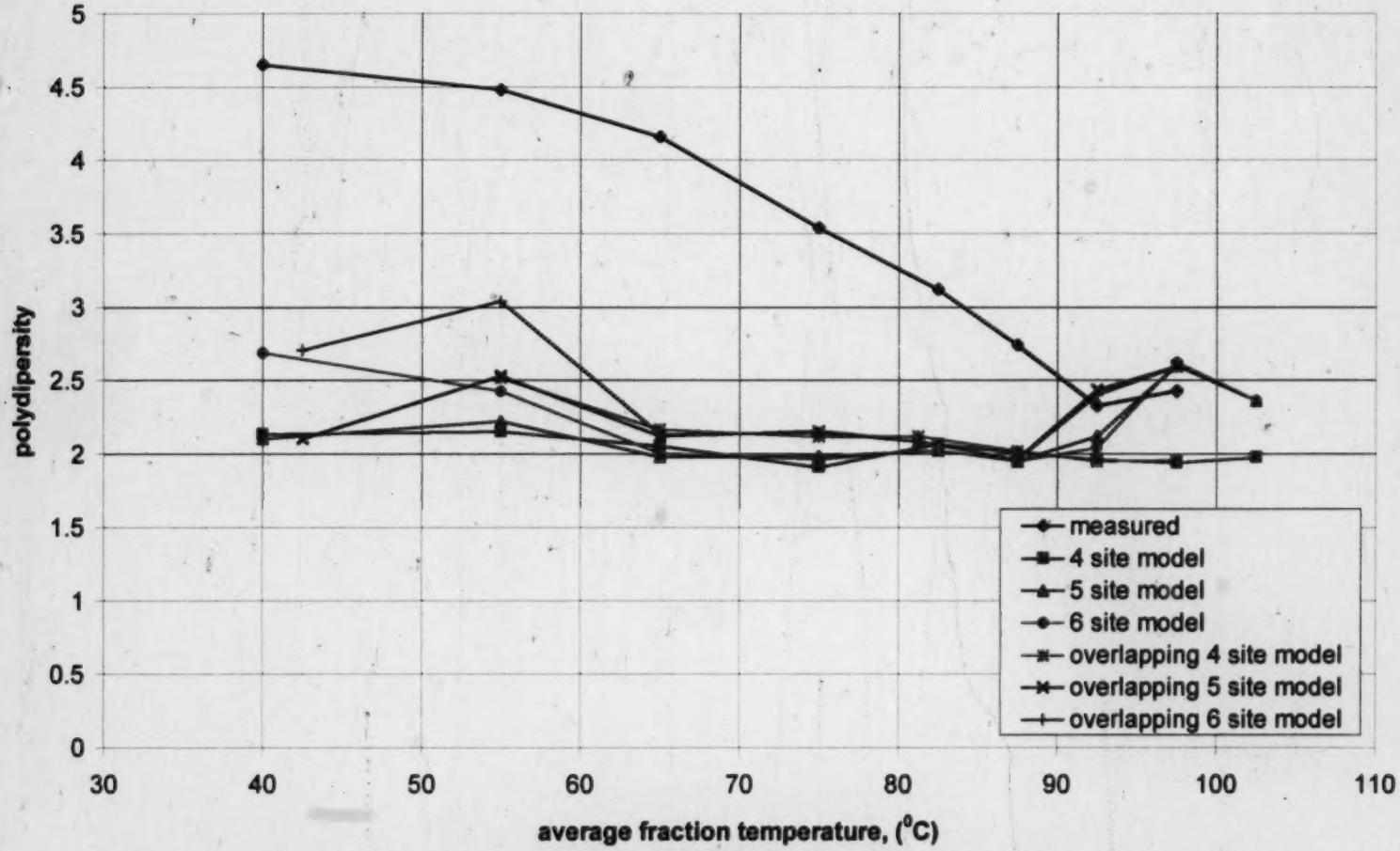

Figure 18. Comparison of the measured preparative TREF fraction polydispersity for Sample 2 with model predictions.

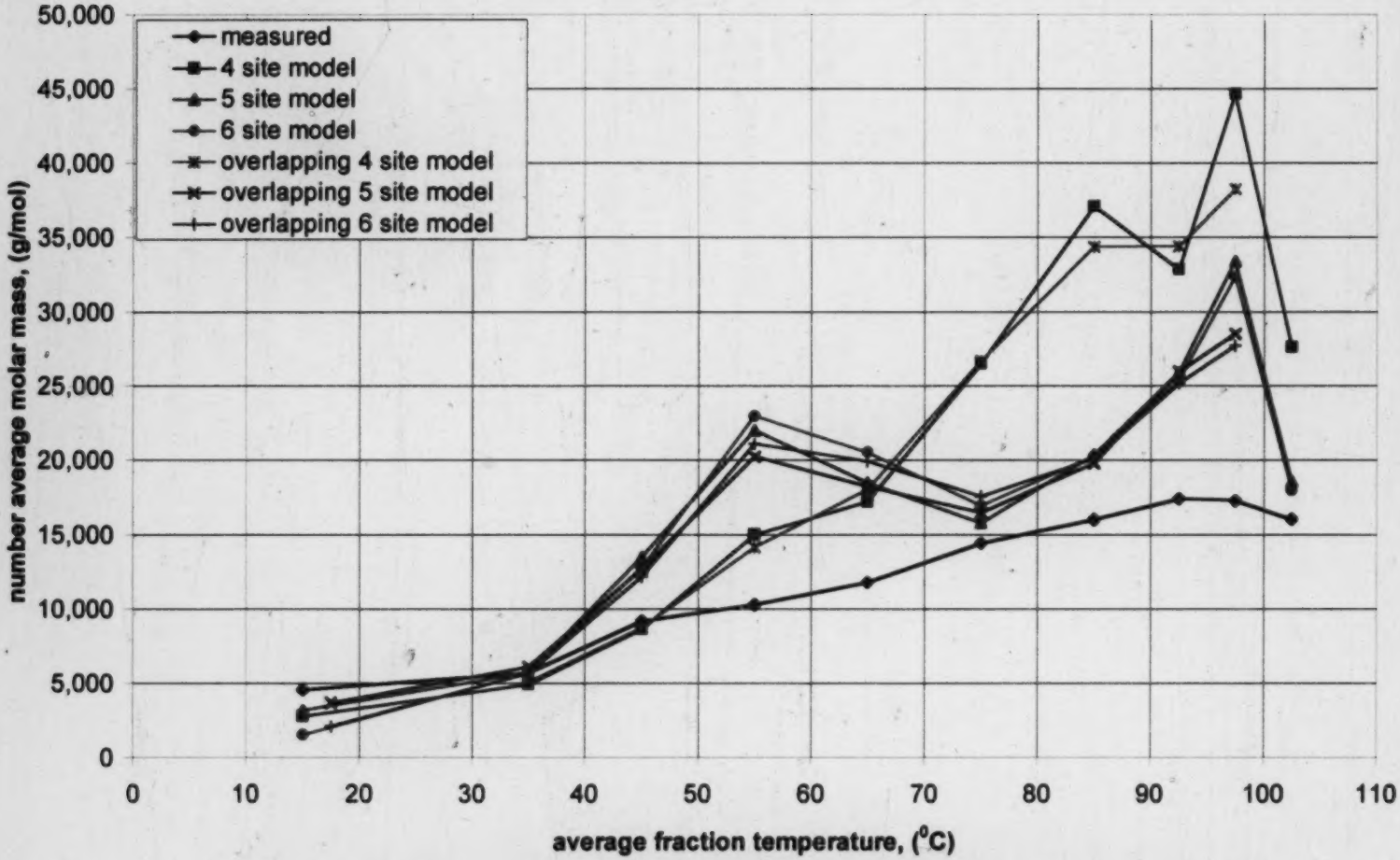

Figure 19. Comparison of the measured preparative TREF number average fraction molar mass for Sample 3 with model predictions.

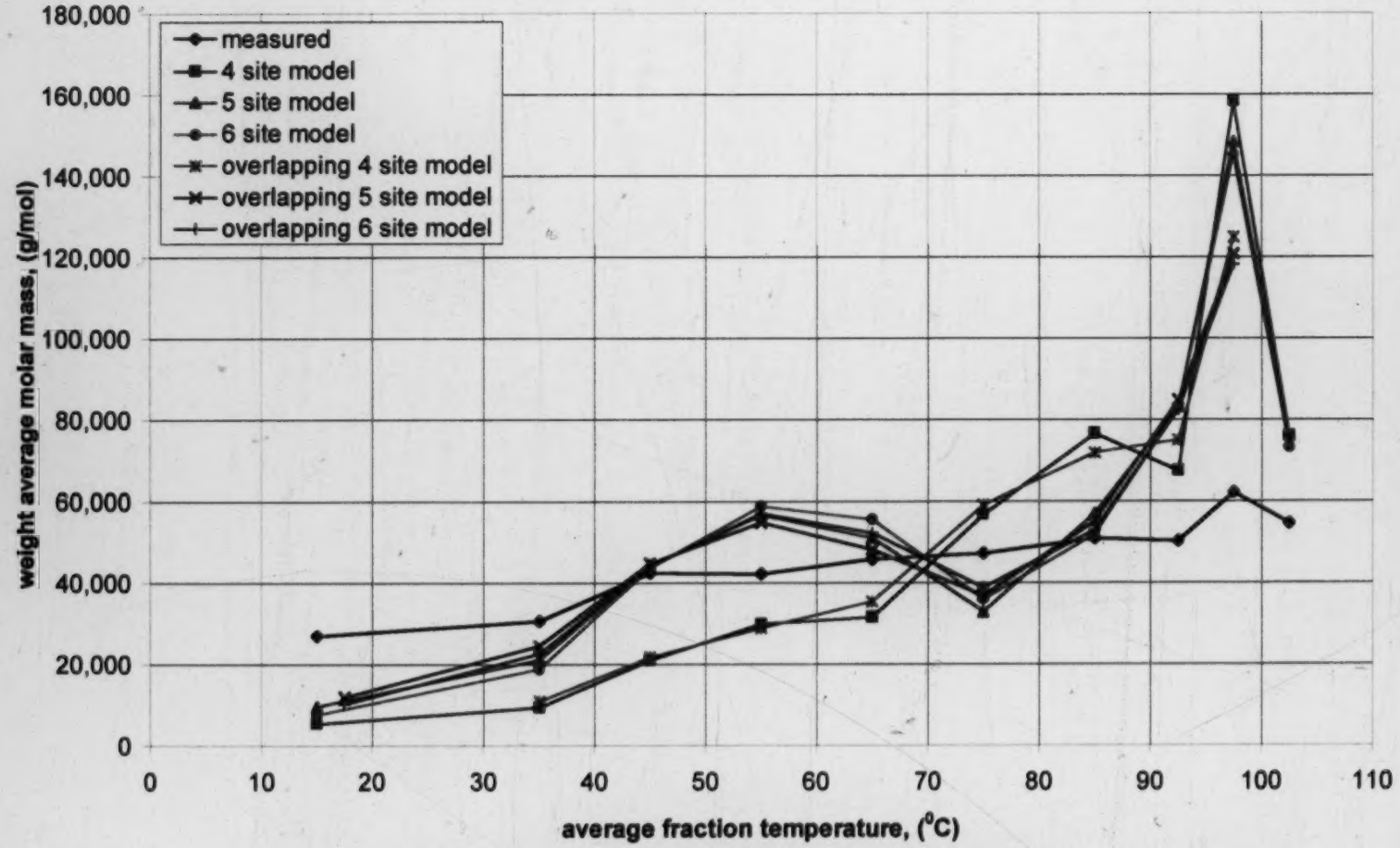

Figure 20. Comparison of the measured preparative TREF weight average fraction molar mass for Sample 3 with model predictions.

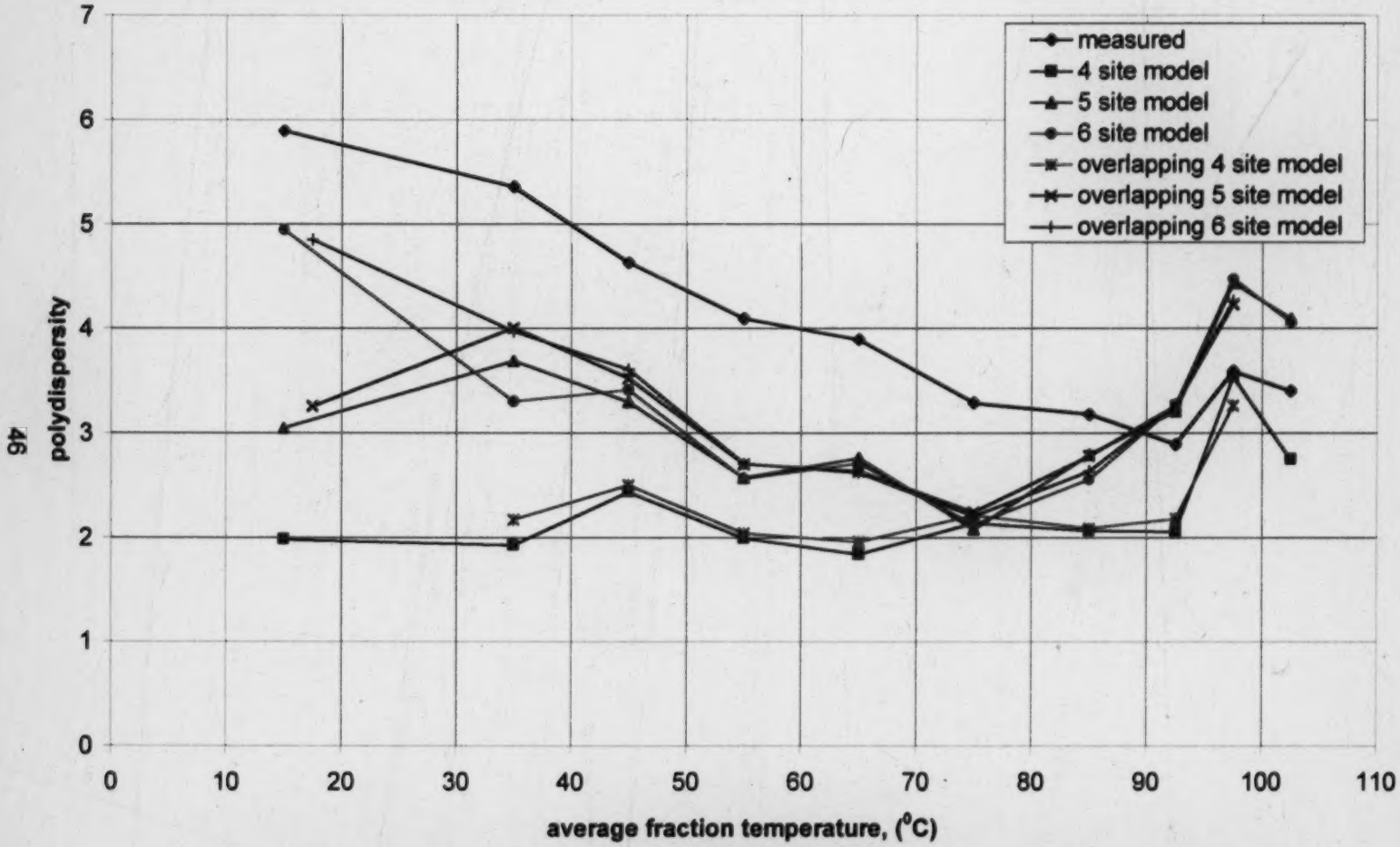

Figure 21. Comparison of the measured preparative TREF fraction polydispersity for Sample 3 with model predictions.

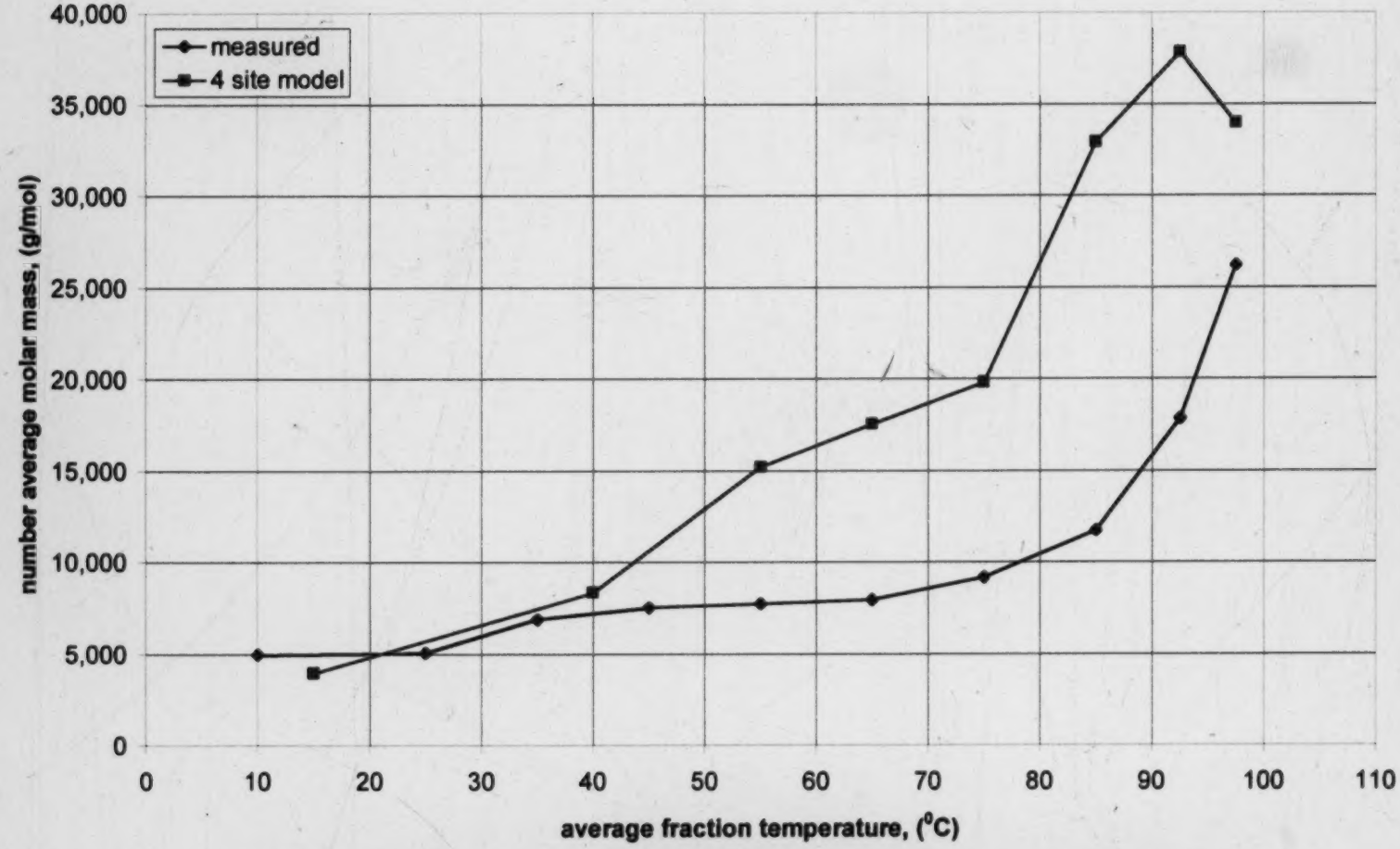

Figure 22. Comparison of the measured preparative TREF number average molar mass for Sample 4 with model predictions.

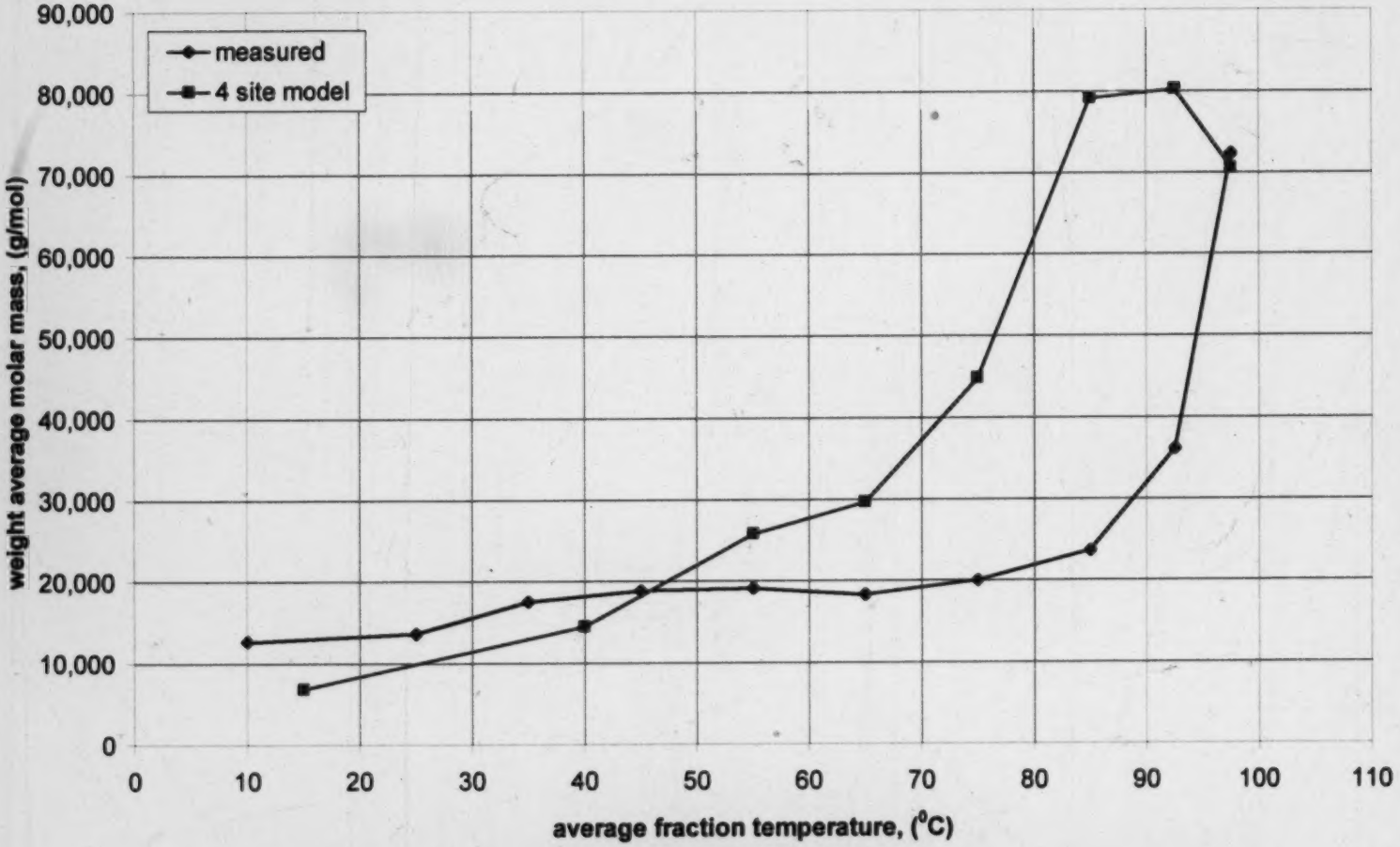

Figure 23. Comparison of the measured preparative TREF weight average molar mass for Sample 4 with model predictions.

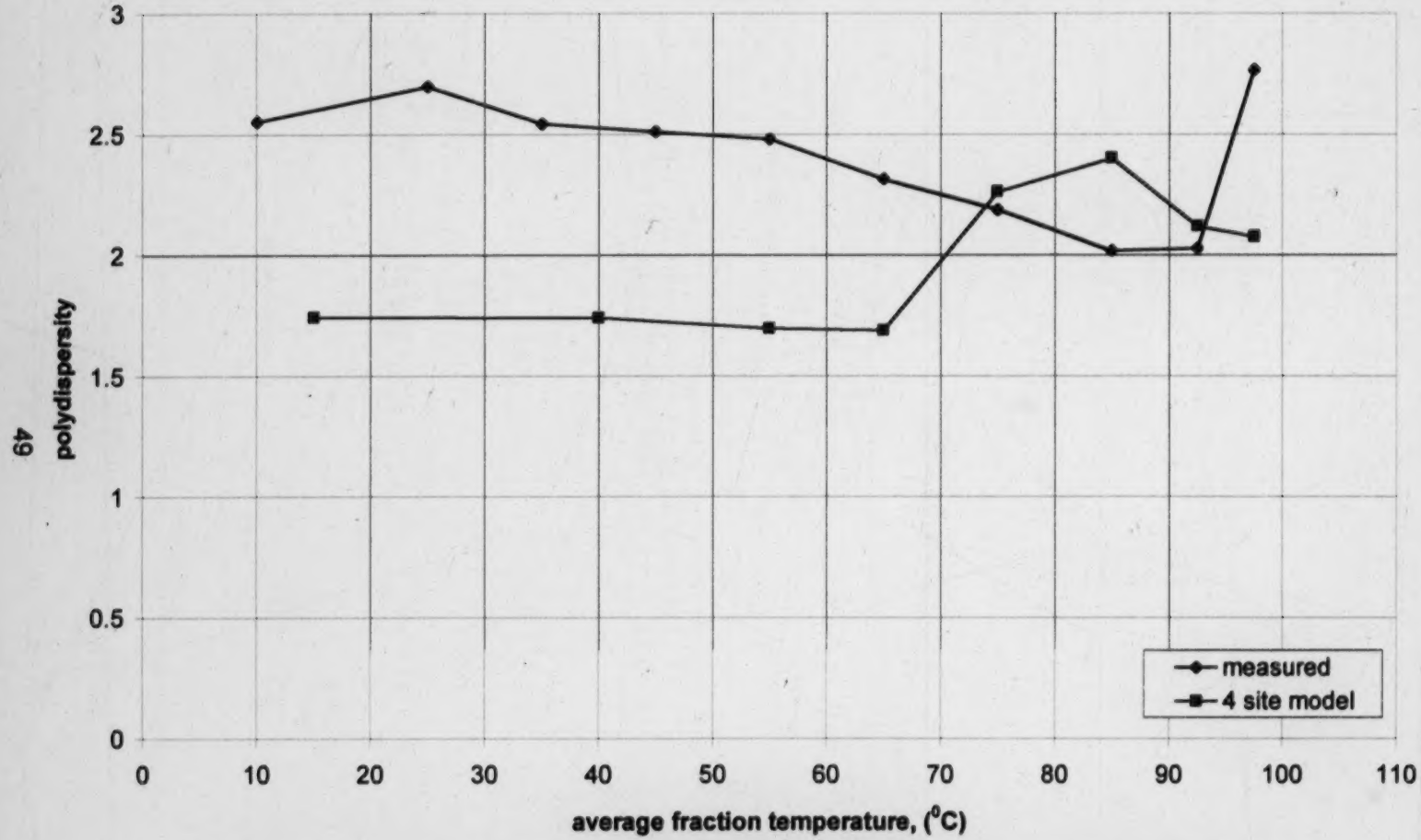

Figure 24. Comparison of the measured preparative TREF fraction polydispersity for Sample 4 with model predictions.

reflect the experimental results, and/or secondly, the measurements, either or both analytical and preparative TREF, are in error. The assumptions used for the model are not entirely valid, e.g. the number of different types of sites was assumed to be four and it is assumed that the parameter or the relative values of parameters for the sites are time independent. The overall fit of the analytical TREF profiles was good; hence, the degree of fit cannot be used to assign validity to the model and the degree of fit does not provide an explanation for the disagreement between the measured and predicted preparative TREF results.

One possible explanation is that the fractionation process is different from the analytical mode to the preparative mode. This could account for having the model fit the analytical TREF and the mass distributions well yet produce poor preparative TREF results. Another possible explanation is that the fractionation process is not consistent. Examination of the previous twelve figures shows that the predicted results follow the same trends for each sample, whereas the measured results do not display similar consistent trends in molar masses and polydispersities for the fractions at the various 1-butene concentrations. Comparing the polydispersity results between the high 1-butene concentration and the low 1-butene concentration show that the measured profiles are very different while the calculated profiles are similar. This could mean that the fractionation mechanism is different for a low branched polymer than a highly branched polymer. For the four site model, Figures 15, 18, 21 and 24 showed that the polydispersity increased when the fractions overlapped. This could indicate that either there is a need for more active sites (i.e. more overlapping of

the sites) or that again the fractionation process is not simple. The next section explores the results of adding more active sites.

4.5 - Models with 5 and 6 active sites

The effect of adding more active sites to the model was explored for two polymers, Sample 2 (10 mL 1-butene) and Sample 3 (20 mL 1-butene). These two polymers were chosen because the fitting of the 4-site model for Samples 1 and 4 was difficult. The difficulty encountered was keeping the sites in the prescribed order of increasing molar mass. Samples 2 and 3 were also chosen since in the 4-site model the value of m(j) needed to be fixed in one case and not in the other (see Section 4.2). Postulating more active sites for these two samples may remove the necessity of fixing the mass fractions for these samples.

Five and six active sites were used to fit the mass distribution and the analytical TREF profile for Sample 2. Figures 25 and 26 show the calculated mass distribution with the measured mass distribution for five and six active sites. When these figures are compared with Figure 1 for four active sites, there is very little difference between the three calculated results. The changes occur in the high and low molecular weight tails of the distribution. The average molar massed and statistical properties of the fits are listed in Table 6.

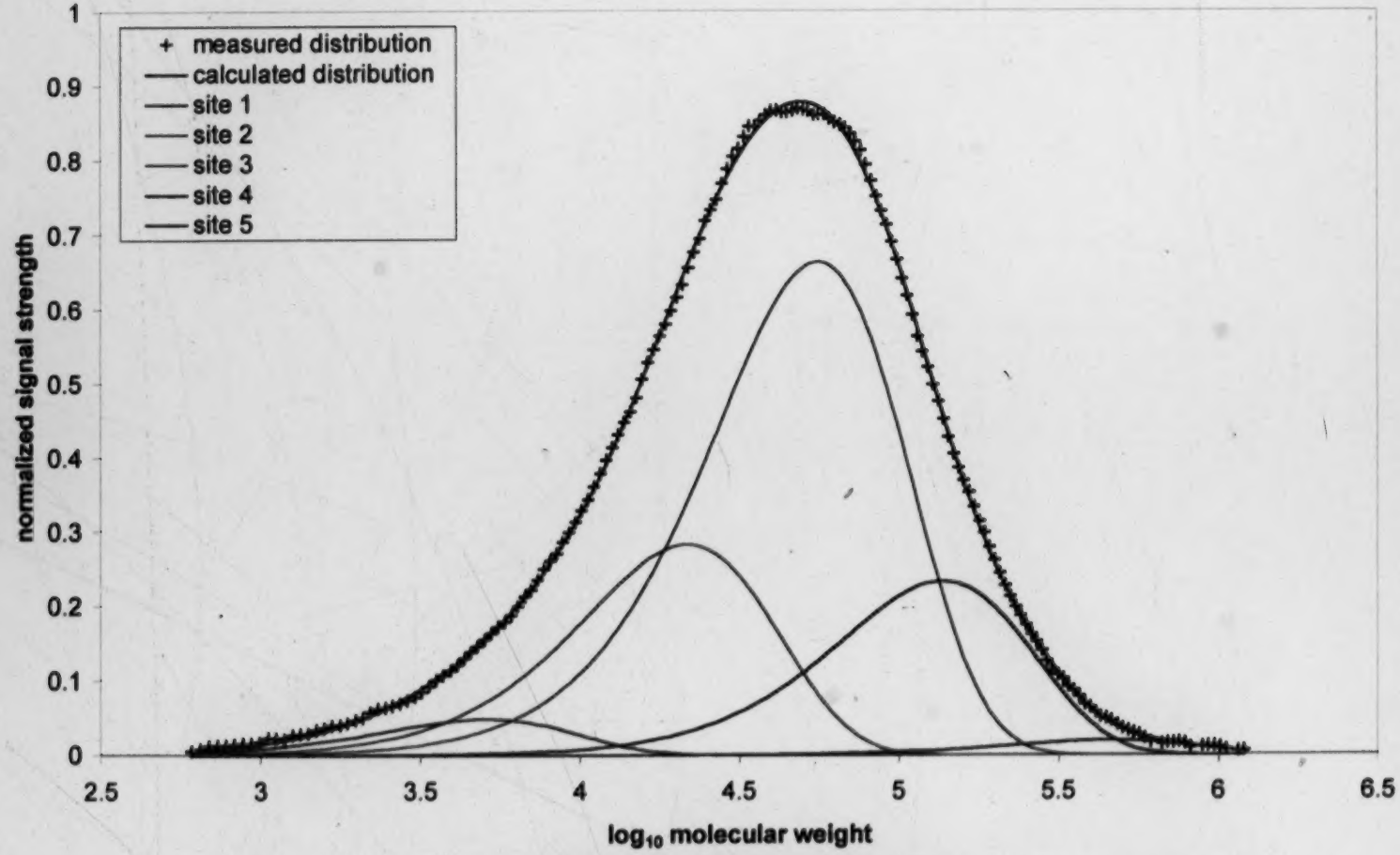

Figure 25. Comparison between the measured mass distribution and the calculated mass distribution using five sites for Sample 2.

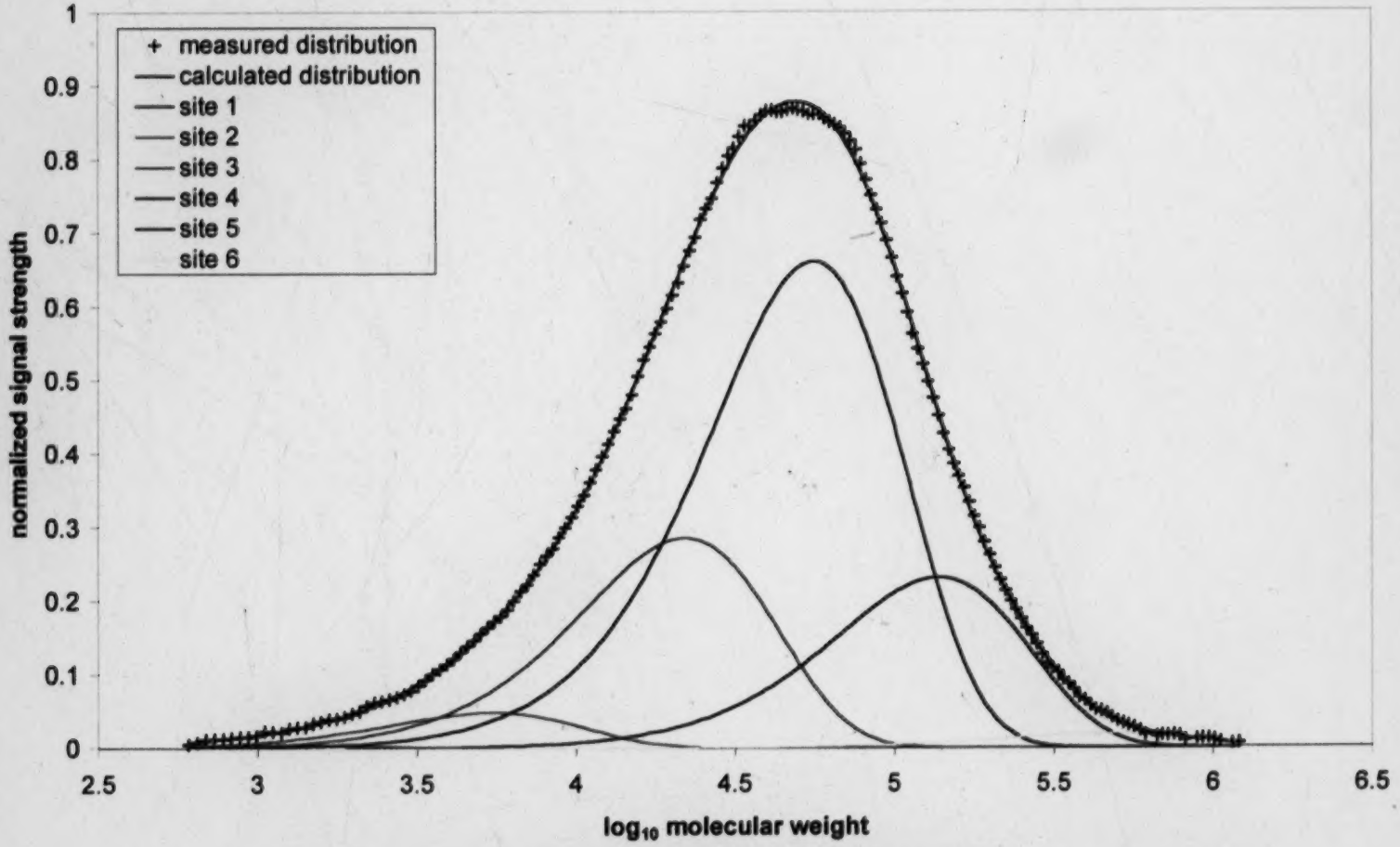

Figure 26. Comparison between the measured mass distribution and the calculated mass distribution using six site for Sample 2.

Table 6. Comparison of calculated mass distributions for 4, 5 and 6 active sites for Sample 2.

	Measured	4 Sites	5 Sites	6 Sites
M_n	17781	17260	17192	15877
M_w	65763	64118	67713	67709
Pd	3.699	3.715	3.939	4.265
r^2	-	0.99957	0.99972	0.99974
χ^2	-	0.00695	0.00452	0.00427
F	-	54818	64642	55496

When the fifth and sixth sites were added the M_w increased significantly and the sixth site decreased the M_n. This has the effect of increasing the polydispersity with each added active site. The r^2 and χ^2 numbers show that the fit was improved by adding the extra active sites. However, it is important to look at the significance of the added parameters. Adding the fifth active site increased the number of fitted parameters by two. The additional parameters improved the fit and are significant. This is reflected by the increase in the F statistic. When two more parameters are added with the sixth active site the fit is improved but the added parameters are not significant. This is reflected by the decrease in the F statistic.

Using these mass distribution parameters the analytical TREF profile was fit using 5 and 6 active sites. Figures 27 and 28 show the analytical TREF profiles fit using 5 active sites and 6 active sites respectively. The statistical results for the four, five and six active site cases are compared in Table 7.

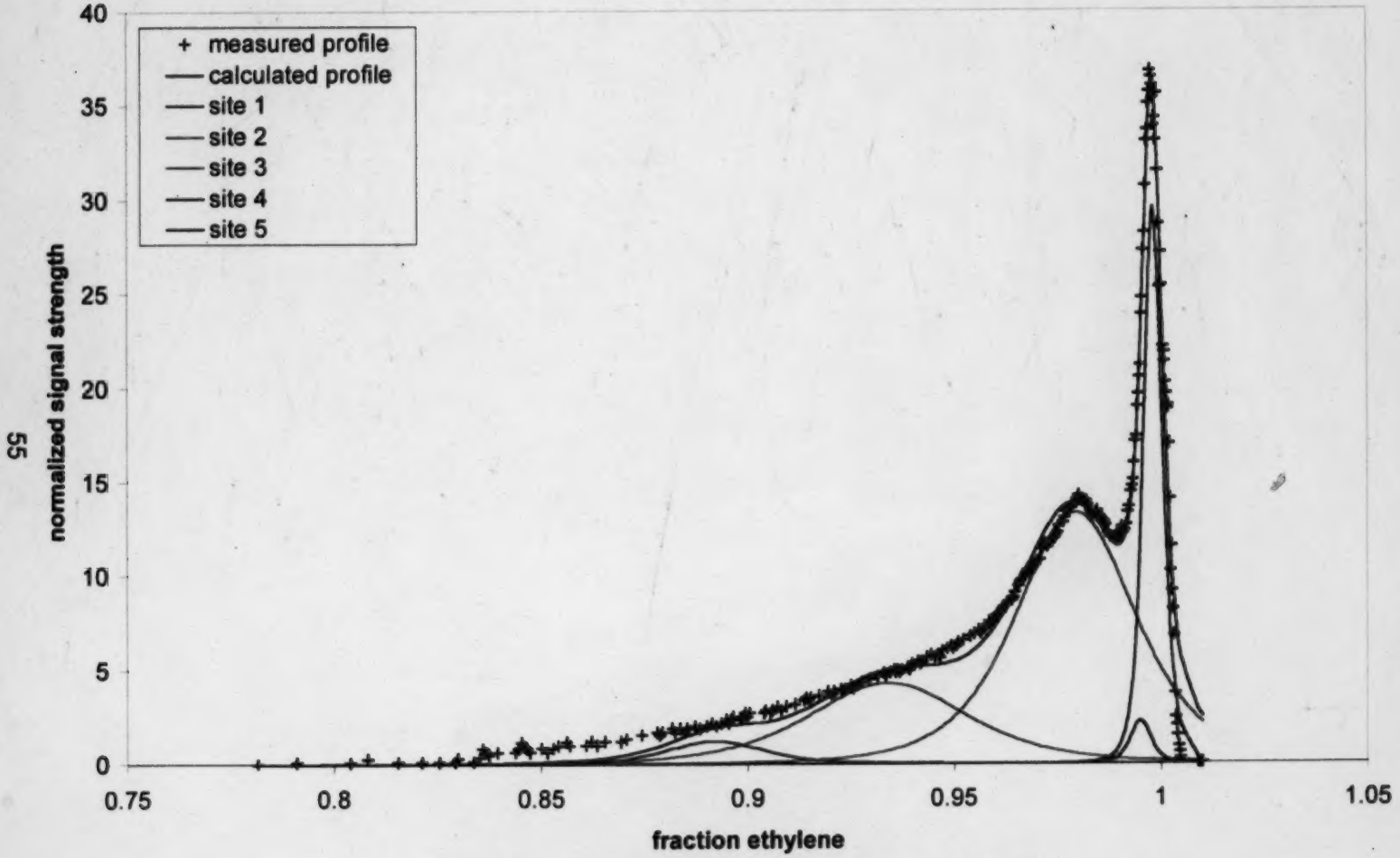

Figure 27. TREF profile for Sample 2 using five sites.

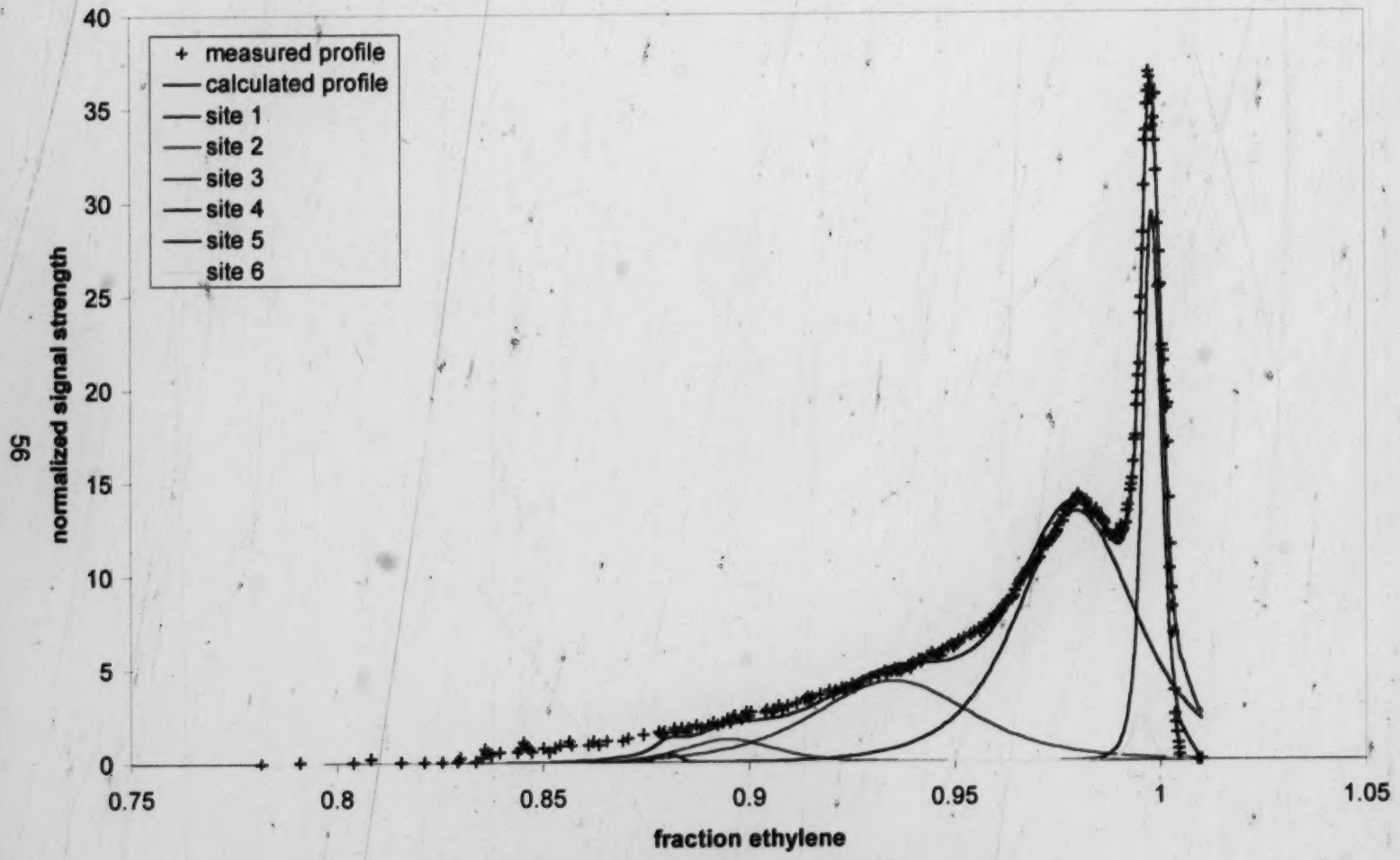

Figure 28. TREF profile for Sample 2 using six sites.

Table 7. Comparison of statisitcal information for the analytical TREF profiles for Sample 2.

	4 sites	5 sites	6 sites
r^2	0.96717	0.97939	0.97946
χ^2	637.80	400.30	398.95
F	984.73	1225.2	997.21

As with the mass distribution fit the addition of one active site is a statistically significant improvement of the fit. The addition of the sixth site did not result in a statistically significant improvement of the fit.

The mass distribution profile for Sample 3 was fit using five and six active sites. Figures 29 and 30 show the calculated profile with the measured profiles for the 5 and 6 site models. The calculated profiles for the 4, 5, and 6 site models are not significantly different. Table 8 compares the statistical results for the models with different number of active sites.

Table 8. Comparison of mass distributions for 4, 5 and 6 active sites for Sample 3.

	Measured	4 Sites	5 Sites	6 Sites
M_n	11545	13495	12771	10312
M_w	51317	52046	52212	52110
Pd	4.445	3.857	4.088	5.053
r^2	-	0.99861	0.99954	0.99981
χ^2	-	0.02309	0.00766	0.00309
F	-	21178	47286	92656

For Sample 3 the addition of the fifth and sixth site were each a statistically significant improvement of the fit. As with the four active site model

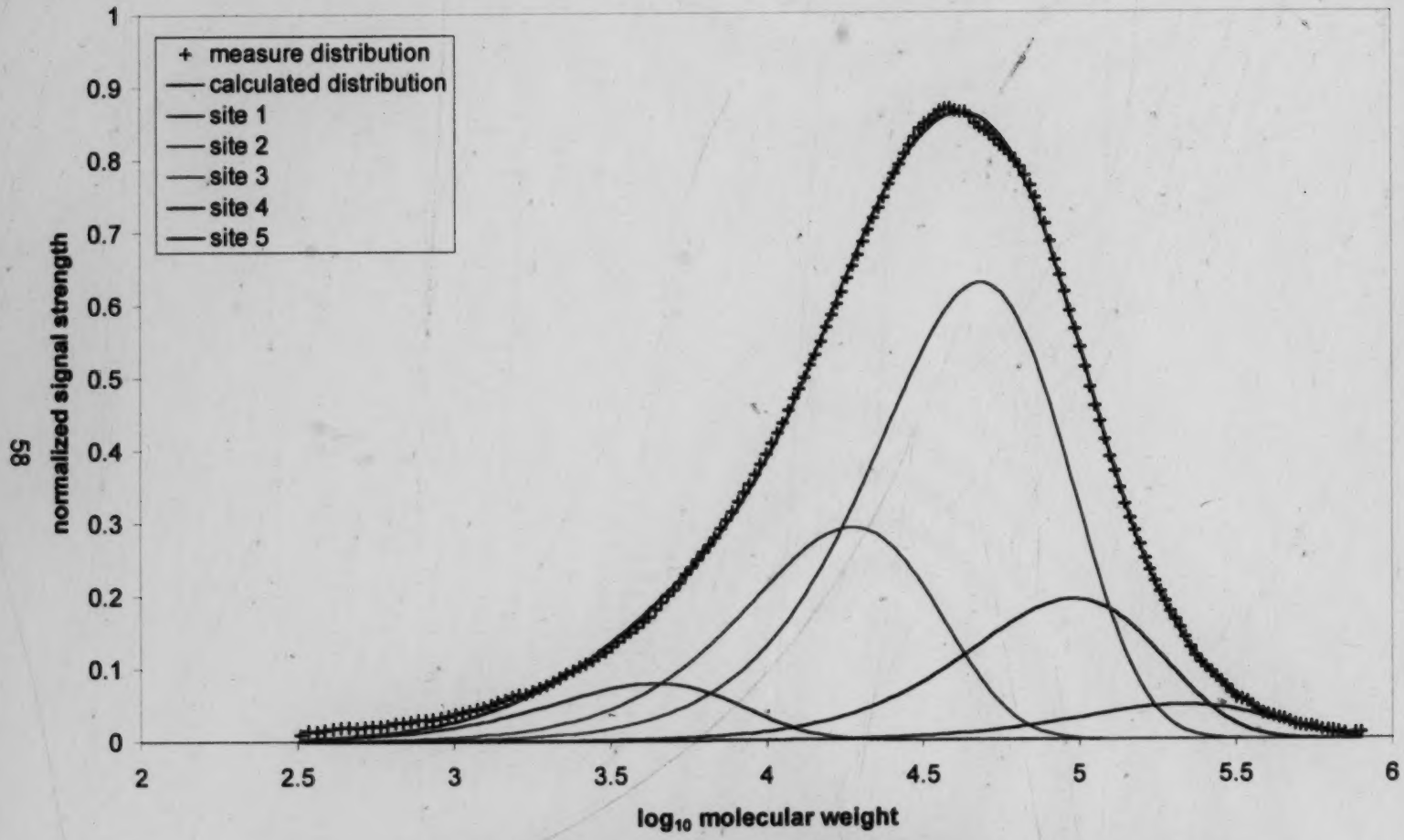

Figure 29. Comparison between the measured mass distribution and the calculated mass distribution for Sample 3 using five sites.

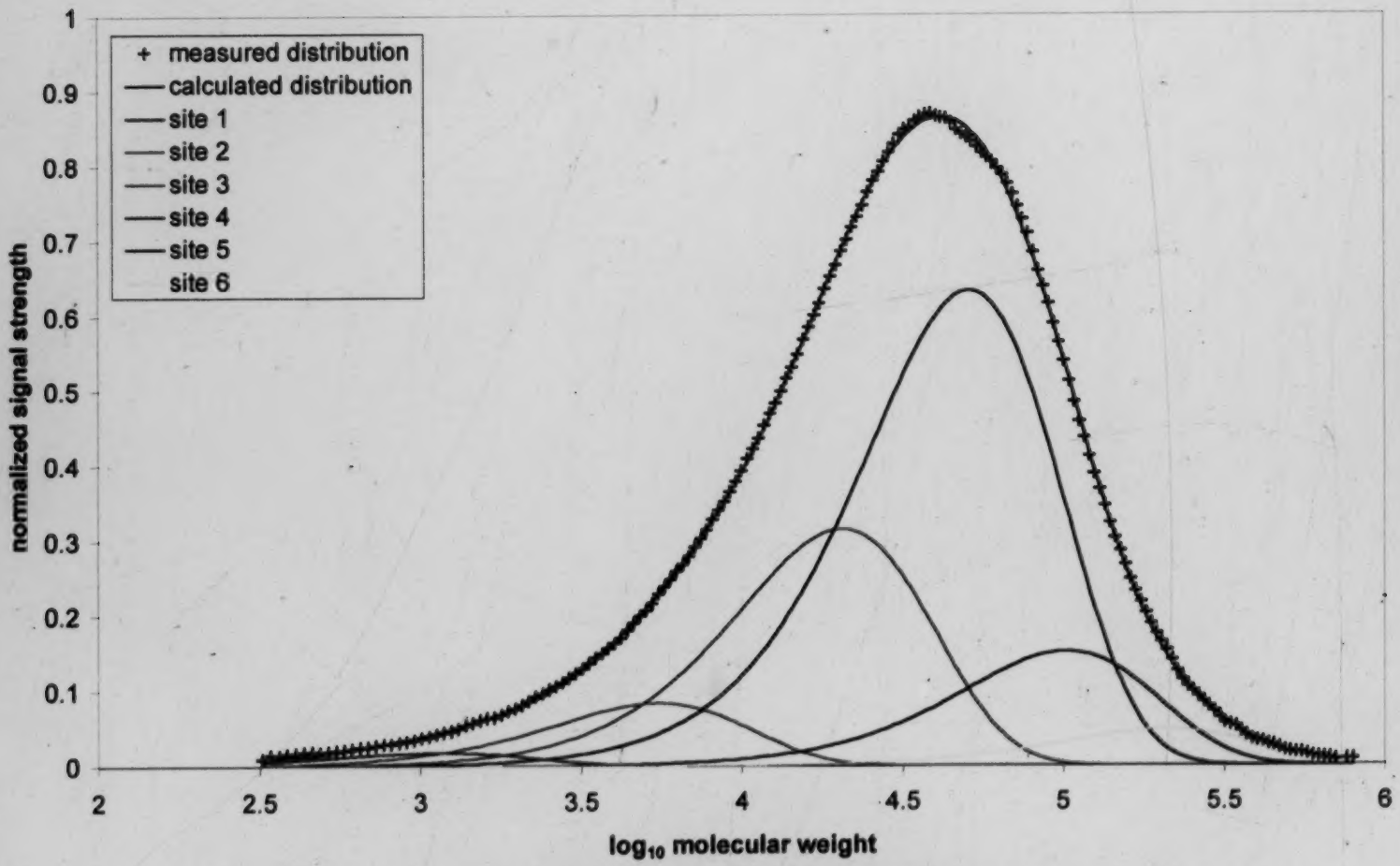

Figure 30. Comparison between the measured mass distribution and the calculated mass distribution for Sample 3 using six sites.

the mass fraction of the homopolymer peak had to be specified so that the analytical TREF profile would be fit properly.

Figures 31 and 32 show the analytical TREF profiles fit using five and six sites. The addition of the 5th and 6th sites improved the fit for the high 1-butene incorporation region over the 4-site model shown in Figure 5. Table 9 compares the statistical results for the analytical TREF profiles.

Table 9. Comparison of statisitcal information for the analytical TREF profiles for Sample 3.

	4 sites	5 sites	6 sites
r^2	0.97371	0.97737	0.97798
χ^2	198.9	171.3	166.6
F	1926.2	2749.1	2305.4

Again, as with Sample 2, using 5 active sites to model the TREF profile is a statistically significant improvement over four active sites and using six sites is not.

A requirement of the model is that the site producing a polymer with the highest molar mass has the least 1-butene incorporation. In all cases, for fits using five and six active sites there was deviation from this requirement. The deviations are different for each case. Table 10 shows the number average molar mass and average ethylene fraction of the TREF profile fits using 5 and 6 sites.

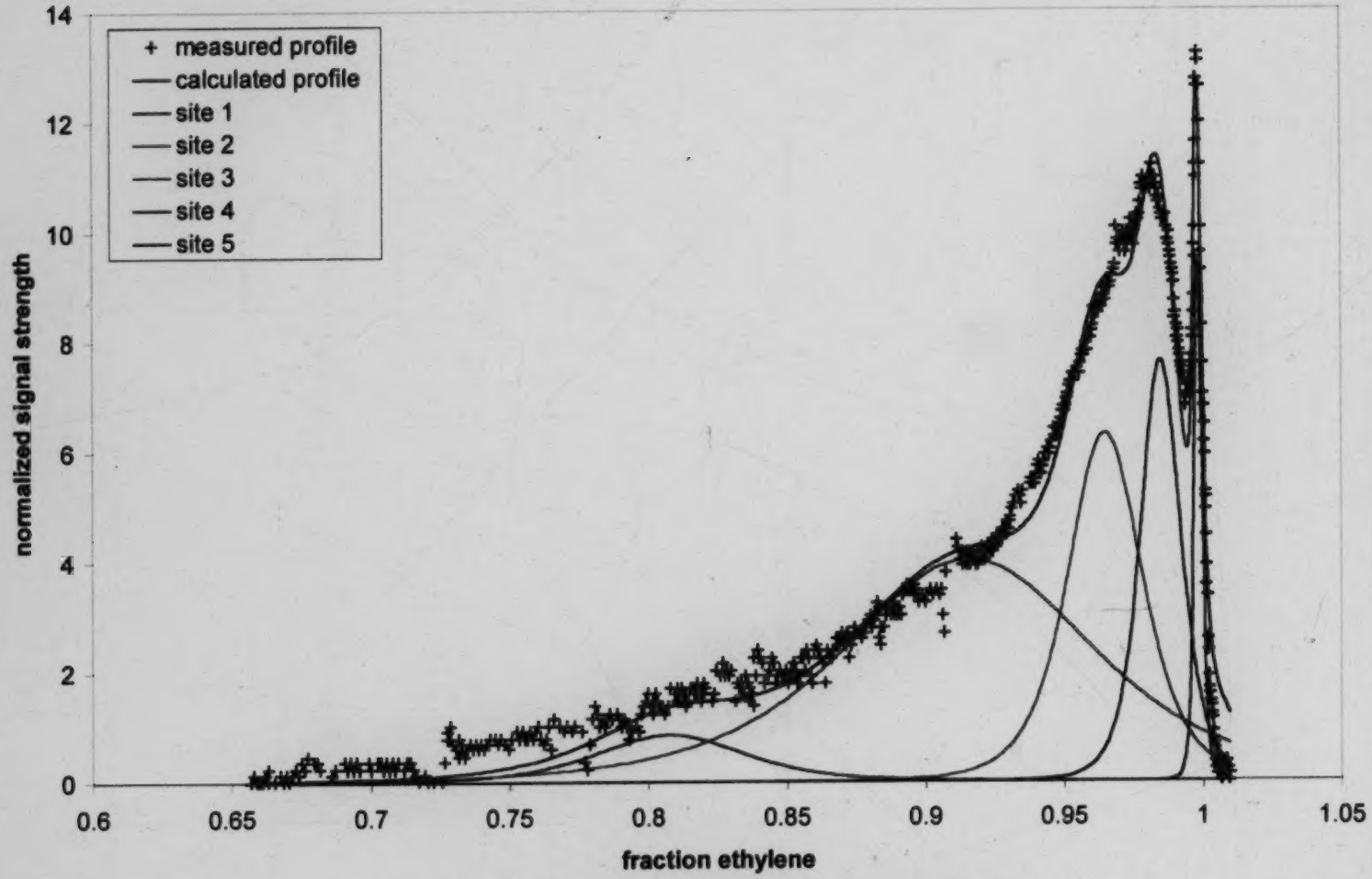

Figure 31. TREF profile for Sample 3 using five sites.

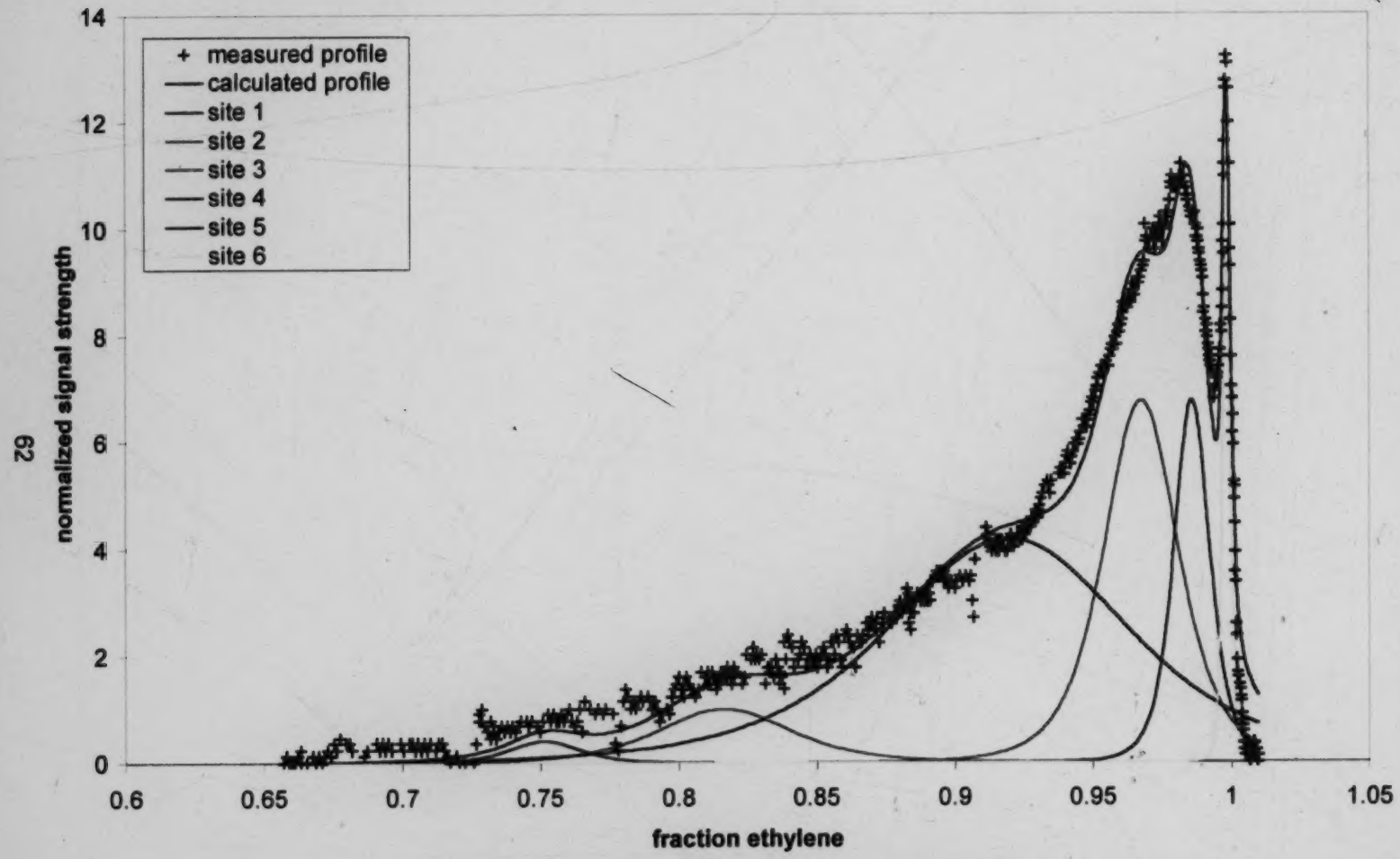

Figure 32. TREF profile for Sample 3 using six sites.

Table 10. Numerical results of fitting TREF profiles using 5 and 6 sites.

			Site 1	Site 2	Site 3	Site 4	Site 5	Site 6
Sample 2	5 Sites	$M_n(j)$	2,547	10,861	27,892	68,546	231,783	n/a
		$F_1(j)$	0.8922	0.9343	0.9796	0.9982	0.9950	n/a
	6 Sites	$M_n(j)$	621	2,736	11,009	28,050	68,954	233,798
		$F_1(j)$	0.8805	0.8952	0.9352	0.9799	0.9982	0.9953
Sample 3	5 Sites	$M_n(j)$	2,184	9,409	24,319	47,954	107,238	n/a
		$F_1(j)$	0.8082	0.9649	0.9174	0.9849	0.9984	n/a
	6 Sites	$M_n(j)$	587	2,744	10,274	25,675	51,212	105,078
		$F_1(j)$	0.7515	0.8168	0.9676	0.9211	0.9858	0.9984

For Sample 3 using the 5-Site model Sites 2 and 3 switched places with respect to molar mass. Using the 6-Site model Sites 3 and 4 are reversed. For Sample 2 using the five site model sites 4 and 5 switched. Using the 6-Site model Sites 5 and 6 switched. These changes may seem minor and may have some real meaning but the basis of the model is being violated. Increasing molar mass with decreasing comonomer incorporation is supported by the experimental preparative TREF results for polyethylene produced with supported Ziegler-Natta catalysts; however, such correlation does not exist for polyethylenes made with metallocene catalysts (Zhang et al., 2000).

The purpose of adding sites was to improve the prediction of the preparative TREF results. The additional overlapping of the sites should lead to an increased polydispersity for each fraction. For Sample 2, Figures 13 and 14 show that the addition of Sites 5 and 6 do not significantly change the molar masses of the fractions. In Figure 15 it is shown that adding active sites

increases the polydispersity of the fractions. However, the additional sites do not increase the polydispersities predicted by the model to the measured ones.

For Sample 3, the additional sites have a greater effect on the preparative TREF predictions. In Figures 16 and 17 it is shown that the additional sites bring the predicted molar masses closer to the measured ones. For the high temperature fractions, the models still over-predict the molar masses. In Figure 18 it is shown that the additional sites result in better agreement between the predicted and measured polydispersities of each fraction.

5.0 - Summary and Conclusions on Modeling

The goal of the work described in this section was to determine if information about the number and nature of catalytic sites can be obtained from measured analytical TREF profiles using the model proposed by Soares and Hamielec (1995). Analysis of the analytic TREF profiles for LLDPE with different 1-butene contents by the four-site model yielded the following information:

1. The amount of 1-butene incorporation differed significantly among the 4 sites (see Figure 9).
2. The dependence of 1-butene incorporation rates on 1-butene concentration varied significantly among the different sites (compare slopes in Figure 9).
3. Each type of site produced polyethylene with different molar masses, but the number average molar mass of the polyethylene by each site was essentially independent of the 1-butene concentration (see Figure 10).
4. The fraction of the total polyethylene produced by each site was a strong function of 1-butene concentration (see Figure 11). It is this variation in relative rates of polyethylene production by the various sites which results in the dependence of the whole polymer molar mass on 1-butuene concentration.
5. The reactivity ratios r_1r_2 were significantly different for the four sites varying in magnitude from about 10^2 to 10^7 (see Figure 12).

It should be pointed out that the above observations are based on the fitting of experimental analytical TREF profiles with the assumption that the catalyst had 4 different types of catalytic sites. There may be more types of sites; however, fitting results using six or more types of sites was found to be statistically unsound.

The model was used to predict preparative TREF behaviour. These predictions were compared to experimental preparative TREF results in order to test the validity of the model. The model was able to predict trends, and to a lesser degree the values, of the number average and weight average molar mass for the various preparative TREF fractions (see Figures 13, 14, 16, 17, 19, 20, 22 and 23); however, the predicted polydispersities of the various fractions were usually lower than the measured ones (see Figures 15, 18, 21 and 24).

The following future work is recommended to further examine the applicability of the model:

1. Develop improvements in the solving method in order to constrain the parameters into the prescribed order.
2. Repeat analytical and preparative TREF profiles with SEC cross-fractionation should be done on each sample to determine the reliability of the experimental results.

6.0 – Part II: Synthesis of Spherical Magnesium Chloride

Polyethylene and other polyolefins can be produced under mild conditions using supported Ziegler-Natta catalysts. Some supports not only add surface area for the distribution of active sites, but also participate chemically to enhance the reaction rates. One such support is magnesium chloride ($MgCl_2$). Titanium supported on $MgCl_2$ can produce a highly active catalyst for the polymerization of ethylene.

A property of the polymer formed using a Ti-$MgCl_2$ catalyst at appropriate reaction conditions is that the polymer replicates the physical shape of the support particle on which it is growing. The replication phenomenon can have very practical applications. A significant amount of polyethylene produced in North America is formed using fluidized bed reactors. The polymer product from these reactors are flakes of polymer. These flakes are then melted, extruded and cut into pellets that are shipped to the users. The pelletization process requires large energy input and pelletizing has some adverse affects on the processibilty of some polyethylenes. If, however, the polymer grows as a spherical pellet in the reactor then no further processing would be necessary. This would result in energy savings and possible product improvements. In order to grow spherical polymer particles; one has to start with a spherical catalyst particle, i.e., spherical support particles.

Magnesium chloride can be formed into spherical particles by several methods. These methods include spray drying, melt quenching and precipitation

reactions. In this part of the thesis, the preparation and characterization of $MgCl_2$ support particles by precipitation will be described.

7.0 - Literature Survey - Catalyst Studies

Highly active fourth-generation Ziegler-Natta catalysts with morphology control can be made by relatively simple procedures. Many studies have been completed that explore the properties of the catalyst support that lead to producing a highly active catalyst.

Guidetti et al. (1980) used x-ray diffraction (XRD) to examine the effects of disorder during the mechanical activation of $TiCl_3$. A model was developed that used two types of disorder that had different amounts of cubic and hexagonal sequences. The concept that the stacking faults on successive layers are cubic, hexagonal or rotational has been expanded and applied to other catalysts and supports. Galli et al. (1983) ball milled $MgCl_2$ and used XRD patterns to show how the structure of the support changed with milling time. A similar study by Gerbasi et al. (1984) with $TiCl_3$ gave results very similar to those obtained by Galli et al. (1984). Both studies showed that as the support or catalyst was activated the disorder appeared as rotational faults with similar XRD patterns. Siew Hew Sam et al. (1986) completed a study on ball milling of VCl_3 and produced an active catalyst that had a similar XRD pattern to active $MgCl_2$ and $TiCl_3$.

The previous papers have shown that the defects of the support lead to active catalysts. The papers did not give a definitive reason as to why the catalysts were active except the observation that the XRD patterns were similar. Lin and Catlow (1993) developed a computer model of disordered $MgCl_2$ that

calculates the surface energy. Molecules of $TiCl_4$ and $TiCl_3$ were placed on the surface and the surface energy was recalculated. This study showed that it was energetically favorable for Ti chlorides to be adsorbed onto the surface of disordered $MgCl_2$.

8.0 - Experimental Procedures

The procedures used to produce $MgCl_2$ catalyst supports, Ziegler-Natta catalysts and the polymerization of ethylene over these catalysts to produce polyethylene are described below. The procedures used to characterize the support and catalyst particles are also described. The characterization methods used were x-ray diffraction, scanning electron microscopy, BET surface area measurement and optical microscopy.

8.1 - Preparation of Magnesium Chloride Support

Spherical magnesium chloride was formed by the reaction between di-*n*-butyl magnesium and 2-chloro-2-methylpropane (*tert*-butyl chloride). The reaction was performed using a one litre glass reactor. Figure 33 shows a schematic of the glass reactor used. The reactor temperature was maintained by circulating water through the reactor jacket. Di-*n*-butyl magnesium and heptane were introduced into the reactor by inserting a syringe needle into the top tee connection on the reactor. To maintain an inert condition in the reactor nitrogen was introduced into the reactor by the side tee connection. The reactor was fitted with removable baffles to increase the turbulence in the reactor and to limit the free body rotation of the fluid in the reactor. The baffles also provided a means to guide a Teflon dip tube to the bottom of the reactor without interfering with the impeller. A syringe pump, shown in Figure 33, was used to inject the

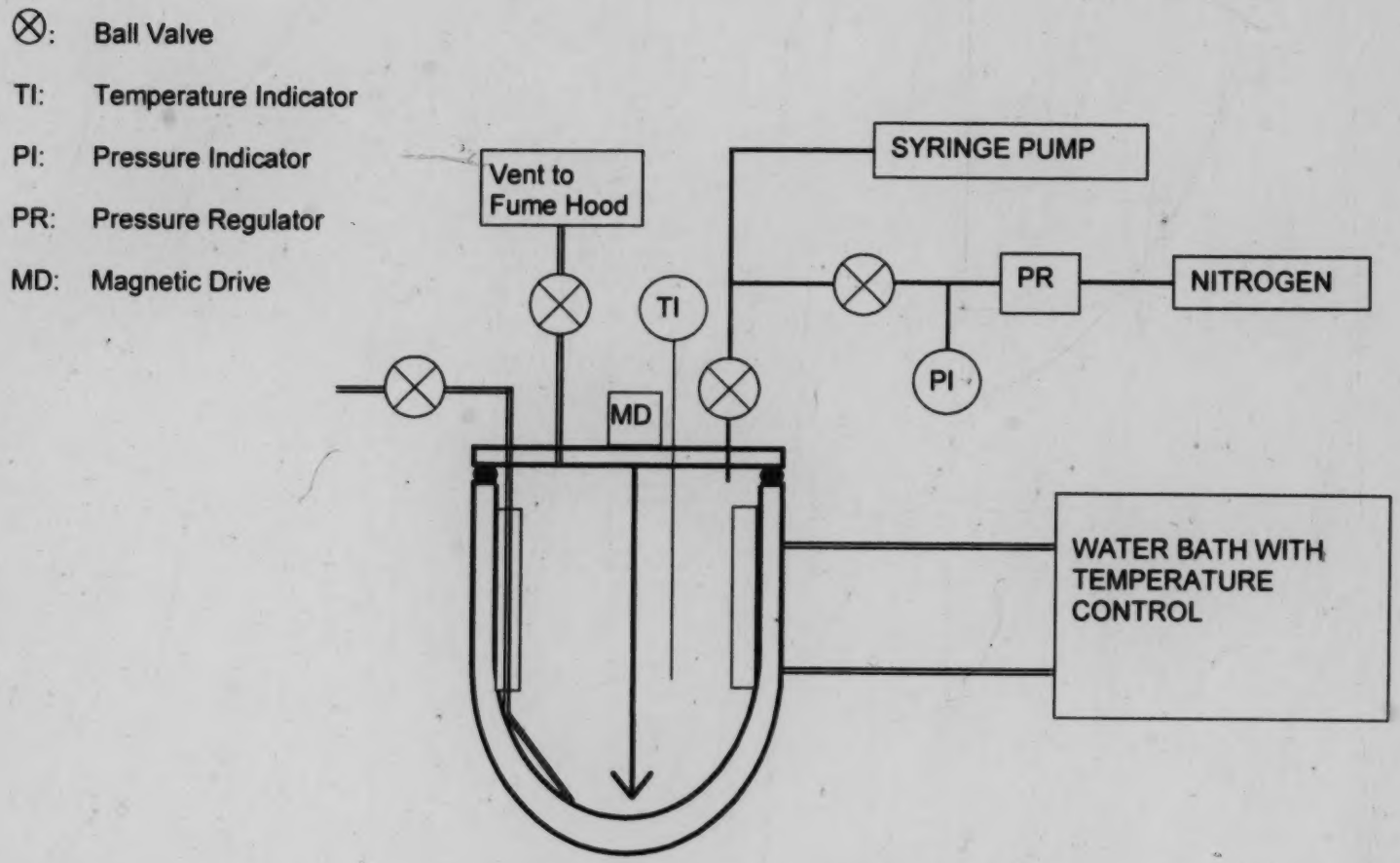

Figure 33. Schematic diagram of the one litre glass reactor.

tert-butyl chloride into the reactor at a slow controlled rate. The reactor was essentially a closed semi-batch reactor. As the reagents were added to the reactor, the heat of reaction caused the temperature to increase; this resulted in a pressure increase, and a vent valve was manually opened to reduce the reactor to the set pressure.

The following procedure was used for the preparation of magnesium chloride particles by reaction:

1. The reactor was evacuated over night at 85°C. This was to remove water and oxygen from the reactor.
2. The reactor was pressurized with nitrogen to 130 kPa and then the nitrogen was purged to atmospheric pressure.
3. The temperature bath was set to the operating temperature of 50°C and 200 mL of heptane was added to the reactor. Then 16 mL of dibutylether was added, followed by the addition of 97 mL of Akzo di-*n*-butyl magnesium (or 110 mL of Aldrich di-*n*-butyl magnesium) to the reactor.
4. The syringe pump line was connected to the top tee and nitrogen was used to purge the line for five minutes. 24 mL of *tert*-butyl chloride and 76 ml of heptane were mixed in a 100 mL syringe. The line was connected to the syringe and placed in the syringe pump.
5. The magnetic drive of the shaft was set at the desired rotation speed. The syringe pump was set to deliver a slow controlled rate of *tert*-butyl chloride to the reactor.

6. After all the *tert*-butyl chloride was added to the reactor it was allowed to react for at least two hours. Two collection bottles, shown in Figure 34, were joined with surgical tubing and evacuated and purged with nitrogen.
7. The collection bottles were connected to the reactor and under pressure the product was forced up the dip tube into the bottles.
8. Most of the heptane was decanted from the bottles under a nitrogen blanket. The remainder of the heptane was evaporated overnight at an elevated temperature. The next day the product was evacuated for 4 to 16 hours at room temperature to evaporate any remaining solvent to produce a free flowing powder.
9. The product was then transferred to a storage bottle in a glove box.

A 2^2 factorial design experiment was performed using the above procedure. The variables changed were the stirrer speed and the rate of *tert*-butyl chloride addition.

8.2 - Preparation of catalyst

The catalyst was prepared by adding titanium tetrachloride to the magnesium chloride particles. The apparatus shown in Figure 35 was used for the titanium addition process. The catalyst preparation procedure consisted of the following steps:

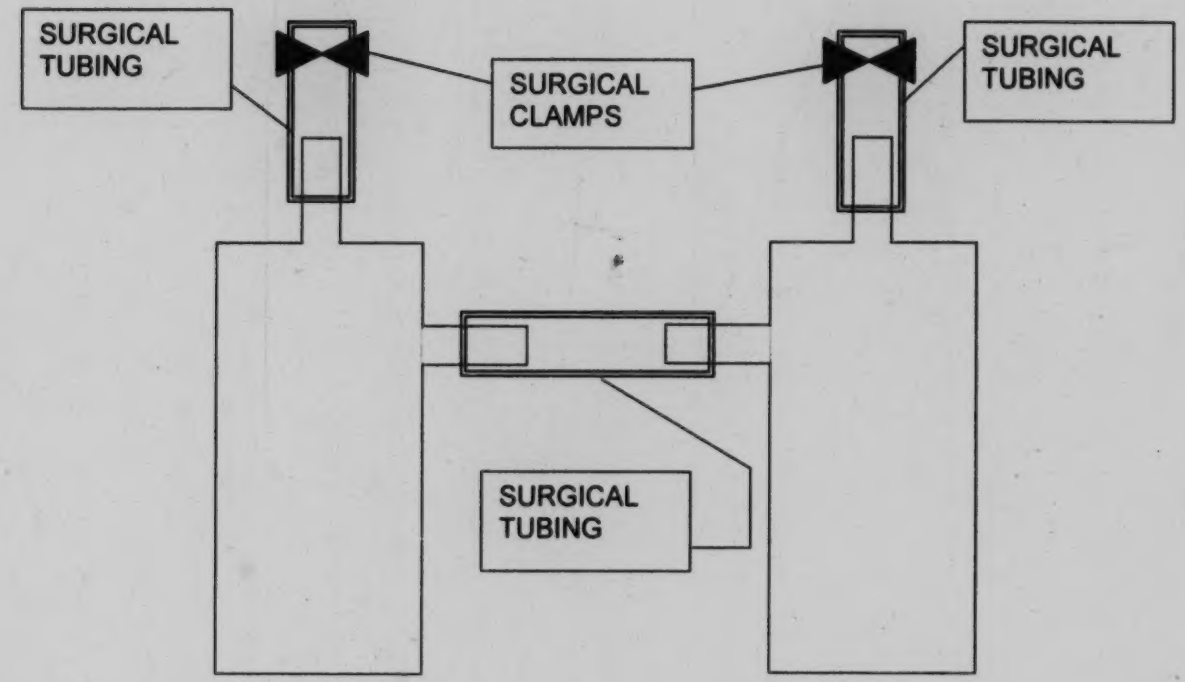

Figure 34. Schematic diagram of the support collection bottles.

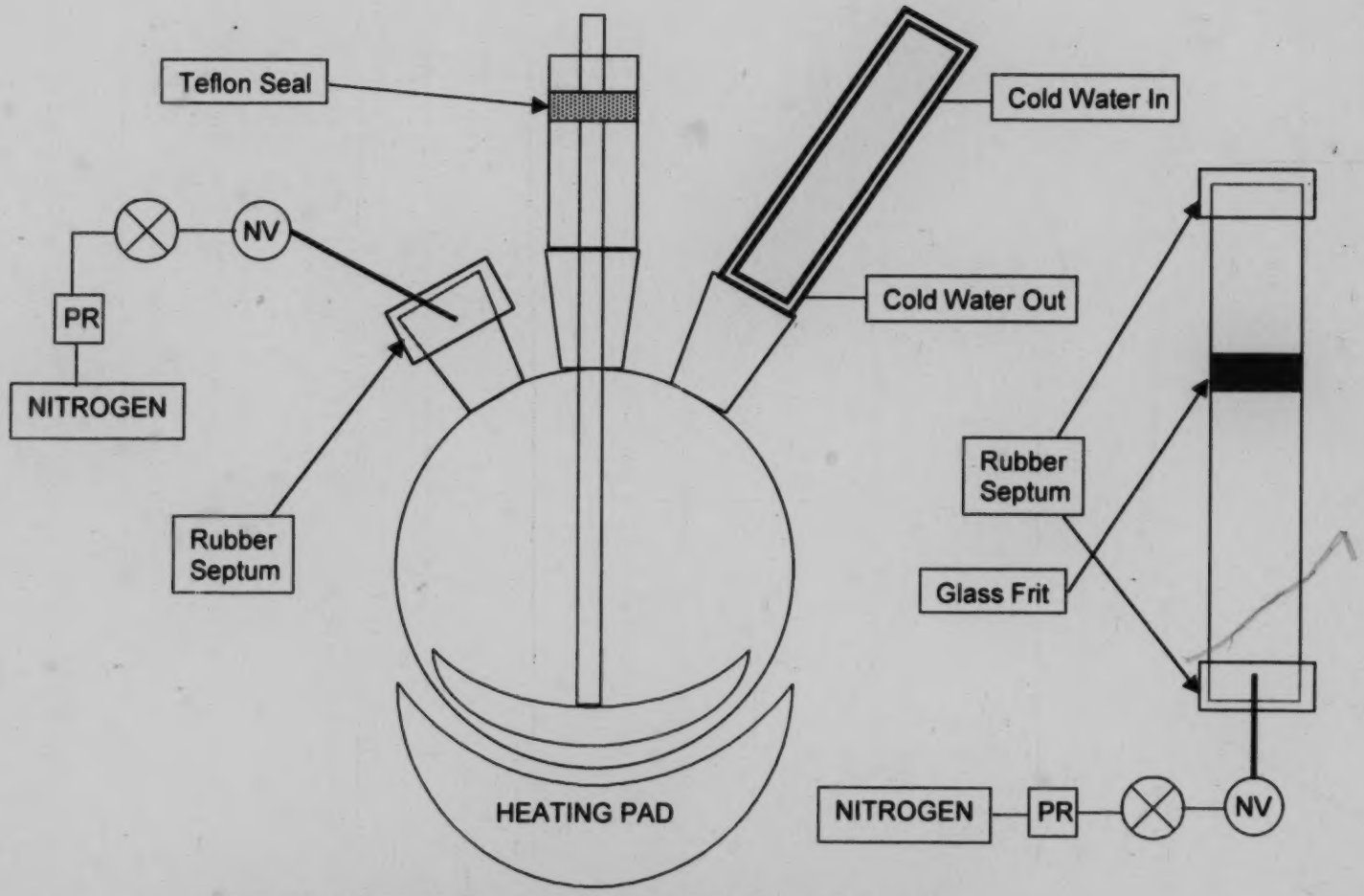

Figure 35. Schematic diagram of the catalyst preparation equipment.

1. Magnesium chloride powder was weighed and placed in a three neck flask. Heptane was added as a solvent. An excess amount of $TiCl_4$ was added to the flask. The flask was sealed and removed from the glove box. Great care must be taken when handling $TiCl_4$ as it reacts violently with air and water.
2. Under a nitrogen purge the contents of the flask were stirred at slow speed and heated to the boiling point of the heptane. A reflux tube was used to reduce solvent losses. The mixture was boiled for one hour.
3. After one hour the magnesium chloride particles were washed three times with a total of 185 mL of heptane. For each wash cycle the solvent was heated to the boil and the particles were stirred for 20 minutes.
4. After the final washing the particles were transferred to a filter and were dried to a free flowing powder using nitrogen. The filter was then placed into the glove box transfer chamber and evacuated overnight.

The catalysts produced were then used in a slurry phase reactor to measure the activity of the catalyst.

8.3 - Ethylene polymerization

A schematic diagram of the reactor used for the polymerization experiments is shown in Figure 36. The description of this equipment has been published previously (Lynch and Wanke, 1991). Polymerizations were conducted in the slurry phase because reproducibility of slurry operation is better than gas-phase operation. The slurry operation followed the following procedure:

1. The reactor was evacuated overnight while immersed in the oil bath at 90°C. The reactor was then pressurized and purged with nitrogen. Heptane (300 mL) was added to the reactor.
2. In the glove box, 2 mL of triethyl aluminum alkyl (TEAL) were drawn into a syringe. The tip was plugged with a rubber septum. The catalyst was suspended in 7 mL of heptane in another syringe.
3. The TEAL was injected into the reactor and the reactor was stirred for 5 minutes. The TEAL acts as a scavenger for residual oxygen and water as well as being the co-catalyst for the supported Ti catalyst. A small amount of ethylene was introduced into the reactor. The catalyst was then injected into the reactor.

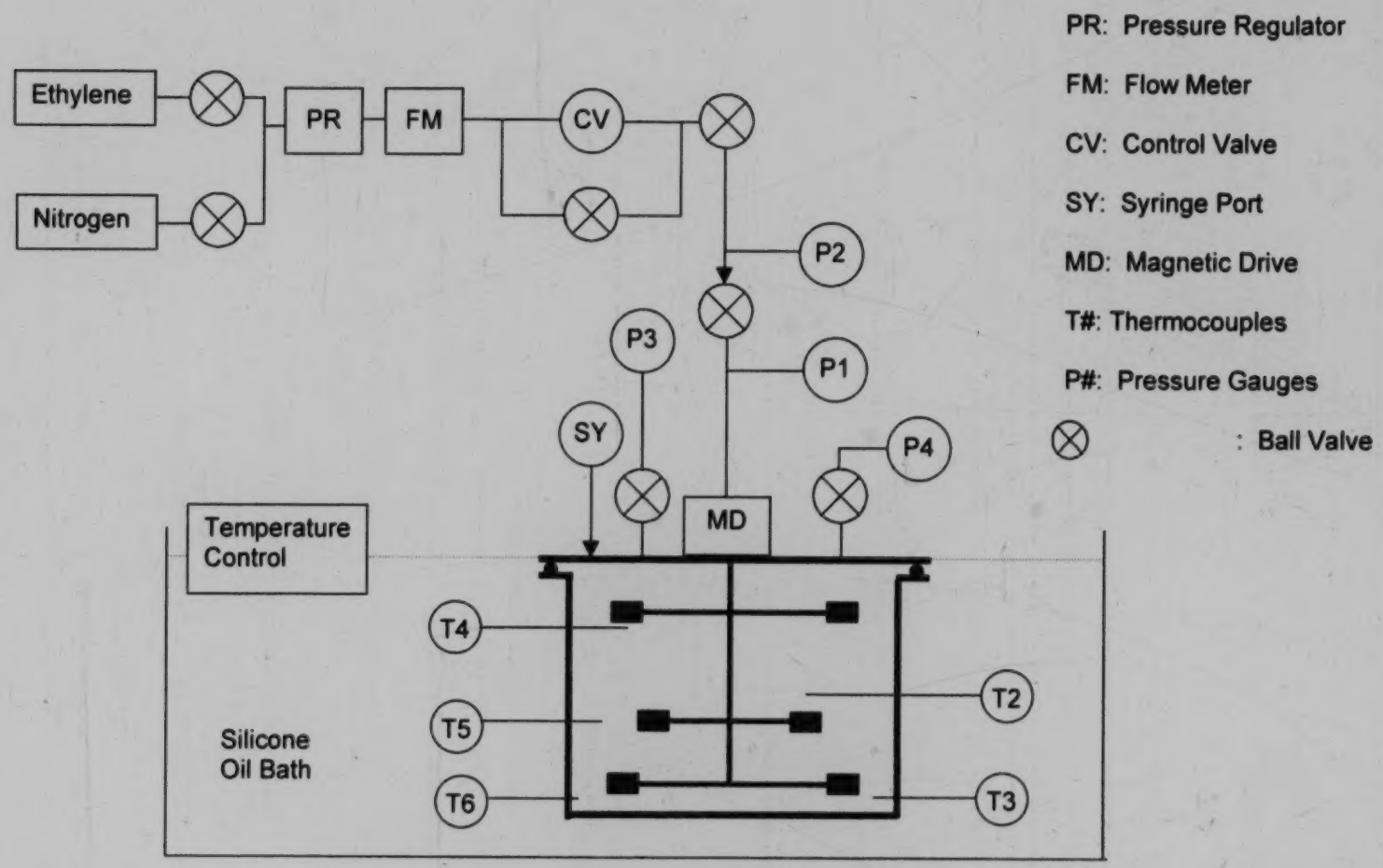

Figure 36. Schematic diagram of the stainless steel reactor.

4. The reactor was slowly pressurized to the final pressure and maintained at this pressure for the duration of the reaction. The ethylene flow was measured and recorded on the computer at 10 s intervals. The bath temperature was changed to try and maintain a constant reactor temperature.
5. After several hours the ethylene flow was stopped and the reactor gas-phase was vented from the reactor to the fume hood.
6. The reactor was cooled and the polymer and solvent removed. Most of the solvent was decanted and the remainder was evaporated in the fume hood.

8.4 - Scanning Electron Microscopy (SEM)

SEM was used to examine the catalyst support particles as well as polymer particles produced. Magnesium chloride is highly hygroscopic and precautions were taken to limit the particle exposure to air and moisture. SEM posts were prepared in the glove box and then sealed in a plastic container. The container top was then wrapped with parafilm to provide a seal. The posts were then quickly transferred to the carbon coating machine. This machine operates in a vacuum. Once the layer of carbon was applied, the sample was transferred to the SEM chamber that was also under vacuum. In total the sample is exposed to the atmosphere for less than 1 minute. The SEM pictures

show the shape of the particles formed and the distribution of sizes produced during the reaction. Other methods were used to characterize the support particles and the catalyst particles formed from the support.

8.5 - BET Measurements

The surface areas of the support particles and catalyst particles were measured using the BET technique. Static in the glove box interfered with accurate weighing of the samples used for BET measurements. The samples were prepared in the following way:

1. Approximately 300 mg of sample was placed in the BET sample holder within the glove box.
2. Two plugs of quartz wool were place in the neck of the sample holder. A second plug was used due to the large amount of particles sticking to the walls of the sample holder. The valve was put on the sample holder and the valve was closed. The BET sample holder assembly was removed from the glove box.
3. The mass of the assembly was measured and then the sample was evacuated at 100°C. The BET measurement was then performed and the final mass of the assembly was measured. The sample was then evacuated at 300°C, and another BET measurement was performed. The final mass of the assembly was measured.

4. After the final BET measurement the assembly was taken apart and each component was weighed separately. The mass of the sample was determined from the measured weights.

The evacuation was performed at the low temperature of 100°C to avoid decomposition of the sample. When the support samples were evacuated at 300°C they turned brown from the original white. However, the surface areas from the two measurements were not significantly different.

8.6 - X-ray diffraction

X-ray diffraction was performed on the support particles to examine the crystal structure of the magnesium chloride. A Philips x-ray diffractometer equipped with a Cu tube and a graphite monochrometer was used to obtain x-ray patterns. The diffractometer was operated in the step scan mode and data were recorded with an online PC.

Special precautions had to be taken for determining the x-ray diffraction pattern because magnesium chloride is hydrophilic. Figure 37 shows the x-ray diffraction sample holder designed for use in the Philips x-ray diffractometer. The sample holder was machined from two pieces of stainless steel bar stock in the machine shop of the Department of Chemical and Materials Engineering. The cover piece had a window removed that covered angles 0° to 180° with a width of 20.6 mm. This window was covered with one layer of 25 μm thick Dupont Kapton 100 HN polyimide film. The Kapton 100 HN was attached to the

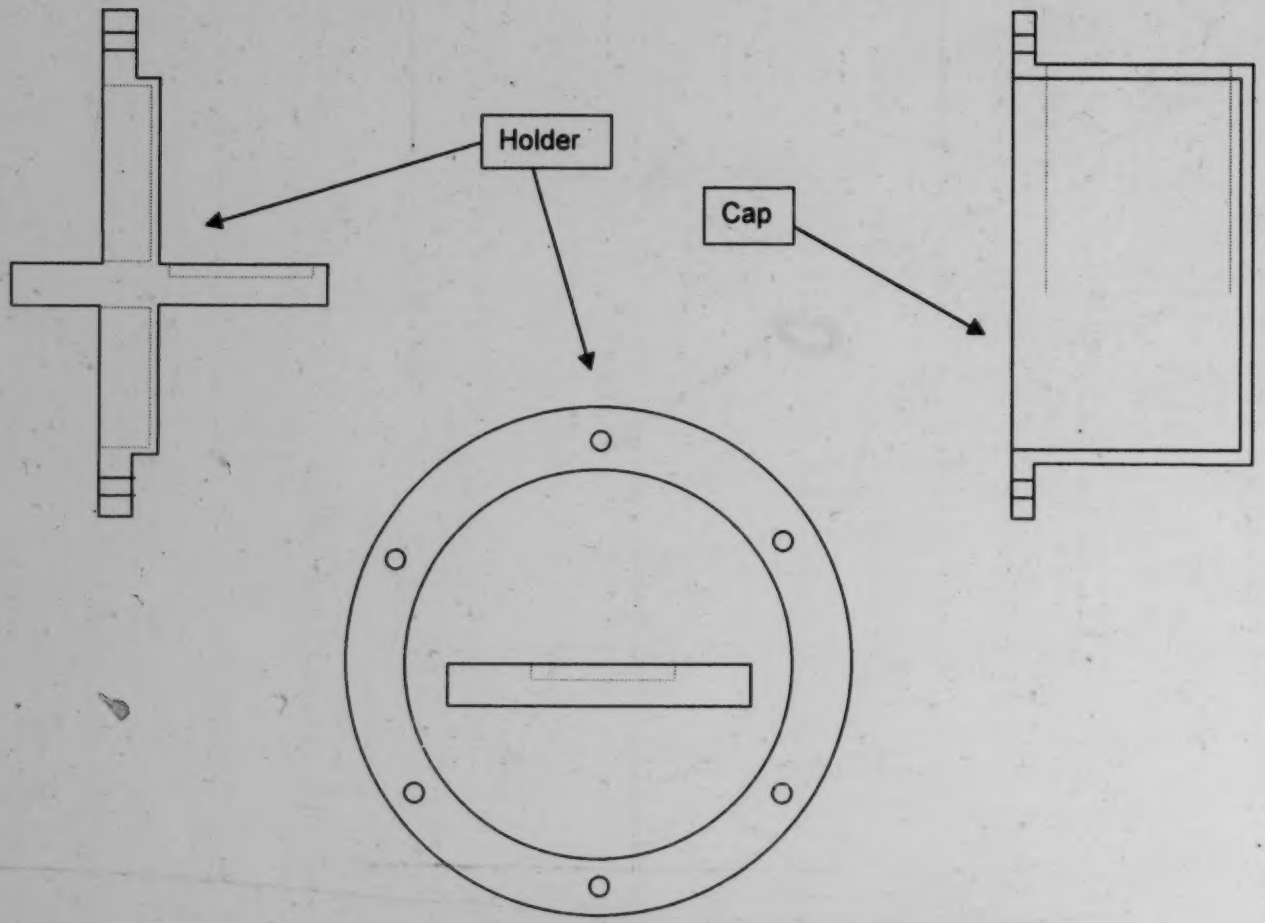

Figure 37. Schematic diagram of air tight XRD sample holder.

cover piece with Crazy glue to ensure an air tight seal. The polyimide film is away from the surface and did not introduce any new lines in the x-ray pattern; however, the film did reduce the signal strength. After the sample holder was made an article by Marigo et al. (1982) was found showing the design of a sample holder very similar to the one described above. The article is in Italian so it is not known the exact makeup of the holder but the figures show the similarities.

For each sample fast and slow scans were performed. The signal to noise ratio for the fast scan was lower than for the slow scan. However, the line shapes of the slow and fast scan were the same. The fast and slow scans were performed to ensure that no significant contamination occurred during the slow scan. Prior x-ray diffraction runs, without the current sample holder, showed that major shape changes in the XRD patterns of the $MgCl_2$ occurred during exposure of the sample to air.

The following procedure was used in the preparation and execution of x-ray diffraction runs on the $MgCl_2$ supports:

1. In the glove box, the support particles were placed into the recess in the sample holder. The powder was packed into the holder using a piece of 1 by ¼ inch aluminum flat bar. More particles were added and flattened until the holder was full and a flat smooth surface was formed.

2. Stopcock grease was spread on the sealing surface of the cover piece. The two pieces were put together and screwed together. The sample holder was then removed from the glove box.
3. The holder was placed in the diffractometer and the slow scan was performed. The slow scan was from 10° to 70° 2θ using a step size of 0.1° 2θ scanning for 20 s per step. The intensity as a function of diffraction angle was recorded using an online computer.
4. Following the slow scan the fast scan was performed. The fast scan was from 10° to 70° 2θ using a step size of 0.1° 2θ scanning for 4 seconds per step.

8.7 - Optical microscope

An optical microscope, Olympus, Model BH-2 equipped with a camera was also used to examine the particle size distribution. A slide for use with the optical microscope was prepared in the following manner inside the glove box:

1. Stopcock grease was spread on a glass slide in a square approximately the size of a cover plate. The grease was spread just around the perimeter to leave the middle free of grease.
2. A small quantity of support particles was placed on the slide. Effort was taken to produce regions where the particles formed a mono-layer of separated particles.

3. A cover slide was then placed on top of the greased slide. The edges of the cover plate were pressed into the grease enough to create a seal but not too much to crush the particles.
4. The particles were examined under the microscope and the images were recorded on videotape.
5. Images were captured using Snappy video capture. The image was then printed and particle outlines were traced onto a transparency.
6. The traced particles were then scanned into another image file. This file was analyzed by image processing software. The software produced the particle area.

9.0 - Results

9.1 - Surface Areas and Shapes of $MgCl_2$ Particles

A true 2^2 factorial designed experiment (Box et al. 1978) was performed to assess the effect of *tert*-butyl chloride addition rate and stirring speed on the particle size and surface area of the support particles. Other properties examined were the crystal structure and activity of the prepared catalysts. The experiment could be viewed as a 2^3 factorial design as experiments were conducted with and without baffles in the reactor. The surface area of the catalyst supports was measured by the BET adsorption method. The surface area measurement for supports RBSP8 through RBSP11 show that the stirring RPM has an effect on surface area and the rate of addition does not have a significant effect. The faster the rate of rotation the higher the surface area. Because replicate runs were not completed it is assumed that the standard error of an effect is the interaction effect. Using this analysis the RPM effect is significant and not a random event. Table 11 compares the reaction conditions with the surface area of the support.

Table 11. Reactor conditions for the catalyst support formation and the BET surface area measurement.

Support	Baffles	Stirring Speed (RPM)	Addition Rate of *tret*-butyl chloride/heptane mixture (mL/h)	BET Surface Area after 100°C evacuation (m^2/g)	BET Surface Area after 300°C evacuation (m^2/g)
RBSP1	NO	500	15	19	19
RBSP2	NO	1000	15	16	24
RBSP3	NO	1000	33	31	53
RBSP4	NO	1500	15	16	37
RBSP5	NO	1000	600	89	65
RBSP8	YES	1000	8	28	29
RBSP9	YES	500	10	22	22
RBSP10	YES	500	30	n/a	22
RBSP11	YES	1000	30	36	29

The results for the reaction with baffles in the reactor show that the surface area of the supports increased with increasing the stirring speed. RBSP 9 and 10 and RBSP 8 and 11 have relatively the same surface area at 300°C while the stirring speed remained constant. However, when examining the experiments conducted using the pitched blade impeller and without baffles the correlation is with reagent addition rate. RBSP2 and RPSP4 were created using the same addition rate and different shaft speed. Their surface areas are similar at 100°C. RBSP2 and RBSP3 were created using the same stirring speed and different reagent addition rate. A complete 2^2 factorial design was not completed for the case without baffles.

The number average particle size was determined for each support by assuming that the particles were spherical. The projected areas measured from the videotape were then used to determine the diameter of a sphere that would

have the same projected area. Table 12 shows the results of the particle size measurements.

Table 12. Support particles mean diameters.

Support Name	Stirring Speed (RPM)	Addition Rate *tert*-butyl chloride/ heptane mixture (mL/h)	Mean Particle Diameter (μm)	Sample Standard Deviation (μm)	Mean A/B ratio
RBSP1	500	15	29.9	4.36	1.31
RBSP2	1000	15	12.4	1.67	1.32
RBSP3	1000	33	14.1	1.85	1.35
RBSP4	1500	15	9.2	1.40	1.30
RBSP8	1000	8	23.3	1.95	1.13
RBSP9	500	10	32.5	3.90	1.21
RBSP10	500	30	13.2	1.30	1.19
RBSP11	1000	30	6.9	0.721	1.18

The 2^2 factorial design experimental results were used to assess the effect of chemical addition and stirring rate on particle size for Supports 8 through 11. The results show that both the stirring rate and the chemical addition rate are significant in determining the particle size. The (RPM x rate) interaction effect is used as the standard deviation of the effects because no replicate runs were completed (Box et al. 1978). The standard error was calculated to be 1.4. The main RPM effect was calculated to be -7.76. The main rate of chemical addition effect was -17.9. Both the RPM effect and the rate effect are significant because each effect value is much greater than the calculated standard error. The results also show that the rate of chemical

addition has a greater effect on particle size than stirring speed. Both effects are inversely proportional to particle size.

The image analysis program measured the major and minor axis projection for each particle. A measure of the particle sphericity is obtained by taking the ratio of the major to minor axis. This assumes that the projected image is representative of the three dimensional solid. The results in the last column of Table 12 show that the reactor with the baffles in place produces particles that were closer to being spherical than in the case in which no baffles were used (compare ratios for RBSP8 to –11 with those for RBSP1 to –4). For the last four experiments the factorial design was used to determine the effect of RPM and *tert*-butyl chloride addition rate on the regularity of the particles. Again it is assumed that the interaction effect is negligible and is a measure of the standard error. This analysis determines the standard error to be 0.037. The main RPM effect is -0.041 and the main chemical addition rate effect is -0.013. The variables are shown not have an effect on the regularity of the formed particles because the value of the effects are the same as or less than the standard error. However, the type of stirring impeller and the use of baffles does have a significant affect on the sphericity of the particles.

9.2 - XRD Results

The x-ray diffraction (XRD) results for the eight catalyst supports show that they have three different crystal structures. The XRD lines for anhydrous

$MgCl_2$ was obtained from the XRD powder database (File 37-0774). The index shows there are 14 possible reflections between 10°2θ and 70°2θ. The strong lines for ordered $MgCl_2$ are at 15.030°2θ, 30.331°2θ, 34.921°2θ, 45.991°2θ, 50.401°2θ, 52.581°2θ, 59.682°2θ, 62.492°2θ and 63.012°2θ. The supports RBSP2 through RBSP5, shown in Figure 38, had similar XRD profiles. The peak at 15°2θ is present but does not have a strong intensity. There is also a fair amount of peak broadening. The two peaks at 30°2θ and 35°2θ show an almost complete merger. The peak at 50°2θ has a high intensity and a fairly narrow peak compared to the other peaks. Samples RBSP2 through RBSP5 show the same basic crystal structure even though the addition rate and the stirrer rates were varied.

Supports RBSP8 through RBSP11, shown in Figure 39, had two different structures. For RBSP8 and RBSP9 the peak at 15°2θ was 3 to 8 times as intense as in the first 4 runs. The peaks at 30°2θ and 34°2θ were separate and distinct with a slightly higher intensity. The peak at 50°2θ again had a high intensity and a fairly narrow width. For these supports the 50°2θ peak width is similar to the other peaks in the profile. The XRD patterns for RBSP8 and RBSP9 have some additional features, i.e. the lines at 28°2θ and 52°2θ are shoulders of the neighboring peak. As well, peaks at 59°2θ and 62°2θ are seen as separate peaks. The x-ray diffraction patterns of these samples show that they had a high degree of order; i.e. the diffraction lines are relatively narrow and of high intensity.

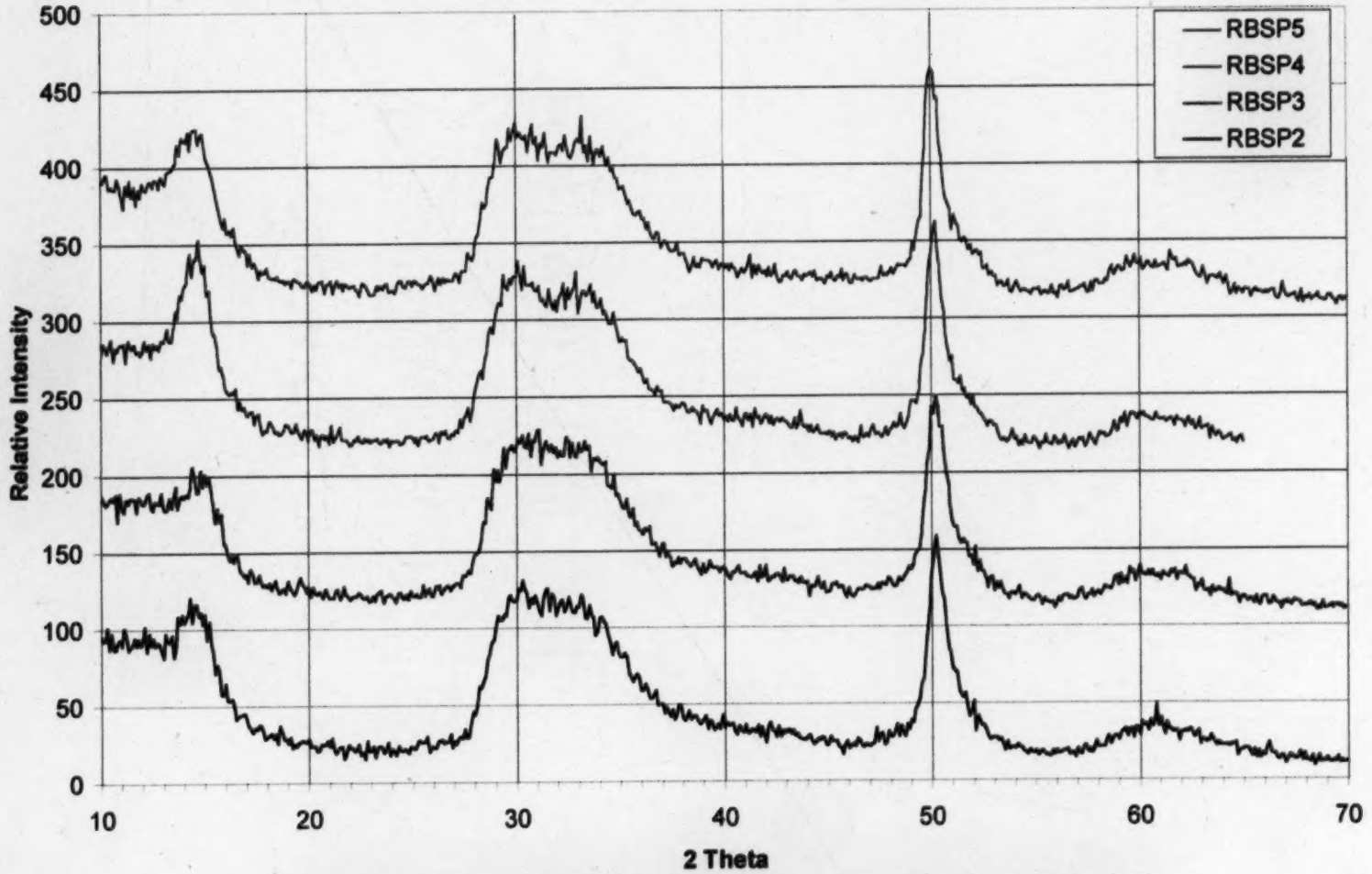

Figure 38. X-ray diffraction patterns for supports RBSP2 through RBSP5.

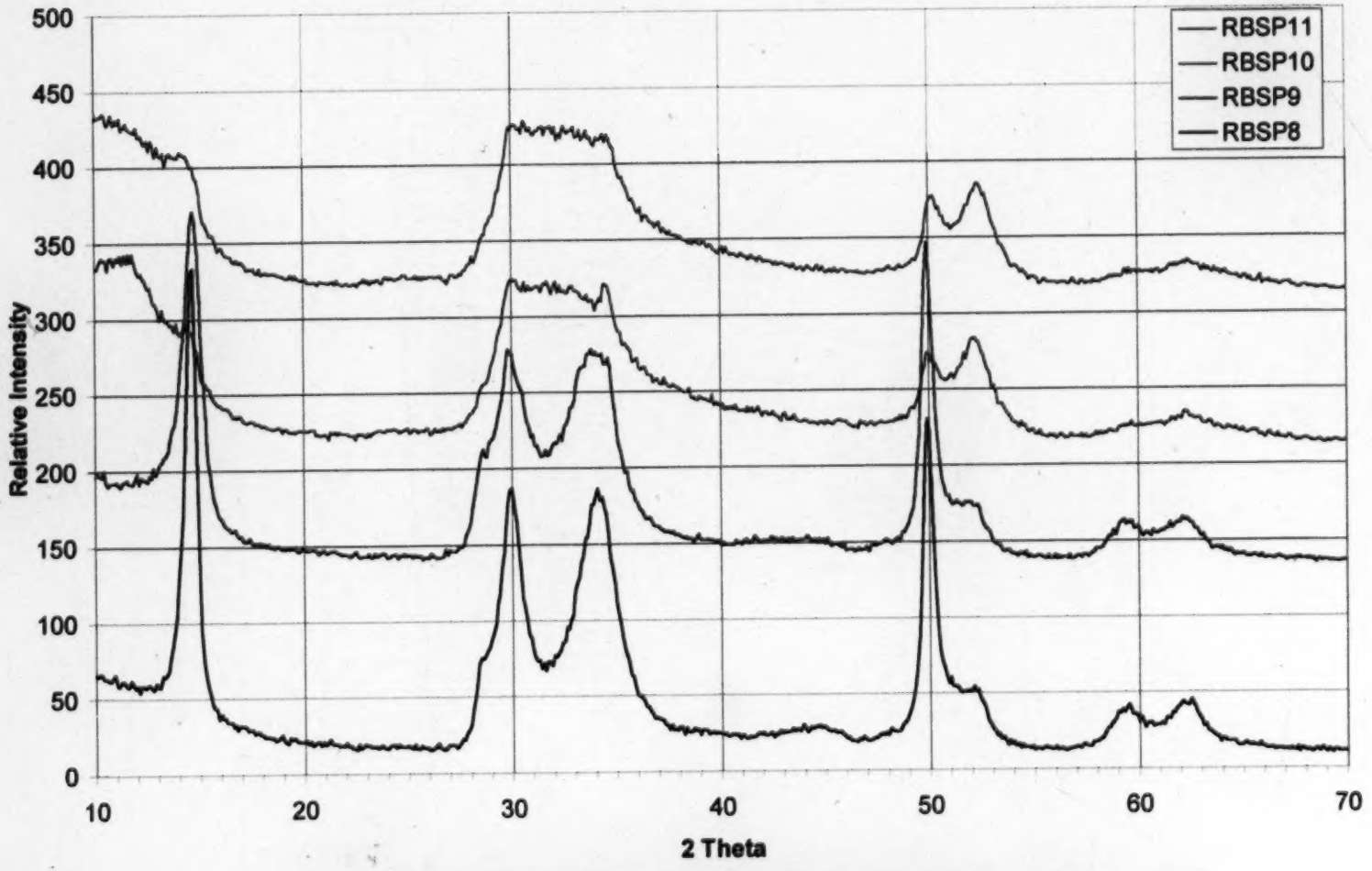

Figure 39. X-ray diffraction patterns for supports RBSP8 through RBSP11.

RBSP10 and RBSP11 showed the third crystal structure. This x-ray diffraction pattern shows a remarkably different structure from the first two. For these supports the peak at 15°2θ was either non-existent or had broadened greatly and shifted to a lower 2θ position. The intensities of the 15°2θ line were much less than that of the previous two structures. The broad band covering 30°2θ and 34°2θ is similar to the first structure in both shape and intensity. The most remarkable change is for the 50°2θ line. The intensity of this line is less than a quarter of the previous two structures. Also occurring is the gain in intensity of the 52.5°2θ reflection. A comparison of the XRD patterns for the three structures is shown in Figure 40; a pattern for crystalline anhydrous $MgCl_2$ is also included.

Giunchi and Allegra (1984) studied the disorder produced in crystalline $MgCl_2$ by ball milling by examining XRD patterns. They developed a procedure which allowed the description of XRD patterns for $MgCl_2$ by four parameters; they state that "the diffracting system is fully specified by the four independent parameters" (Giunchi and Allegra, 1984). Two parameters are related to size of the crystalline domain and the other two with the "monodimensional disorder produced by different interlayer shifts" (Giunchi and Allegra, 1984). They actually used three disorder parameters, i.e. p_{cub} the probability of a cubic-like shift between two adjacent layers, p_{hex} the probability of a hexagonal-like shift between layers and p_{rot} the probability of two layers mutually rotated 60°. The three disorder parameters are not linearly independent since the sum of the three must equal unity. Guinchi and Allegra (1984) used these parameters to

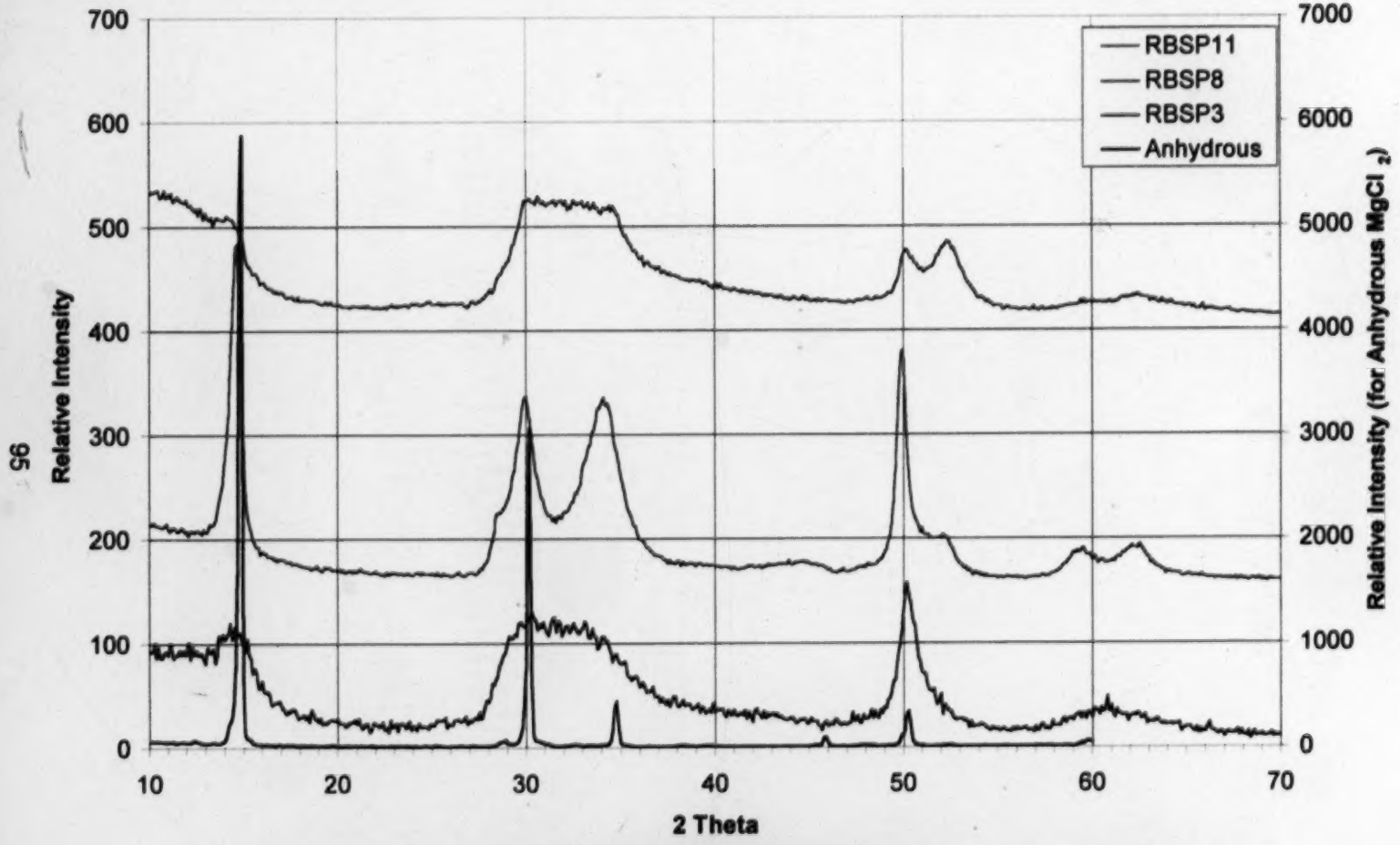

Figure 40. Comparison of the X-ray diffraction patterns of the catalyst supports with anhydrous magnesium chloride.

describe the structural changes caused by ball milling $MgCl_2$. Their results show that as the disorder of the $MgCl_2$ increased, the value of p_{rot} increased. Values of "p_{cub}=p_{hex}=0.25, p_{rot}=0.5 correspond to the hypothetical completely random model." Using the procedures described by Guinchi and Allegra (1984) the XRD patterns shown in Figures 38 and 39 were analyzed. To improve the resolution of the 15°2θ peak the background was removed. The equation of the background was obtained from the XRD pattern of the sample holder without any sample. A least squares regression obtained the following equation.

$$z = -7.53\times10^{-7}x^5 + 1.86\times10^{-4}x^4 - 1.81\times10^{-2}x^3 + 8.63\times10^{-1}x^2 - 2.05\times10^{1}x + 205 \quad (20)$$

where z is the intensity of the diffracted x-rays and x is the diffraction angle in °2θ . After Equation 20 was subtracted from the XRD patterns of Figures 38 and 39 the width at half height was measured for the peaks at 15°2θ and 50°2θ. From these peak widths two parameters, α and γ, were obtained according to the method described by Guinchi and Allegra (1984). Using the following equations the average lengths of the crystal domain were obtained (Giunchi and Allegra, 1984).

$$\langle L_{av} \rangle = \frac{a}{\alpha} \quad (21)$$

$$\langle L_{cv} \rangle = \frac{2c}{\gamma} \quad (22)$$

Where a is the width of the ideal close packed hexagonal crystal unit cell and c is distance between layers.

The disorder parameters, described by Guinchi and Allegra (1984), could not be calculated from the patterns in Figures 38 and 39 because the 30°2θ and 34°2θ lines were not well resolved. The method presented by Guinchi and Allegra (1984) does not lend itself to cases where these two lines are not resolved. However, the shape of the broad band covering 30°2θ to 34°2θ can be used to qualitatively describe the degree of disorder. The α and γ parameters, and the calculated crystalline dimensions calculated from these parameters (Equations 21 and 22), and the qualitative disorder for the $MgCl_2$ samples are listed in Table 13.

Table 13. Catalyst support crystal structure parameters.

Support Name	γ	α	$\langle L_{a'} \rangle$ (Å)	$\langle L_{c'} \rangle$ (Å)	Level of Disorder
RBSP2	0.44	0.049	74	27	high
RBSP3	0.30	0.047	78	39	high
RBSP4	0.34	0.044	83	35	high
RBSP5	0.37	0.041	88	32	high
RBSP8	0.10	0.026	141	117	low
RBSP9	0.17	0.028	128	70	low
RBSP10	0.30	0.080	45	39	very high
RBSP11	0.37	0.075	49	32	very high

Some general observations can be made from the results shown in Table 13. The XRD patterns for RBSP2, -3, -4 and -5 were all similar (see Figure 38), and hence the crystal sizes are also similar. For these XRD patterns the level of disorder was rated as high because the 30°2θ and 34°2θ lines are not resolved. RBSP8 and -9 have similar XRD patterns as shown in Figure 39. Table 13

shows that the crystal size is very much larger than RBSP2 through –5. As shown in Figure 39 there is good separation of the 30°2θ and 34°2θ peaks and so the disorder is rated as low. For RBSP10 and –11 the disorder is rated as very high because the band between 30°2θ and 34°2θ is even less resolved that was the case for RBSP2 to –5. The crystal size is also smaller that that of RBSP2 through –5.

The XRD patterns show that three distinct crystal structures were formed as a result of the different preparation methods. The results for RBSP2 to RBSP5 show that the crystal structure did not change significantly with changes in process conditions in the absence of baffles in the reactor. However, changes in crystal structure did occur for samples RBSP8 to RBSP11. For those supports baffles had been added to the reactor to improve mixing. The impeller had also been changed from a pitched blade impeller to a Rushton turbine impeller to induce more turbulent mixing. These changes in reactor geometry and mixing intensity resulted in changes in the degree of order in the crystal structure with changes in the rate of reactant addition. The change in shaft rotation speed did not have a perceived effect on the degree of order in the structure.

Crystal structure appears to be a function of the turbulent eddies induced by the impeller and the chemical addition rate. The chemical addition rate only changes the crystal structure when there is a sufficiently high level of turbulence. This interaction of stirring and reactant addition rate could be the result of the size turbulent eddy formation and the dissipation rate to larger eddies. A

possible speculation is that each turbulent eddy created by the impeller acts as a reactor cell. The turbulence facilitates the bringing together of reactants. At the higher addition rate the $MgCl_2$ layers formed do not align themselves with as much order as at the lower reaction rate. This hypothesis may be plausible for RBSP8 though RBSP11 but does not account for the fact that with addition rate change for RBSP2 through RBSP5 there is no perceivable change in the crystal structure.

The reactor geometry, i.e. the addition of baffles, had a pronounced effect on crystal structure. The hypothesis does not explain why increasing the impeller speed does not affect crystal structure. With the higher impeller speed there is more energy entering the reactor. This higher energy should produce more turbulence, and according the above hypothesis this should result in a more disordered structure. Hence, additional experimentation is required to determine the reasons why reactor geometry influences the crystal structure of $MgCl_2$ made by precipitation.

9.3 - Polymerization Results

Four of the catalyst supports were used to prepare $TiCl_4$ on $MgCl_2$ catalyst. $TiCl_4$ was added to the catalyst support as described in Section 8.2. The Ti contents of the catalysts were measured by Mrs. Bu using cplorimetric titration analysis (Vogel, 1961). In Table 14 the Ti contents and average polymerization activities of these catalysts are tabulated.

Table 14. Measured Titanium content and catalyst activity.

Support Name	Catalyst Name	Titanium Content (mass%)	Polymer Name	Average Polymerization Activity $\left(\frac{\text{g polymer}}{\text{mole Ti·kPa·min}}\right)$
RBSP3	RBCT3	0.102	SLROB03	2718
RBSP2	RBCT4	0.118	SLROB04	2491
RBSP11	RBCT5	0.094	SLROB05	5610
RBSP8	RBCT6	0.067	SLROB06	1177

Detailed information about the polymerization conditions and activity profiles are given in Appendix C. The activities as well as the shapes of the activity profiles appear to be a function of the crystal structure. RBCT3 and RBCT4 were from the first set of supports produced and which had similar crystal structures (see Figure 38) had similar activities and similar activity profiles. RBCT3 was made from a support (RBSP3) with a smaller surface area than the support used for RBCT4 (support RBSP2). The difference in surface area could account for the small difference in activity. The support used to make RBCT5 (support RBSP11) had the highest degree of disorder (see Table 13) and RBCT5 had significantly higher activity than the other three catalysts. The RBCT6 catalyst had the lowest activity. The support used to make this catalyst (RBSP8) had the most ordered structure of the four supports used to make catalysts, (see Table 13). This is consistent with experiments using ball milled $MgCl_2$ as the catalyst support (Galli et al., 1983, Gerbasi et al., 1984).

These results show that the activity of the catalyst is more dependent on the crystal structure of the $MgCl_2$ support than on the surface area of the support. The products from all the polymerization runs consisted of fine powders, i.e. replication of catalyst particle shape into polymer particle shape did not occur. This could be due to two factors; the support particles may have disintegrated when the $TiCl_4$ was added or the initial activity of the catalyst was high enough to fragment the catalyst into separate particles during polymerization. To prevent the catalyst breakup during polymerization, a pre-polymerization step should be carried out before the polymerization (Wu, et al., 1999). The disintegration of the particles during polymerization is the more probable cause for the lack of particle replication because the SEM results presented below indicate that most of the catalyst particles were intact after the addition of the $TiCl_4$.

9.4 - Scanning Electron Microscopy Results

SEM was used to determine if there was any correlation between the reactor conditions and the surface features of the particles formed. SEM was also used to compare the support particles with the catalyst particles to determine if changes in particle morphology occurred due to the treatment with $TiCl_4$. The SEM results are summarized in Table 15, and the micrographs are shown in Figures 41 through 64.

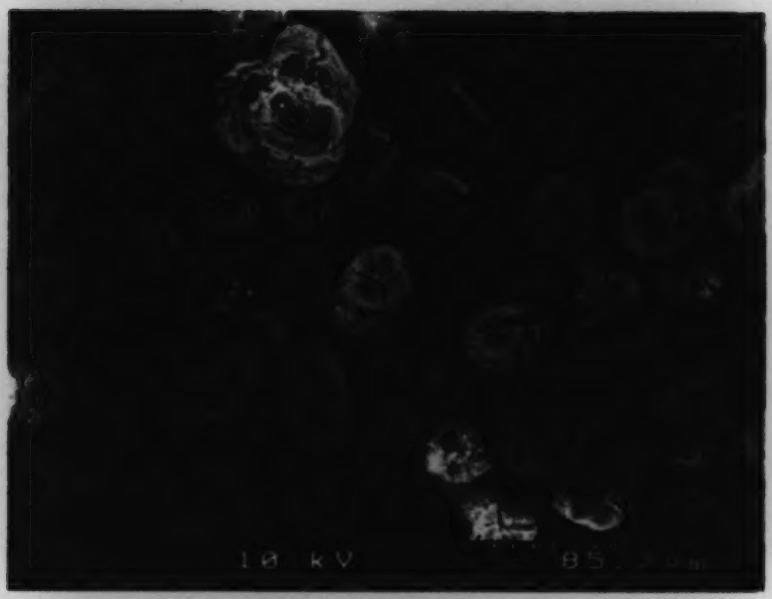

Figure 41. SEM picture of $MgCl_2$ support RBSP1.
(85.7 μm ———————)

Figure 42. SEM picture of $MgCl_2$ support RBSP1.
(15 μm ———————)

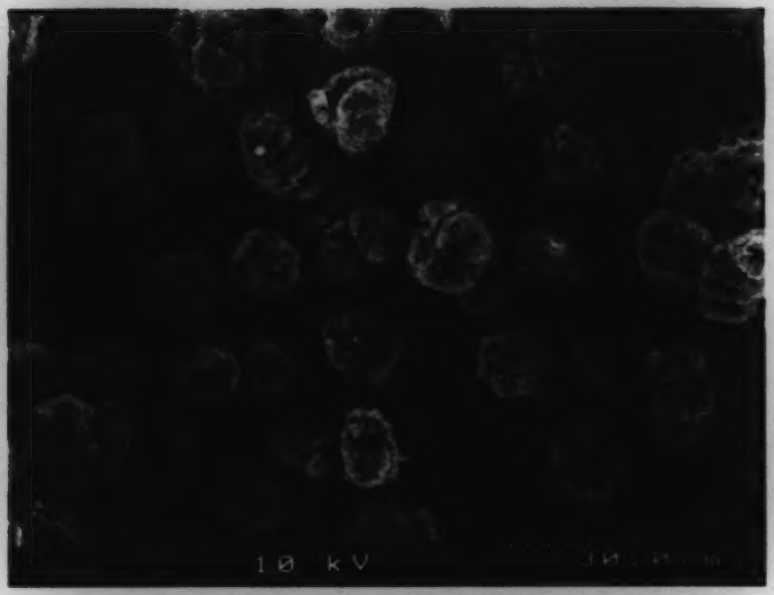

Figure 43. SEM picture of $MgCl_2$ support RBSP2.
(30.0 μm ——————)

Figure 44. SEM picture of $MgCl_2$ support RBSP2.
(3.00 μm ——————)

Figure 45. SEM picture of $MgCl_2$ support RBSP3.
(20.0 μm ——————)

Figure 46. SEM picture of $MgCl_2$ support RBSP3.
(3.00 μm ——————)

Figure 47. SEM picture of $MgCl_2$ support RBSP4.
(20.0 μm ——————)

Figure 48. SEM picture of $MgCl_2$ support RBSP4.
(3.00 μm ——————)

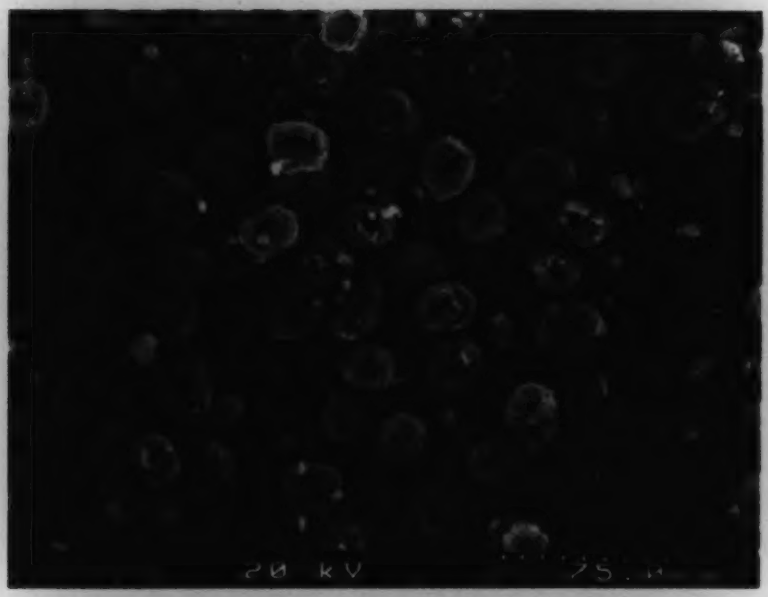

Figure 49. SEM picture of $MgCl_2$ support RBSP8.
(75.0 μm——————)

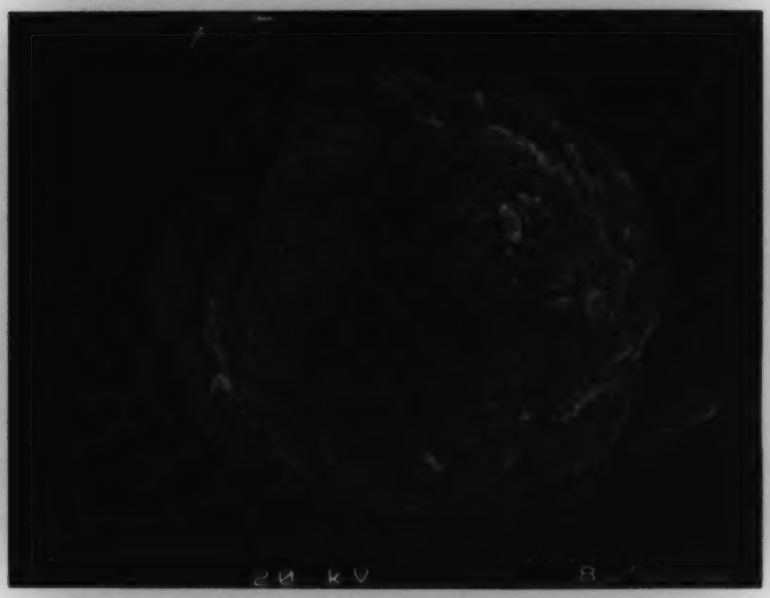

Figure 50. SEM picture of $MgCl_2$ support RBSP8.
(8.57 μm——————)

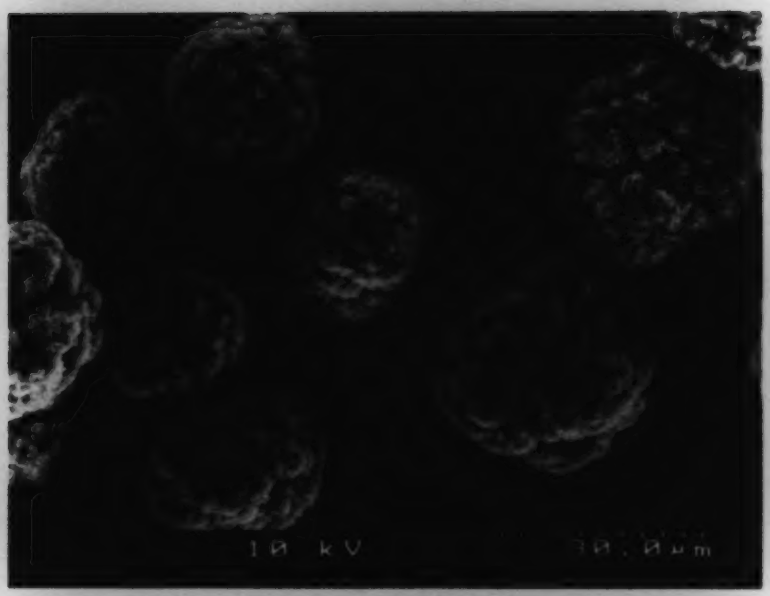

Figure 51. SEM picture of $MgCl_2$ support RBSP9.
(30.0 μm——————)

Figure 52. SEM picture of $MgCl_2$ support RBSP9.
(6.00 μm——————)

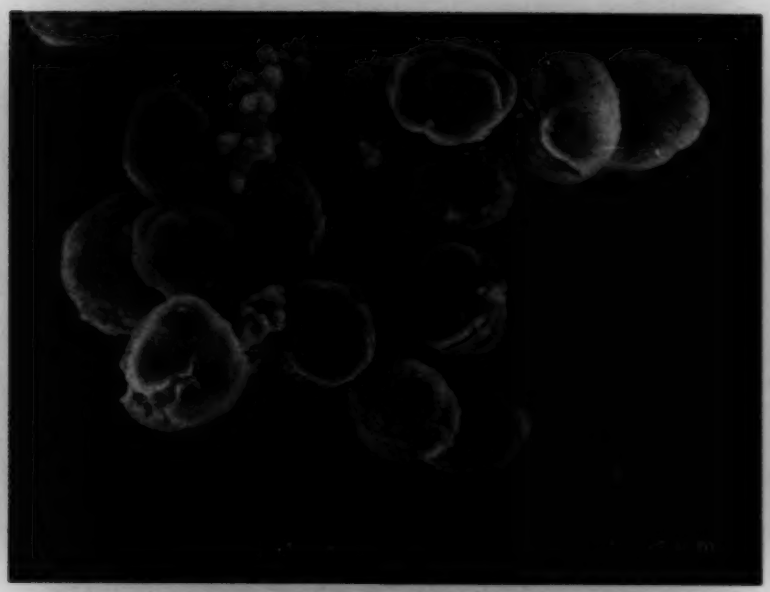

Figure 53. SEM picture of $MgCl_2$ support RBSP10.
(20.0 μm——————)

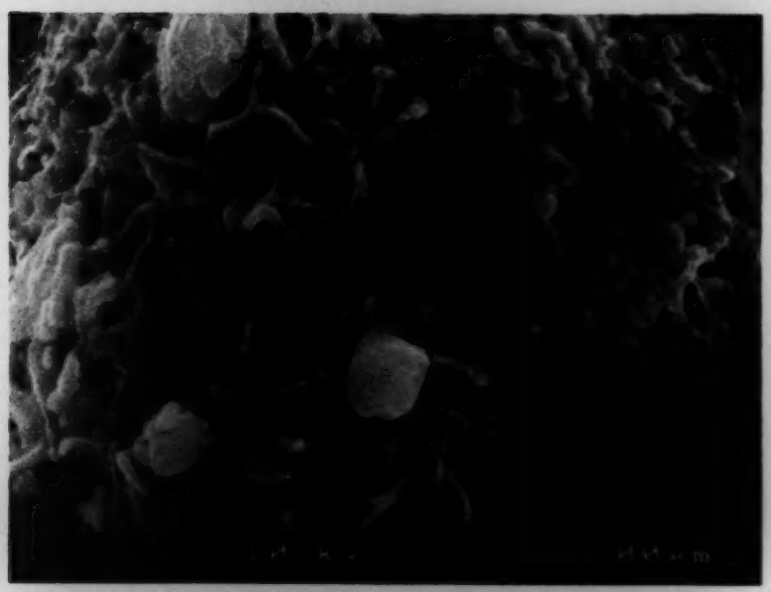

Figure 54. SEM picture of $MgCl_2$ support RBSP10.
(3.00 μm——————)

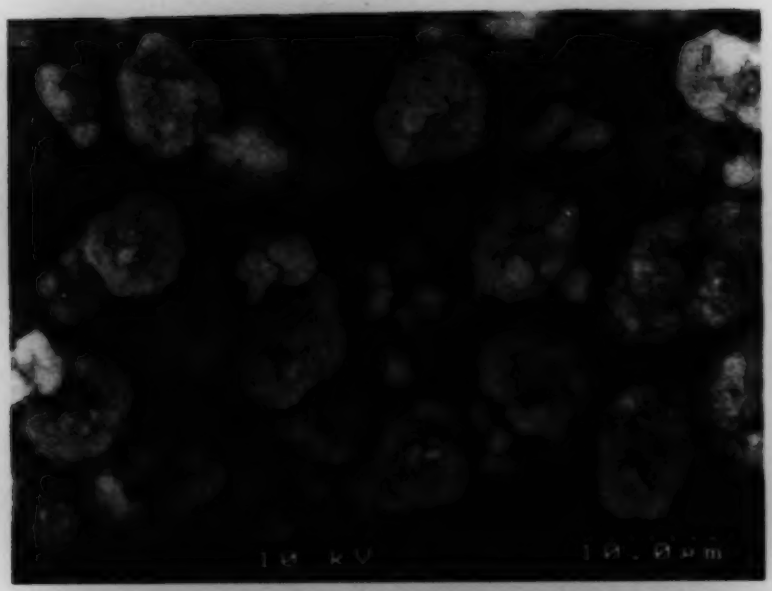

Figure 55. SEM picture of $MgCl_2$ support RBSP11.
(10.0 μm——————)

Figure 56. SEM picture of $MgCl_2$ support RBSP11.
(3.00 μm——————)

Figure 57. SEM picture of the catalyst RBCT3.
(20.0 μm ——————)

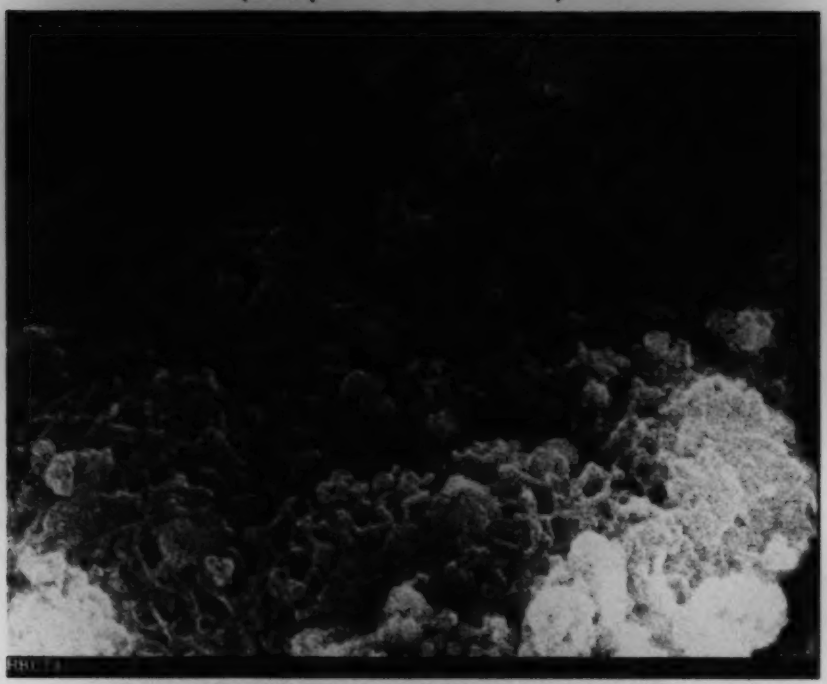

Figure 58. SEM picture of the catalyst RBCT3.
(3.00 μm——————)

Figure 59. SEM picture of the catalyst RBCT4.
(30.0 μm——————)

Figure 60. SEM picture of the catalyst RBCT4.
(3.00 μm——————)

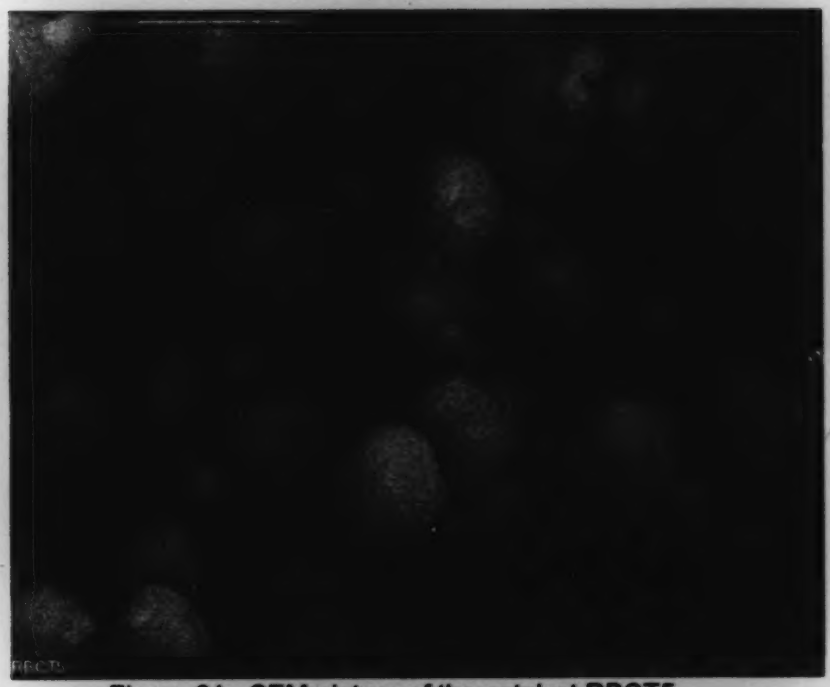

Figure 61. SEM picture of the catalyst RBCT5.
(10.0 μm——————)

Figure 62. SEM picture of the catalyst RBCT5.
(3.00 μm——————)

Figure 63. SEM picture of the catalyst RBCT6.
(75.0 μm————————)

Figure 64. SEM picture of the catalyst RBCT6.
(8.57 μm————————)

Table 15. Summary of SEM results.

Sample	Figures	Comments on Surface Structure	Comments on Surface Hydration
RBSP1	41 & 42	large cracks and pores	no major hydration apparent
RBSP2	43 & 44	no large visible pores	hydration apparent by agglomerated surface
RBSP3	45 & 46	agglomerates are larger than RBSP2; no large visible pores	hydration apparent by large agglomeration at surface
RBSP4	47 & 48	large visible pores; similar to RBSP1	some hydration
RBSP8	49 & 50	large visible pores; some particle fragmentation	no significant hydration
RBSP9	51 & 52	open structure; highly complex surface features	no hydration present
RBSP10	53 & 54	agglomeration of large particles; large pores on some particles none on others	some hydration effects present
RBSP11	55 & 56	irregular particle shapes; few surface features visible	some hydration
RBCT3	57 & 58	made from RBSP3; large pores present; different than support	no significant hydration
RBCT4	59 & 60	made form RBSP2; large pores similar to support	no significant hydration
RBCT5	61 & 62	made from RBSP11; surface features not visible	significant hydration
RBCT6	63 & 64	made from RBSP8; large pores similar to support; some particle fragmentation	some hydration

Direct comparison of the catalyst structure with the structure of the support from which the catalyst was made is difficult due to the hydration of the surface. A direct comparison of the supports is also made difficult due to the surface hydration. In Section 8.4 it was assumed that the exposure time was minimal but

the preceding figures show the extent of the hydration damage. From the comparison of RBCT6 with RBSP8 and RBCT4 with RBSP2 it appears that the $TiCl_4$ treatment does not significantly change the macroscopic structure of the particles. The SEM micrographs show features of the particles which are 0.1 μm (100 nm) or greater; this is significantly larger than the crystal size of about 10nm (100 Å) or less (see Table 13).

10.0 – Summary and Conclusions

Highly active catalysts were produced with $MgCl_2$ supports prepared by a precipitation reaction, and the support crystal structure, which was found to have a significant influence on the catalyst activity, was affected by the reactor geometry (baffles) and the reaction conditions (rate of addition of reagents). Powder X-ray diffraction, using a specially constructed specimen holder to avoid hydration of the $MgCl_2$, was found to be an excellent tool for investigating the disorder of the $MgCl_2$ structure.

This study showed that the following conditions needed to be used to produce a support by precipitation that can be used to prepare a highly active catalyst:

1. The reactor needs to have baffles to prevent free body rotation of the fluid in the reactor.
2. The addition rate of *tert*-butyl chloride to the reactor should be at least 30 mL/h.

The activity of the catalysts produced did not appear to depend on the stirring speed used in the preparation of the support, but the size of the support particles produced was a function of the stirring speed.

The following work should be completed to validate the conclusions of this section:

1. Replicate runs for the preparation of the supports need to be done to obtain the standard errors for the factorial design.

2. A prepolymerization step should be included prior to the polymerization experiments in order to determine whether the supports produced by precipitation do result in catalysts which can yield good replication, i.e. morphology control of the produced polymer particles.
3. Replicate SEM pictures need to be taken to determine the effect of exposure time on the surface structures observed by SEM. From this information, new methods of handling SEM specimens may need to be developed.
4. An improved method, possibly involving fitting of XRD profiles, should be used for determining the disorder and size parameters since the current method yields parameter values with a high uncertainty.

11.0 – References

Borrajo, J., C. Cordon, J. M. Carella, S. Toso, and G. Goizueta, "Modelling the Fractionation Process in TREF Systems: Thermodynamic Simple Approach", *Journal of Polymer Science: Part B: Polymer Physics*, **33**, 1627-1632 (1995).

Box, G. E. P., W. G. Hunter, J. S. Hunter, *Statistics for Experimenters: An Introduction to Design, Data Analysis, and Model Building*, John Wiley & Sons, New York, 1978, Chapter 10.

Chakravarty, Jayant, *Characterization of Polyolefins by Temperature Rising Elution Fractionation (TREF)*, M.Sc. thesis, University of Alberta, Edmonton, Alberta, Canada, 1993.

Eliçabe, G., J. Carella, and J. Borrajo, "Modeling the Fractionation Process in TREF Systems. II. Numerical Analysis", *Journal of Polymer Science: Part B: Polymer Physics*, **34**, 527-533 (1996a).

Eliçabe, G., C. Cordon, and J. Carella, "Modeling the Fractionation Process in TREF Systems. III. Model Validation With Low Molecular Weight Homopolymers", *Journal of Polymer Science: Part B: Polymer Physics*, **34**, 1147-1154 (1996b).

Galli, P., P. Barbè. G. Guidetti, R. Zannetti, A. Martorana, A. Marigo, M. Bergozza, and A. Fichera, "The activation of $MgCl_2$-supported Ziegler-Natta catalysts: A structural investigation", *European Polymer Journal*, **19**, 19-24 (1983).

Gerbasi, R., A. Marigo, A. Martorana, R. Zannetti, G. P. Guidetti, and G. Baruzzi, "The activation of $MgCl_2$-supported Ziegler-Natta catalysts – II", *European Polymer Journal*, **20**(10), 967-970 (1984).

Giunchi, G., and G. Allegra, "Structural Disorder in Microcrystalline $MgCl_2$", *Journal of Applied Crystallography*, **17**, 172-178 (1984).

Guidetti, G., R. Zannetti, D. Ajo, A. Marigo, and M. Vadali, "A Crystallographic Study of Disorder in Titanium Trichloride, A Component of Ziegler-Natta Catalysts for Stereospecific Polymerization", *European Polymer Journal*, **16**, 1007-1015 (1980).

Huang, James Chin-Kuang, *Ethylene and 1-Butene Copolymerization: Catalytic Gas-Phase Synthesis and Characterization*, M.Sc. thesis, University of Alberta, Edmonton, Alberta, Canada, 1995.

Huang. J. C. –K., Y. Lacombe, D. T. Lynch, and S. E. Wanke, "Effects of Hydrogen and 1-Butene Concentrations on the Molecular Properties of Polyethylene Produced by Catalytic Gas-Phase Polymerization", *Industrial & Engineering Chemistry Research*, **36**(4), 1136-1143 (1997).

Karoglanian, S. A., I. R. Harrison, "The similarity of compositional distribution information generated by DSC and TREF", *Thermochimica Acta*, **288**, 239-245 (1996).

Kelusky, E. C., C. T. Elston, and R. E. Murry, "Characterizing Polyethylene-Based Blends With Temperature Rising Elution Fractionation (TREF) Techniques", *Polymer Engineering and Science*, **27**(20), 1562-1571 (1987).

Lacombe, Yves, *TREF and SEC Characterization of Ethylene/1-Butene Copolymers Produced at various 1-Butene and Hydrogen Pressures*, M.Sc. thesis, University of Alberta, Edmonton, Alberta, Canada, 1995.

Lin, J. S., and C. R. A. Catlow, "Computer-modelling Studies on $MgCl_2$-supported Ziegler-Natta Catalysts", *Journal of Materials Chemistry*, **3**(12), 1217-1225 (1993).

Lynch, D. T., and S. E. Wanke, "Reactor Design and Operation for Gas-Phase Ethylene Polymerization Using Ziegler-Natta Catalysts", *The Canadian Journal of Chemical Engineering*, **69**, 332-339 (1991).

Marigo, A., R. Gerbasi, A. Martorana, and R. Zannetti, "Un dispositivo per l'indagine diffrattometrica a raggi X di sostanze sensibili all'aria (Device for x-ray diffraction studies on air-sensitive substances)", *Chimia e l'industria*, **64**, 785-786 (1982).

Power Diffraction Data File, 37-0774.

Press, W. H., S. A. Teukolsky, W. T. Vetterling, and B. P. Flannery, *Numerical Recipies in FORTRAN: The Art of Scientific Computing*, 2nd ed., Cambridge University Press, New York, 1992, Chapters 2 and 15.

Siew Hew Sam, D., P. Courtine, J. C. Jannel, D. Lalart, and K. Bujadoux, "Characterisation of δ-VCl_3, A highly active Ziegler-Natta catalyst obtained by ball-milling", *European Polymer Journal*, **22**(2), 89-95 (1986).

Simha, R., and H. Branson, "Theory of Chain Copolymerization Reactions", *The Journal of Chemical Physics*, **12**(6), 253-267 (1944).

Soares, J. B. P., and A. E. Hamielec, "Analyzing TREF data by Stockmayer's bivariate distribution", *Macromolecular Theory and Simulation*, **4**, 305-324 (1995).

Soares, J. B. P., Department of Chemical Engineering, McMaster University, private communication, 1997.

Starck, P., "Studies of the Comonomer Distributions in Low Density Polyethylenes Using Temperature Rising Elution Fractionation and Stepwise Crystallization by DSC", *Polymer International*, **40**, 111-122 (1996).

Stockmayer, W. H., "Distribution of Chain Lengths and Compositions in Copolymers", *The Journal of Chemical Physics*, **13**(6), 199-207 (1945).

Tacx, J. C. J. F., H. N. Linssen, and A. L. German, "Effect of Molar Mass Ratio on Monomers on the Mass Distribution of Chain Lengths and Compositions in Copolymers: Extension of the Stockmayer Theory", *Journal of Polymer Science: Part A: Polymer Chemistry*, **26**, 61-69 (1988).

Vogel, A.I., In *A Text-Book of Quantitative Inorganic Analysis Including Elementary Instrumental Analysis*, 3rd ed., Longmans, London, 1961.

Wild, L., T. R. Ryle, D. C. Knobeloch, and I. R. Peat, "Determination of Branching Distributions in Polyethylene and Ethylene Copolymers", *Journal of Polymer Science: Polymer Physics Edition*, **20**, 441-455 (1982).

Wu, L., D.T. Lynch, and S.E. Wanke, "Kinetics of Gas-Phase Ethylene Polymerization with Morphology-Controlled $MgCl_2$-Supported $TiCl_4$ Catalyst", *Macromolecules*, **32**, 7990-7998 (1999).

Zhang, M., D.T. Lynch and S.E. Wanke, "Characterization of Commercial Linear Low-Density Polyethylene by TREF-DSC and TREF-SEC Cross-Fractionation", *Journal of Applied Polymer Science*, **75**, 960-967 (2000).

APPENDIX A: FORTRAN Programs for TREF and Molar Mass Analysis

The complete FORTRAN 77 code for the programs "mass" and "tref" are presented in this appendix. These programs were use for the analysis of the ATREF profiles. The equations and nomenclature used in these programs are described in Appendix B.

LISTING OF PROGRAM mass

```
PROGRAM mass


      INTEGER COUNT,mNDATA,mMA,mia(30),mNCA,mITERATION,
     -      mIMAX,maxdata,i,j,peaks,control

      Parameter (maxdata=5000)

      REAL*8 mX(maxdata),mY(maxdata),mXVAR,mYVAR,mSIG(maxdata),
     -   mA(30),mCOVAR(30,30),mALPHA(30,30),mCHISQ,mALAMDA,
     - mycalc(maxdata),bchi,diff

      external massdist

      character description*40,mrunname*8,mdatafile*40,moutfile*40,
     -  num(9)*1,mlogfile*40,mrestart*40

      num(1)='1'
      num(2)='2'
      num(3)='3'
      num(4)='4'
      num(5)='5'
      num(6)='6'
      num(7)='7'
      num(8)='8'
      num(9)='9'

      read*, description,peaks
      read*, description,mimax
      read*, description,control

      mMA=peaks*2

      do i=1,mma
         read*, description,ma(i),mia(i)
      enddo


      if(control.eq.1) then
         ma(peaks*2)=1.0D+00
         do i=1,(peaks-1)
            ma(peaks*2)=ma(peaks*2)-ma(i*2)
         enddo
      endif

      read*, description,mrunname

      mdatafile=mrunname//'.dat'
      mlogfile=mrunname//'.'//num(peaks)//'peaks.log'
      moutfile=mrunname//'.'//num(peaks)//'peaks.out'

      open(unit=80,file=mdatafile,status='old')
      open(unit=83,file=moutfile,status='new')
      open(unit=84,file=mlogfile,status='new')

      COUNT=0
```

```
5     READ(80,*,END=15) mXVAR,myvar
         COUNT = COUNT+1
         mX(COUNT) = mXVAR
         mY(COUNT) = mYVAR
         GO TO 5
15    mNDATA=COUNT
      WRITE(6,*) mNDATA
      DO J=1,mNDATA
         mSIG(J)=1.0D+00
      enddo

      mNCA=mMA

      mALAMDA=-1.0D+00
      count=0
      bchi=mchisq
      CALL MRQMIN(mX,mY,mSIG,mNDATA,mA,mia,mma,mCOVAR,mALPHA,
     -            mNCA,mCHISQ,massdist,mALAMDA,mycalc,peaks)
      mITERATION=1
      diff=dabs(bchi-mchisq)

      do i=1,mma
         write(84,*) ma(i)
      enddo
      write(84,*) malamda,mchisq
      write(6,*) malamda,mchisq,diff
40    IF(diff.GE.1.0D-30.AND.mITERATION.LT.mIMAX.
     -   AND.count.lt.10) THEN
         count=0
         mITERATION=mITERATION+1
         bchi=mchisq
         CALL MRQMIN(mX,mY,mSIG,mNDATA,mA,miA,mma,mCOVAR,mALPHA,
     -            mNCA,mCHISQ,massdist,mALAMDA,mycalc,peaks)

         diff=dabs(bchi-mchisq)
         write(84,*) miteration
         do i=1,mma
            write(84,*) ma(i)
         enddo
         write(84,*) malamda,mchisq
         write(6,*) malamda,mchisq,diff
         GOTO 40
      elseif (diff.lt.1D-30.and.miteration.lt.mimax.
     -        and.count.lt.10) then
         count=count+1
         bchi=mchisq
         miteration=miteration+1
         CALL MRQMIN(mX,mY,mSIG,mNDATA,mA,miA,mma,mCOVAR,mALPHA,
     -            mNCA,mCHISQ,massdist,mALAMDA,mycalc,peaks)

         diff=dabs(bchi-mchisq)
         write(84,*) miteration
         do i=1,mma
            write(84,*) ma(i)
         enddo
         write(84,*) malamda,mchisq
         write(6,*) malamda,mchisq,diff
         GOTO 40

      ELSEIF (count.ge.10.and.miteration.lt.mimax) THEN
```

```
      mALAMDA=0
      CALL MRQMIN(mX,mY,mSIG,mNDATA,mA,mia,mma,mCOVAR,mALPHA,
     -           mNCA,mCHISQ,massdist,mALAMDA,mycalc,peaks)

      write(84,*) malamda,mchisq
      write(6,*) malamda,mchisq,diff
      DO I=1,mMA
         WRITE(84,*) mA(I)
      enddo
      do i=2,mndata
         write(83,*) mx(i),my(i),mycalc(i)
      enddo
c     flush the buffer for this stuff
      call flush_(83)
      call sort(ma,peaks)
      call peakplot(mx,peaks,ma,mrunname,mndata,num)
      call massout(num,ma,mma,peaks,mia,mrunname,mrestart)
      call stats(mma,ma,peaks,mchisq,my,mcovar,mndata,mycalc,mia,
     -      mrunname,num,mx,massdist)
      ELSE
      mALAMDA=0
      CALL MRQMIN(mX,mY,mSIG,mNDATA,mA,mia,mma,mCOVAR,mALPHA,
     -           mNCA,mCHISQ,massdist,mALAMDA,mycalc,peaks)

      WRITE(84,*) 'MAXIMUM ITERAITONS EXCEDED'
      write(6,*) malamda,mchisq,diff
      write(84,*) miteration,malamda,mchisq
      DO I=1,mMA
         WRITE(84,*) mA(I)
      enddo
      do i=2,mndata
         write(83,*) mx(i),my(i),mycalc(i)
      enddo
      call flush_(83)
      call sort(ma,peaks)
      call peakplot(mx,peaks,ma,mrunname,mndata,num)
      call massout(num,ma,mma,peaks,mia,mrunname,mrestart)
      call stats(mma,ma,peaks,mchisq,my,mcovar,mndata,mycalc,mia,
     -      mrunname,num,mx,massdist)

      ENDIF

      END


      subroutine mrqmin(x,y,sig,ndata,a,ia,ma,covar,alpha,nca,
     +   chisq,funcs,alamda,ycalc,peaks)
      integer ma,nca,ndata,ia(30),MMAX,maxdata,peaks
      parameter (maxdata=5000)
      real*8 alamda,chisq,a(30),alpha(30,30),covar(30,30),
     +    sig(maxdata),x(maxdata),y(maxdata),ycalc(maxdata)
      external funcs
      parameter (MMAX=30)
      integer j,k,l,m,mfit
      real*8 ochisq,atry(MMAX),beta(MMAX),da(MMAX)
      save ochisq,atry,beta,da,mfit
      if(alamda.lt.0.0D+00)then
         mfit=0
         do j=1,ma
            if (ia(j).ne.0) then
```

```
            mfit=mfit+1
         endif
      enddo
      alamda=1.0D-3
      call mrqcof(x,y,sig,ndata,a,ia,ma,alpha,beta,nca,
     -              chisq,funcs,ycalc,peaks)
      ochisq=chisq
      do j=1,ma
         atry(j)=a(j)
      enddo
   endif
   j=0
   do l=1,ma
      if(ia(l).ne.0) then
         j=j+1
         k=0
         do m=1,ma
            if(ia(m).ne.0) then
               k=k+1
               covar(j,k)=alpha(j,k)
            endif
         enddo
         covar(j,j)=alpha(j,j)*(1.0D+00+alamda)
         da(j)=beta(j)
      endif
   enddo
   call gaussj(covar,mfit,nca,da,1,1)
   if(alamda.eq.0.) then
      call covsrt(covar,nca,ma,ia,mfit)
      return
   endif
   j=0
   do l=1,ma
      if(ia(l).ne.0) then
         j=j+1
         atry(l)=a(l)+da(j)
      endif
   enddo

   call mrqcof(x,y,sig,ndata,atry,ia,ma,covar,da,
     -      nca,chisq,funcs,ycalc,peaks)
   if(chisq.lt.ochisq) then
      alamda=5.0D-1*alamda
      ochisq=chisq
      j=0
      do l=1,ma
         if(ia(l).ne.0) then
            j=j+1
            k=0
            do m=1,ma
               if(ia(m).ne.0) then
                  k=k+1
                  alpha(j,k)=covar(j,k)
               endif
            enddo
            beta(j)=da(j)
            a(l)=atry(l)
         endif
      enddo
   else
```

```
      alamda=1.0D+1*alamda
      chisq=ochisq
    endif
    return
    end


    subroutine mrqcof(x,y,sig,ndata,a,ia,ma,alpha,beta,nalp,
   +     chisq,funcs,ycalc,peaks)
    integer ma,nalp,ndata,ia(30),MMAX,maxdata,peaks
    parameter (maxdata=5000)
    real*8 chisq,a(30),alpha(30,30),beta(30),sig(maxdata),
   +     x(maxdata),y(maxdata),ycalc(maxdata)
    external funcs
    parameter (MMAX=30)
    integer mfit,i,j,k,l,m
    real*8 dy,sig2i,wt,ymod,dyda(MMAX)
    mfit=0
    do j=1,ma
      if (ia(j).ne.0) mfit=mfit+1
    enddo
    do j=1,mfit
      do k=1,j
        alpha(j,k)=0.0D+00
      enddo
      beta(j)=0.0D+00
    enddo
    chisq=0.0D+00
    do i=1,ndata
      if (i.eq.1) then
        call constrain(x(i),a,ymod,dyda,ma,peaks)
      else
        call funcs(x(i),a,ymod,dyda,ma,peaks)
      endif
      sig2i=1.0D+00/(sig(i)*sig(i))
      dy=y(i)-ymod
      ycalc(i)=ymod
      j=0
      do l=1,ma
        if(ia(l).ne.0) then
          j=j+1
          wt=dyda(l)*sig2i
          k=0
          do m=1,l
            if(ia(m).ne.0) then
              k=k+1
              alpha(j,k)=alpha(j,k)+wt*dyda(m)
            endif
          enddo
          beta(j)=beta(j)+dy*wt
        endif
      enddo
      chisq=chisq+dy*dy
    enddo
    do j=2,mfit
      do k=1,j-1
        alpha(k,j)=alpha(j,k)
      enddo
    enddo
    return
```

```
      end


      subroutine covsrt(covar,npc,ma,ia,mfit)
      integer ma,mfit,npc,ia(30)
      real*8 covar(30,30)
      integer i,j,k
      real*8 swap
      do i=mfit+1,ma
         do j=1,i
            covar(i,j)=0.0D+00
            covar(j,i)=0.0D+00
         enddo
      enddo
      k=mfit
      do j=ma,1,-1
         if(ia(j).ne.0) then
            do i=1,ma
               swap=covar(i,k)
               covar(i,k)=covar(i,j)
               covar(i,j)=swap
            enddo
            do i=1,ma
               swap=covar(k,i)
               covar(k,i)=covar(j,i)
               covar(j,i)=swap
            enddo
            k=k-1
         endif
      enddo
      return
      end

      subroutine gaussj(a,n,np,b,m,mp)
      integer m,mp,n,np,NMAX
      real*8 a(30,30),b(30,mp)
      parameter (NMAX=30)
      integer i,icol,irow,j,k,l,ll,indxc(NMAX),indxr(NMAX),
     +     ipiv(NMAX)
      real*8 big,dum,pivinv
      do j=1,n
         ipiv(j)=0
      enddo
      do i=1,n
         big=0.0D+00
         do j=1,n
            if(ipiv(j).ne.1) then
               do k=1,n
                  if (ipiv(k).eq.0) then
                     if (dabs(a(j,k)).ge.big) then
                        big=dabs(a(j,k))
                        irow=j
                        icol=k
                     endif
                  else if (ipiv(k).gt.1) then
                     pause 'singular matrix in gaussj'
                  endif
               enddo
            endif
         enddo
```

```
        ipiv(icol)=ipiv(icol)+1
        if (irow.ne.icol) then
           do l=1,n
              dum=a(irow,l)
              a(irow,l)=a(icol,l)
              a(icol,l)=dum
           enddo
           do l=1,m
              dum=b(irow,l)
              b(irow,l)=b(icol,l)
              b(icol,l)=dum
           enddo
        endif
        indxr(i)=irow
        indxc(i)=icol
        if (a(icol,icol).eq.0.) pause 'singular matrix in gaussj2'
        pivinv=1.0D+00/a(icol,icol)
        a(icol,icol)=1.0D+00
        do l=1,n
           a(icol,l)=a(icol,l)*pivinv
        enddo
        do l=1,m
           b(icol,l)=b(icol,l)*pivinv
        enddo
        do ll=1,n
           if(ll.ne.icol) then
              dum=a(ll,icol)
              a(ll,icol)=0.0D+00
              do l=1,n
                 a(ll,l)=a(ll,l)-a(icol,l)*dum
              enddo
              do l=1,m
                 b(ll,l)=b(ll,l)-b(icol,l)*dum
              enddo
           endif
        enddo
     enddo
     do l=n,1,-1
        if(indxr(l).ne.indxc(l)) then
           do k=1,n
              dum=a(k,indxr(l))
              a(k,indxr(l))=a(k,indxc(l))
              a(k,indxc(l))=dum
           enddo
        endif
     enddo
     return
     end


     SUBROUTINE massdist(X,A,YFIT,DYDA,MA,peaks)

*  THIS PROGRAM RETURNS THE FUNCTION EVALUATION AND DERIVATIVES AT
*  ONE X


     REAl*8 X,A(30),YFIT,dyda(30),r
     INTEGER MA,peaks,i
```

```
      yfit=0.0D+00

      r=1.0D+1**x

      do i=1,peaks

      DYDA(i*2-1)=a(i*2)*dlog(1.0D+1)*r**2.0D+0*a(i*2-1)*
     -           dexp(-a(i*2-1)*r)*(2.0d+0-r*a(i*2-1))

      DYDA(i*2)=a(i*2-1)**2.0D+0*r**2.0D+0*dlog(1.0D+1)*
     -          dexp(-a(i*2-1)*r)

      YFIT=yfit+a(i*2)*a(i*2-1)**2.0d+0*r**2.0d+0*dlog(1.0D+1)*
     -          dexp(-a(i*2-1)*r)

      enddo

      RETURN
      END


      subroutine constrain(X,A,YFIT,DYDA,MA,peaks)

      integer ma,peaks,wfrac,i
      real*8 x,a(30),yfit,dyda(30)

      do i=1,ma
         dyda(i)=0.0D+00
      enddo

      yfit=0.0D+00

      do i=1,peaks
         dyda(i*2)=1
         yfit=yfit+a(i*2)
      enddo

      return
      end


      subroutine massout(num,a,ma,peaks,ai,runname,mrestart)

      integer i,ma,peaks,ai(30)
      real*8 a(30),mw,mni,mn,pd
      character num(9)*1,runname*8,des1*30,des2*30,mrestart*40

      mw=0.0D+00
      mni=0.0D+00

      do i=1,peaks
         mw=mw+2.0D+00/a(i*2-1)*a(i*2)
         mni=mni+a(i*2)*a(i*2-1)
      enddo

      mn=1.0D+00/mni
      pd=mw/mn

      mrestart=runname//'.'//num(peaks)//'peaks.rst'
```

```
      open(unit=85,file=mrestart,status='new')

      do i=1,peaks
         des1='''tau peak '//num(i)//''''
         des2='''weight frac peak '//num(i)//''''
         write(85,*) des1,a(i*2-1),ai(i*2-1)
         write(85,*) des2,a(i*2),ai(i*2)
      enddo

      write(85,*) 'Number averaged MW',mn
      write(85,*) 'Weight averaged MW',mw
      write(85,*) 'Polydispersity',pd

      close(unit=85,status='keep')

      return
      end


      subroutine stats(ma,a,peaks,chisq,y,covar,ndata,
     -                 ycalc,ia,runname,num,x,funcs)

      integer i,ma,ia(30),ndata,peaks,maxdata

      parameter (maxdata=5000)

      real*8 a(30),chisq,y(maxdata),ycalc(maxdata),ssr,ssy,ytotal,
     - covar(30,30),yave,mfit,v,scf,f,r2,sn(30),tn(30),b(30),
     - x(maxdata)

      external funcs

      character num(9)*1,runname*8,statname*40,heading*30

      ssr=0.0D+00
      do i=2,ndata
         ssr=ssr+(ycalc(i)-y(i))**2.0D+00
      enddo
      ytotal=0.0D+00
      do i=2,ndata
         ytotal=ytotal+y(i)
      enddo
      yave=ytotal/dble(real(ndata-1))
      ssy=0.0D+00
      do i=2,ndata
         ssy=ssy+(y(i)-yave)**2.0D+00
      enddo
      mfit=0.0D+00
      do i=1,ma
         if(ia(i).ne.0) mfit=mfit+1.0D+00
      enddo
      v=dble(real(ndata-1))-mfit
      scf=dsqrt(ssr/v)
      call mrqcof2(x,y,scf,ndata,a,ia,ma,covar,funcs,
     -             peaks)
      call gaussj(covar,idint(mfit),30,b,1,1)
      call covsrt(covar,30,ma,ia,idint(mfit))
      F=((ssy-ssr)/(mfit-1))/(ssr/v)
      r2=1.0D+00-(ssr/ssy)
      do i=1,ma
```

```
      if(ia(i).ne.0) then
        sn(i)=scf*dsqrt(covar(i,i))
        tn(i)=a(i)/sn(i)*1.0D+2
      endif
    enddo

    statname=runname//'.'//num(peaks)//'peaks.sta'
    open(unit=97,file=statname,status='new')

    write(97,*) 'r^2     ',r2
    write(97,*) 'X^2     ',chisq
    write(97,*) 'F       ',f
    write(97,*) 'Description  ','Parameter            ',
   - 'Standard error      ','t-value'
    do i=1,peaks
      heading='Peak '//num(i)
      write(97,*) heading
      write(97,*) 'tau          ',a(2*i-1),sn(2*i-1),tn(2*i-1)
      write(97,*) 'weight frac ',a(2*i),sn(2*i),tn(2*i)
    enddo

    close(unit=97,status='keep')

    return
    end

    subroutine sort(a,peaks)

    integer j,peaks,last
    real*8 a(30),hold1,hold2
    logical sorted

    sorted=.false.

    last=peaks-1

65  if (.not.sorted) then
      sorted=.true.
      do j=1,last
        if (a(j*2-1).lt.a((j+1)*2-1)) then
          hold1=a((j+1)*2-1)
          hold2=a((j+1)*2)
          a((j+1)*2-1)=a(j*2-1)
          a((j+1)*2)=a(j*2)
          a(j*2-1)=hold1
          a(j*2)=hold2
          sorted=.false.
        endif
      enddo
      last=last-1
      go to 65
    endif

    return
    end


    subroutine peakplot(x,peaks,a,runname,ndata,num)

    integer peaks,ndata,i,j
```

```
      real*8 op(10),a(30),x(ndata),ratio,b,d,r
      character runname*8,peakname*40,num(9)*1

      peakname=runname//'.'//num(peaks)//'peaks.pks'

      open(unit=75,file=peakname,status='new')

      do i=2,ndata
         do j=1,peaks
            r=(1.0d+1)**x(i)
            op(j)=a(j*2)*a(j*2-1)**2.0d+0*r**2.0d+0*dlog(1.0D+1)*
     -        dexp(-a(j*2-1)*r)
         enddo

         if (peaks.eq.1) then
            write(75,*) x(i),op(1)
         else if (peaks.eq.2) then
            write(75,*) x(i),op(1),op(2)
         else if (peaks.eq.3) then
            write(75,*) x(i),op(1),op(2),op(3)
         else if (peaks.eq.4) then
            write(75,*) x(i),op(1),op(2),op(3),op(4)
         else if (peaks.eq.5) then
            write(75,*) x(i),op(1),op(2),op(3),op(4),op(5)
         else if (peaks.eq.6) then
            write(75,*) x(i),op(1),op(2),op(3),op(4),op(5),op(6)
         else if (peaks.eq.7) then
            write(75,*) x(i),op(1),op(2),op(3),op(4),op(5),op(6),
     -      op(7)
         else if (peaks.eq.8) then
            write(75,*) x(i),op(1),op(2),op(3),op(4),op(5),op(6),
     -      op(7),op(8)
         else if (peaks.eq.9) then
            write(75,*) x(i),op(1),op(2),op(3),op(4),op(5),op(6),
     -      op(7),op(8),op(9)
         endif

      enddo

      close(unit=75,status='keep')
      call flush_(75)

      return
      end

      subroutine mrqcof2(x,y,sig,ndata,a,ia,ma,alpha,
     +     funcs,peaks)
      integer ma,ndata,ia(30),MMAX,maxdata,peaks
      parameter (maxdata=5000)
      real*8 a(30),alpha(30,30),sig,
     +     x(maxdata),y(maxdata)
      external funcs
      parameter (MMAX=30)
      integer mfit,i,j,k,l,m
      real*8 dy,sig2i,wt,ymod,dyda(MMAX)

      mfit=0
      do j=1,ma
         if (ia(j).ne.0) mfit=mfit+1
      enddo
```

```
do j=1,mfit
   do k=1,j
      alpha(j,k)=0.0D+00
   enddo
enddo
do i=2,ndata
   call funcs(x(i),a,ymod,dyda,ma,peaks)
   sig2i=1.0D+00/(sig*sig)
   dy=y(i)-ymod
   j=0
   do l=1,ma
      if(ia(l).ne.0) then
         j=j+1
         wt=dyda(l)*sig2i
         k=0
         do m=1,l
            if(ia(m).ne.0) then
               k=k+1
               alpha(j,k)=alpha(j,k)+wt*dyda(m)
            endif
         enddo
      endif
   enddo
enddo
do j=2,mfit
   do k=1,j-1
      alpha(k,j)=alpha(j,k)
   enddo
enddo

return
end
```

LISTING OF RPROGRAM tref

```
PROGRAM tref

      INTEGER COUNT,i,j,peaks,tNDATA,tMA,maxdata,start,
     -     tia(30),tNCA,tITERATION,tIMAX,tconst

      Parameter (maxdata=5000)

      REAL*8 mycalc(maxdata),tX(maxdata),tY(maxdata),tXVAR,tYVAR,
     -  tSIG(maxdata),tA(30),tCOVAR(30,30),tALPHA(30,30),
     - tCHISQ,tALAMDA,tycalc(maxdata),bchi,diff

      external myfunc

      character description*40,mrunname*8,
     -  num(9)*1,mrestart*40,trestart*40,trunname*8,
     - tdatafile*40,toutfile*40,tlogfile*40,tinitial*40

      num(1)='1'
      num(2)='2'
      num(3)='3'
      num(4)='4'
      num(5)='5'
      num(6)='6'
      num(7)='7'
      num(8)='8'
      num(9)='9'

      read*, description,peaks
      read*, description,timax

      read*, description,trunname
      read*, description,mrunname

      tma=peaks*4

      tdatafile=trunname//'.dat'
      tlogfile=trunname//'.'//num(peaks)//'peaks.log'
      toutfile=trunname//'.'//num(peaks)//'peaks.out'
      mrestart=mrunname//'.'//num(peaks)//'peaks.rst'

      open(unit=90,file=tdatafile,status='old')
      open(unit=93,file=toutfile,status='new')
      open(unit=94,file=tlogfile,status='new')
      open(unit=96,file=mrestart,status='old')


      do i=1,peaks
         read*, description,ta(i*4-3),tia(i*4-3)
         read(96,*) description,ta(i*4-2),tia(i*4-2)
         read*, description,ta(i*4-1),tia(i*4-1)
         read(96,*) description,ta(i*4),tia(i*4)
      enddo

*     read whether weight frcation is variable or not

      read*, description, tconst
```

```
      if (tconst.eq.0) then
         start=1
         do i=1,peaks
            tia(i*4)=0
            tia(i*4-2)=0
         enddo
      else
         start=2
         do i=1,peaks
            tia(i*4-2)=0
         enddo
      endif

      COUNT=0

25     READ(90,*,END=35) tXVAR,tyvar
         COUNT = COUNT+1
         tX(COUNT) = tXVAR
         tY(COUNT) = tYVAR
         GO TO 25

35    tNDATA=COUNT

      WRITE(6,*) tNDATA

      DO J=1,tNDATA
         tSIG(J)=1.0D+00
      enddo

      tNCA=tMA

      tALAMDA=-1.0D+00
      count=0
      bchi=tchisq
      CALL MRQMIN(tX,tY,tSIG,tNDATA,tA,tia,tma,tCOVAR,tALPHA,
     -            tNCA,tCHISQ,myfunc,tALAMDA,tycalc,peaks,tconst)
      tITERATION=1
      diff=dabs(bchi-tchisq)

      do i=1,tma
         write(94,*) ta(i)
      enddo
      write(94,*) talamda,tchisq
      write(6,*) talamda,tchisq,diff
50    IF(diff.GE.1.0D-20.AND.tITERATION.LT.tIMAX.
     -   AND.count.lt.10) THEN
         count=0
         tITERATION=tITERATION+1
         bchi=tchisq
         CALL MRQMIN(tX,tY,tSIG,tNDATA,tA,tiA,tma,tCOVAR,tALPHA,
     -              tNCA,tCHISQ,myfunc,tALAMDA,tycalc,peaks,tconst)
         diff=dabs(bchi-tchisq)
         write(94,*) titeration
         do i=1,tma
            write(94,*) ta(i)
         enddo
         write(94,*) talamda,tchisq
         write(6,*) talamda,tchisq,diff
         GOTO 50
       elseif (diff.lt.1D-20.and.titeration.lt.timax.
```

```
-       and.count.lt.10) then
     count=count+1
     bchi=tchisq
     titeration=titeration+1
     CALL MRQMIN(tX,tY,tSIG,tNDATA,tA,tiA,tma,tCOVAR,tALPHA,
-           tNCA,tCHISQ,myfunc,tALAMDA,tycalc,peaks,tconst)
     diff=dabs(bchi-tchisq)
     write(94,*) titeration
     do i=1,tma
        write(94,*) ta(i)
     enddo
     write(94,*) talamda,tchisq
     write(6,*) talamda,tchisq,diff
     GOTO 50

 ELSEIF (count.ge.10.and.titeration.lt.timax) THEN
     tALAMDA=0
     CALL MRQMIN(tX,tY,tSIG,tNDATA,tA,tia,tma,tCOVAR,tALPHA,
-           tNCA,tCHISQ,myfunc,tALAMDA,tycalc,peaks,tconst)
     write(94,*) talamda,tchisq
     write(6,*) talamda,tchisq,diff
     DO I=1,tMA
        WRITE(94,*) tA(I)
     enddo
     do i=start,tndata
        write(93,*) tx(i),ty(i),tycalc(i)
     enddo
     call peakplot(tx,peaks,ta,trunname,tndata,num,tconst)
     call trefout(num,ta,tma,peaks,tia,trunname,trestart)
     call stats(tma,ta,peaks,tchisq,ty,tcovar,tndata,tycalc,tia,
-        trunname,num,tx,myfunc,tconst)
 ELSE
     tALAMDA=0
     CALL MRQMIN(tX,tY,tSIG,tNDATA,tA,tia,tma,tCOVAR,tALPHA,
-           tNCA,tCHISQ,myfunc,tALAMDA,tycalc,peaks,tconst)
     WRITE(94,*) 'MAXIMUM ITERAITONS EXCEDED'
     write(6,*) talamda,tchisq,diff
     write(94,*) titeration,talamda,tchisq
     DO I=1,tMA
        WRITE(94,*) tA(I)
     enddo
     do i=start,tndata
        write(93,*) tx(i),ty(i),tycalc(i)
     enddo
     call peakplot(tx,peaks,ta,trunname,tndata,num,tconst)
     call trefout(num,ta,tma,peaks,tia,trunname,trestart)
     call stats(tma,ta,peaks,tchisq,ty,tcovar,tndata,tycalc,tia,
-        trunname,num,tx,myfunc,tconst)
 ENDIF

 END


 subroutine mrqmin(x,y,sig,ndata,a,ia,ma,covar,alpha,nca,
+   chisq,funcs,alamda,ycalc,peaks,wfrac)
 integer ma,nca,ndata,ia(30),MMAX,maxdata,peaks
 parameter (maxdata=5000)
 real*8 alamda,chisq,a(30),alpha(30,30),covar(30,30),
+    sig(maxdata),x(maxdata),y(maxdata),ycalc(maxdata)
 external funcs
```

```
      parameter (MMAX=30)
      integer j,k,l,m,mfit,wfrac
      real*8 ochisq,atry(MMAX),beta(MMAX),da(MMAX)
      save ochisq,atry,beta,da,mfit
      if(alamda.lt.0.0D+00)then
         mfit=0
         do j=1,ma
            if (ia(j).ne.0) then
               mfit=mfit+1
            endif
         enddo
         alamda=1.0D-3
         call mrqcof(x,y,sig,ndata,a,ia,ma,alpha,beta,nca,
     -              chisq,funcs,ycalc,peaks,wfrac)
         ochisq=chisq
         do j=1,ma
            atry(j)=a(j)
         enddo
      endif
      j=0
      do l=1,ma
         if(ia(l).ne.0) then
            j=j+1
            k=0
            do m=1,ma
               if(ia(m).ne.0) then
                  k=k+1
                  covar(j,k)=alpha(j,k)
               endif
            enddo
            covar(j,j)=alpha(j,j)*(1.0D+00+alamda)
            da(j)=beta(j)
         endif
      enddo
      call gaussj(covar,mfit,nca,da,1,1)
      if(alamda.eq.0.) then
         call covsrt(covar,nca,ma,ia,mfit)
         return
      endif
      j=0
      do l=1,ma
         if(ia(l).ne.0) then
            j=j+1
            atry(l)=a(l)+da(j)
         endif
      enddo

      call mrqcof(x,y,sig,ndata,atry,ia,ma,covar,da,
     -      nca,chisq,funcs,ycalc,peaks,wfrac)
      if(chisq.lt.ochisq) then
         alamda=5.0D-1*alamda
         ochisq=chisq
         j=0
         do l=1,ma
            if(ia(l).ne.0) then
               j=j+1
               k=0
               do m=1,ma
                  if(ia(m).ne.0) then
                     k=k+1
```

```
                alpha(j,k)=covar(j,k)
              endif
            enddo
            beta(j)=da(j)
            a(l)=atry(l)
          endif
        enddo
      else
        alamda=1.0D+1*alamda
        chisq=ochisq
      endif
      return
      end


      subroutine mrqcof(x,y,sig,ndata,a,ia,ma,alpha,beta,nalp,
     +     chisq,funcs,ycalc,peaks,wfrac)
      integer ma,nalp,ndata,ia(30),MMAX,maxdata,peaks,wfrac
      parameter (maxdata=5000)
      real*8 chisq,a(30),alpha(30,30),beta(30),sig(maxdata),
     +     x(maxdata),y(maxdata),ycalc(maxdata)
      external funcs
      parameter (MMAX=30)
      integer mfit,i,j,k,l,m
      real*8 dy,sig2i,wt,ymod,dyda(MMAX)
      mfit=0
      do j=1,ma
        if (ia(j).ne.0) mfit=mfit+1
      enddo
      do j=1,mfit
        do k=1,j
          alpha(j,k)=0.0D+00
        enddo
        beta(j)=0.0D+00
      enddo
      chisq=0.0D+00
      do i=1,ndata
        if (i.eq.1.and.(wfrac.eq.4)) then
          call constrain(x(i),a,ymod,dyda,ma,peaks)
        else
          call funcs(x(i),a,ymod,dyda,ma,peaks)
        endif
        sig2i=1.0D+00/(sig(i)*sig(i))
        dy=y(i)-ymod
        ycalc(i)=ymod
        j=0
        do l=1,ma
          if(ia(l).ne.0) then
            j=j+1
            wt=dyda(l)*sig2i
            k=0
            do m=1,l
              if(ia(m).ne.0) then
                k=k+1
                alpha(j,k)=alpha(j,k)+wt*dyda(m)
              endif
            enddo
            beta(j)=beta(j)+dy*wt
          endif
        enddo
```

```
      chisq=chisq+dy*dy
   enddo
   do j=2,mfit
      do k=1,j-1
         alpha(k,j)=alpha(j,k)
      enddo
   enddo
   return
   end


   subroutine covsrt(covar,npc,ma,ia,mfit)
   integer ma,mfit,npc,ia(30)
   real*8 covar(30,30)
   integer i,j,k
   real*8 swap
   do i=mfit+1,ma
      do j=1,i
         covar(i,j)=0.0D+00
         covar(j,i)=0.0D+00
      enddo
   enddo
   k=mfit
   do j=ma,1,-1
      if(ia(j).ne.0) then
         do i=1,ma
            swap=covar(i,k)
            covar(i,k)=covar(i,j)
            covar(i,j)=swap
         enddo
         do i=1,ma
            swap=covar(k,i)
            covar(k,i)=covar(j,i)
            covar(j,i)=swap
         enddo
         k=k-1
      endif
   enddo
   return
   end

   subroutine gaussj(a,n,np,b,m,mp)
   integer m,mp,n,np,NMAX
   real*8 a(30,30),b(30,mp)
   parameter (NMAX=30)
   integer i,icol,irow,j,k,l,ll,indxc(NMAX),indxr(NMAX),
  +    ipiv(NMAX)
   real*8 big,dum,pivinv
   do j=1,n
      ipiv(j)=0
   enddo
   do i=1,n
      big=0.0D+00
      do j=1,n
         if(ipiv(j).ne.1) then
            do k=1,n
               if (ipiv(k).eq.0) then
                  if (dabs(a(j,k)).ge.big) then
                     big=dabs(a(j,k))
                     irow=j
```

```
                  icol=k
               endif
            else if (ipiv(k).gt.1) then
               pause 'singular matrix in gaussj'
            endif
         enddo
      endif
   enddo
   ipiv(icol)=ipiv(icol)+1
   if (irow.ne.icol) then
      do l=1,n
         dum=a(irow,l)
         a(irow,l)=a(icol,l)
         a(icol,l)=dum
      enddo
      do l=1,m
         dum=b(irow,l)
         b(irow,l)=b(icol,l)
         b(icol,l)=dum
      enddo
   endif
   indxr(i)=irow
   indxc(i)=icol
   if (a(icol,icol).eq.0.) pause 'singular matrix in gaussj2'
   pivinv=1.0D+00/a(icol,icol)
   a(icol,icol)=1.0D+00
   do l=1,n
      a(icol,l)=a(icol,l)*pivinv
   enddo
   do l=1,m
      b(icol,l)=b(icol,l)*pivinv
   enddo
   do ll=1,n
      if(ll.ne.icol) then
         dum=a(ll,icol)
         a(ll,icol)=0.0D+00
         do l=1,n
            a(ll,l)=a(ll,l)-a(icol,l)*dum
         enddo
         do l=1,m
            b(ll,l)=b(ll,l)-b(icol,l)*dum
         enddo
      endif
   enddo
enddo
do l=n,1,-1
   if(indxr(l).ne.indxc(l)) then
      do k=1,n
         dum=a(k,indxr(l))
         a(k,indxr(l))=a(k,indxc(l))
         a(k,indxc(l))=dum
      enddo
   endif
enddo
return
end

SUBROUTINE myfunc(X,A,YFIT,DYDA,MA,peaks)
```

```
* THIS PROGRAM RETURNS THE FUNCTION EVALUATION AND DERIVATIVES AT
* ONE X


      REAl*8 X,A,YFIT,DYDA,B,DBDF,D,DDDF,ratio,dbdrr
      INTEGER MA,peaks,i
      DIMENSION A(30),DYDA(30)
*      WRITE(6,*) 'Entered FUNCS'

      ratio=4.8D+1/2.4D+1

      yfit=0.0D+00
      do i=1,peaks

      B=(1.0D+00-a(4*i-3))*a(4*i-3)*(1.0D+00+4.0D+00*
     - (1.0D+00-a(4*i-3))*
     - a(4*i-3)*(-1.0D+00+a(4*i-1)))**5.0D-1

      dbdf=5.0D-1*(1.0D+00-a(4*i-3))*a(4*i-3)*(4.0D+00*
     - (1.0D+00-a(4*i-3))*
     - (-1.0D+00+a(4*i-1))-4.0D+00*a(4*i-3)*(-1.0D+00+a(4*i-1)))/
     -   (1.0D+00+4.0D+00*(1.0D+00-a(4*i-3))*a(4*i-3)*
     - (-1.0D+00+a(4*i-1)))**5.0D-1+
     -  (1.0D+00-a(4*i-3))*(1.0D+00+4.0D+00*(1.0D+00-
     - a(4*i-3))*a(4*i-3)*(-1.0D+00+a(4*i-1)))**5.0D-1-
     -  a(4*i-3)*(1.0D+00+4.0D+00*(1.0D+00-a(4*i-3))*a(4*i-3)*
     - (-1.0D+00+a(4*i-1)))**5.0D-1

      dbdrr=2.0D+00*(1.0D+00-a(4*i-3))**2.0D+00*a(4*i-3)**2.0D+00/
     - (1.0D+00+4.0D+00*
     - (1.0D+00-a(4*i-3))*a(4*i-3)*(-1.0D+00+a(4*i-1)))**5.0D-1

      D=(1.0D+00-ratio)/(ratio+a(4*i-3)*(1.0D+00-ratio))

      DDDF=-(1.0D+00-ratio)**2.0D+00/(ratio+a(4*i-3)*
     - (1.0D+00-ratio))**2.0D+00

      DYDA(i*4-3)=a(4*i)*(-3.0D+00*a(4*i-2)*(1.0D+00+
     - (-a(4*i-3)+X)*D)*DBDF/
     -   (8.0D+00*dSqrt(2.0D+00)*(1.0D+00+(-a(4*i-3)+X)**2.0D+00/
     - (2.0D+00*a(4*i-2)*B))
     -   **(5.0D+00/2.0D+00)*(a(4*i-2)*B)**(3.0D+00/2.0D+00))-
     -  1.5D+1*(1.0D+00+(-a(4*i-3)+X)*D)*(-((-a(4*i-3)+X)/
     - (a(4*i-2)*B))-
     -  (-a(4*i-3)+X)**2.0D+00*DBDF/(2.0D+00*a(4*i-2)*B**2.0D+00))/
     - (8.0D+00*dSqrt(2.0D+00)*(1.0D+00+(-a(4*i-3)+X)**2.0D+00/
     - (2.0D+00*a(4*i-2)*B))**(7.0D+00/2.0D+00)*dSqrt(a(4*i-2)*B))+
     -  3.0D+00*(-D+(-a(4*i-3)+X)*DDDF)/
     -  (4.0D+00*dSqrt(2.0D+00)*(1.0D+00+(-a(4*i-3)+X)**2.0D+00/
     - (2.0D+00*a(4*i-2)*B))**(5.0D+00/2.0D+00)*dSqrt(a(4*i-2)*B)))

      DYDA(i*4-2)=a(4*i)*(-3.0D+00*B*(1.0D+00+(-a(4*i-3)+X)*D)/
     -   (8.0D+00*dSqrt(2.0D+00)*(1.0D+00+(-a(4*i-3)+X)**2.0D+00/
     - (2.0D+00*a(4*i-2)*B))**(5.0D+00/2.0D+00)*(a(4*i-2)*B)**
     - (3.0D+00/2.0D+00))+
     -  1.5D+1*(-a(4*i-3)+X)**2.0D+00*(1.0D+00+(-a(4*i-3)+X)*D)/
     -   (1.6D+1*dSqrt(2.0D+00)*a(4*i-2)**2.0D+00*(1.0D+00+
     - (-a(4*i-3)+X)
     -  **2.0D+00/(2.0D+00*a(4*i-2)*B))**(7.0D+00/2.0D+00)*
     - B*dSqrt(a(4*i-2)*B)))
```

```
 DYDA(i*4-1)=a(4*i)*(-3.0D+00*a(4*i-2)*(1.0D+00+d*
-  (-a(4*i-3)+x))*dbdrr/
-    (8.0D+00*dSqrt(2.0D+00)*(1.0D+00+(-a(4*i-3)+x)**2.0D+00/
-  (2.0D+00*a(4*i-2)*b))**(5.0D+00/2.0D+00)*(a(4*i-2)*b)**
-  (3.0D+00/2.0D+00))+
-   1.5D+1*(-a(4*i-3)+x)**2.0D+00*(1.0D+00+d*(-a(4*i-3)+x))*dbdrr/
-  (1.6D+1*dSqrt(2.0D+00)*a(4*i-2)*(1.0D+00+(-a(4*i-3)+x)**2.0D+00/
-  (2.0D+00*a(4*i-2)*b))**(7.0D+00/2.0D+00)*b**2.0D+00*
-      dSqrt(a(4*i-2)*b)))

 DYDA(i*4)=3.0D+00*(1.0D+00+(-a(4*i-3)+X)*D)/
-   (4.0D+00*dSqrt(2.0D+00)*(1.0D+00+(-a(4*i-3)+X)**2.0D+00/
-  (2.0D+00*a(4*i-2)*B))**(5.0D+00/2.0D+00)*dSqrt(a(4*i-2)*B))

 YFIT=yfit+a(4*i)*(3.0D+00*(1.0D+00+(-a(4*i-3)+X)*D)/
-   (4.0D+00*dSqrt(2.0D+00)*(1.0D+00+(-a(4*i-3)+X)**2.0D+00/
-  (2.0D+00*a(4*i-2)*B))**(5.0D+00/2.0D+00)*dSqrt(a(4*i-2)*B)))

 enddo

 RETURN
 END



 subroutine constrain(X,A,YFIT,DYDA,MA,peaks)

 integer ma,peaks,i
 real*8 x,a(30),yfit,dyda(30)

 do i=1,ma
    dyda(i)=0.0D+00
 enddo

 yfit=0.0D+00

 do i=1,peaks
    dyda(i*4)=1
    yfit=yfit+a(i*4)
 enddo

 return
 end



 subroutine trefout(num,a,ma,peaks,ai,runname,trestart)

 integer i,ma,peaks,ai(30)
 real*8 a(30)
 character num(9)*1,runname*8,des1*30,des2*30,trestart*40,
- des3*30,des4*30

 trestart=runname//'.'//num(peaks)//'peaks.rst'

 open(unit=95,file=trestart,status='new')

 do i=1,peaks
    des1='''F peak '//num(i)//''''
```

```
      des2='''tau peak '//num(i)//''''
      des3='''r1r2 peak '//num(i)//''''
      des4='''weight frac peak '//num(i)//''''
      write(95,*) des1,a(i*4-3),ai(i*4-3)
      write(95,*) des2,a(i*4-2),ai(i*4-2)
      write(95,*) des3,a(i*4-1),ai(i*4-1)
      write(95,*) des4,a(i*4),ai(i*4)
   enddo

   close(unit=95,status='keep')

   return
   end


   subroutine stats(ma,a,peaks,chisq,y,covar,ndata,
  -             ycalc,ia,runname,num,x,funcs,tconst)

   integer i,ma,ia(30),ndata,fit,peaks,maxdata,tconst,start

   parameter (maxdata=5000)

   real*8 a(30),chisq,y(maxdata),ycalc(maxdata),ssr,ssy,ytotal,
  - covar(30,30),yave,mfit,v,scf,f,r2,sn(30),tn(30),b(30),
  - x(maxdata)

   external funcs

   character num(9)*1,runname*8,statname*40,heading*30

   if (tconst.eq.0) then
      start=1
   else
      start=2
   endif

   ssr=0.0D+00

   do i=start,ndata
      ssr=ssr+(ycalc(i)-y(i))**2.0D+00
   enddo

   ytotal=0.0D+00

   do i=start,ndata
      ytotal=ytotal+y(i)
   enddo

   yave=ytotal/dble(real(ndata-1))

   ssy=0.0D+00

   do i=start,ndata
      ssy=ssy+(y(i)-yave)**2.0D+00
   enddo

   mfit=0.0D+00

   do i=1,ma
      if(ia(i).ne.0) mfit=mfit+1.0D+00
```

```
      enddo

      v=dble(real(ndata-1))-mfit

      scf=dsqrt(ssr/v)

      call mrqcof2(x,y,scf,ndata,a,ia,ma,covar,funcs,
     -           peaks,start)
      call gaussj(covar,idint(mfit),30,b,1,1)
      call covsrt(covar,30,ma,ia,idint(mfit))

      F=((ssy-ssr)/(mfit-1))/(ssr/v)

      r2=1.0D+00-(ssr/ssy)

      do i=1,ma
         if(ia(i).ne.0) then
            sn(i)=scf*dsqrt(covar(i,i))
            tn(i)=a(i)/sn(i)*1.0D+2
         endif
      enddo

      statname=runname//'.'//num(peaks)//'peaks.sta'
      open(unit=97,file=statname,status='new')

      write(97,*) 'r^2     ',r2
      write(97,*) 'X^2     ',chisq
      write(97,*) 'F       ',f
      write(97,*) 'Description  ','Parameter           ',
     - 'Standard error      ','t-value'
      do i=1,peaks
         heading='Peak '//num(i)
         write(97,*) heading
         write(97,*) 'F           ',a(4*i-3),sn(4*i-3),tn(4*i-3)
         write(97,*) 'tau         ',a(4*i-2),sn(4*i-2),tn(4*i-2)
         write(97,*) 'r1r2        ',a(4*i-1),sn(4*i-1),tn(4*i-1)
         write(97,*) 'weight frac ',a(4*i),sn(4*i),tn(4*i)
      enddo

      close(unit=97,status='keep')

      return
      end


      subroutine peakplot(x,peaks,a,runname,ndata,num,tconst)

      integer peaks,ndata,i,j,tconst,start
      real*8 op(10),a(30),x(ndata),ratio,b,d,r
      character runname*8,peakname*40,num(9)*1

      peakname=runname//'.'//num(peaks)//'peaks.pks'

      open(unit=75,file=peakname,status='new')

      if (tconst.eq.0) then
         start=1
      else
         start=2
      endif
```

```
do i=start,ndata
      do j=1,peaks
        ratio=4.8D+1/2.4D+1
        B=(1.0D+00-a(4*j-3))*a(4*j-3)*(1.0D+00+4.0D+00*
-            (1.0D+00-a(4*j-3))*
-           a(4*j-3)*(-1.0D+00+a(4*j-1)))**5.0D-1
        D=(1.0D+00-ratio)/(ratio+a(4*j-3)*(1.0D+00-ratio))


        op(j)=a(4*j)*(3.0D+00*(1.0D+00+(-a(4*j-3)+X(i))*D)/
-  (4.0D+00*dSqrt(2.0D+00)*(1.0D+00+(-a(4*j-3)+X(i))**2.0D+00/
- (2.0D+00*a(4*j-2)*B))**(5.0D+00/2.0D+00)*dSqrt(a(4*j-2)*B)))

      enddo

   if (peaks.eq.1) then
      write(75,*) x(i),op(1)
   else if (peaks.eq.2) then
      write(75,*) x(i),op(1),op(2)
   else if (peaks.eq.3) then
      write(75,*) x(i),op(1),op(2),op(3)
   else if (peaks.eq.4) then
      write(75,*) x(i),op(1),op(2),op(3),op(4)
   else if (peaks.eq.5) then
      write(75,*) x(i),op(1),op(2),op(3),op(4),op(5)
   else if (peaks.eq.6) then
      write(75,*) x(i),op(1),op(2),op(3),op(4),op(5),op(6)
   else if (peaks.eq.7) then
      write(75,*) x(i),op(1),op(2),op(3),op(4),op(5),op(6),
-     op(7)
   else if (peaks.eq.8) then
      write(75,*) x(i),op(1),op(2),op(3),op(4),op(5),op(6),
-     op(7),op(8)
   else if (peaks.eq.9) then
      write(75,*) x(i),op(1),op(2),op(3),op(4),op(5),op(6),
-     op(7),op(8),op(9)
   endif

enddo

close(unit=75,status='keep')
call flush_(75)

return
end

subroutine mrqcof2(x,y,sig,ndata,a,ia,ma,alpha,
+    funcs,peaks,start)

integer ma,ndata,ia(30),MMAX,maxdata,peaks,wfrac,start
parameter (maxdata=5000)
real*8 a(30),alpha(30,30),sig,
+    x(maxdata),y(maxdata)
external funcs
parameter (MMAX=30)
integer mfit,i,j,k,l,m
real*8 dy,sig2i,wt,ymod,dyda(MMAX)

mfit=0
```

```
do j=1,ma
   if (ia(j).ne.0) mfit=mfit+1
enddo
do j=1,mfit
   do k=1,j
      alpha(j,k)=0.0D+00
   enddo
enddo
do i=start,ndata
   call funcs(x(i),a,ymod,dyda,ma,peaks)
   sig2i=1.0D+00/(sig*sig)
   dy=y(i)-ymod
   j=0
   do l=1,ma
      if(ia(l).ne.0) then
         j=j+1
         wt=dyda(l)*sig2i
         k=0
         do m=1,l
            if(ia(m).ne.0) then
               k=k+1
               alpha(j,k)=alpha(j,k)+wt*dyda(m)
            endif
         enddo
      endif
   enddo
enddo
do j=2,mfit
   do k=1,j-1
      alpha(k,j)=alpha(j,k)
   enddo
enddo

return
end
```

APPENDIX B: Equations and Nomenclature for Statistical Analysis

The statistical calculations that were utilised in the programs in Appendix A will be presented along with the definitions of the symbols used.

ycalc(i) is the calculated curve value for the i^{th} data point

y(i) is the measured value for the i^{th} data point

ndata is the number of data point plus one

mfit is the number of fitted parameters

ssr is the sum of squares of residuals and is represented by Equation B1.

$$ssr = \sum_{2}^{ndata} (y_i - ycalc_i)^2 \tag{B1}$$

ytotal is the sum of all y(i)s

yave is the mean value of the y(i) and is given by Equation B2.

$$yave = \frac{ytotal}{ndata - 1} \tag{B2}$$

ssy is the sum of squares about the mean and is given by Equation B3.

$$ssy = \sum_{2}^{ndata} (y_i - yave)^2 \tag{B3}$$

v is the number of degrees of freedom and is given by Equation B4.

$$v = (ndata - 1) - mfit \tag{B4}$$

scf is the standard error of the curve fit and is given by Equation B5.

$$scf = \sqrt{\frac{ssr}{v}} \tag{B5}$$

The F statistic is calculated using Equation B6.

$$F = \frac{\frac{ssy - ssr}{mfit - 1}}{\frac{ssr}{v}} \qquad \text{(B6)}$$

The covariance matrix is calculated by calling the subroutines MRQCOF, GAUSSJ, and COVSRT. The covariance matrix is used in calculating the standard error of the fitted parameters and the t value of the fitted parameters. The standard error of the n^{th} parameter (S_n) is given by Equation B7.

$$S_n = scf\sqrt{V_{nn}} \qquad \text{(B7)}$$

Where V_{nn} is the n^{th} diagonal element of the covariance matrix.

The t value for the n^{th} parameter (t_n) is given by Equation B8.

$$t_n = \frac{a_n}{S_n} \times 100 \qquad \text{(B8)}$$

Where a_n is the value of the n^{th} parameter.

The formulas used in calculation the curve fit statistics were taken from the operating manual pages 141 to 143 for the program PeakFit purchased from SPSS Inc., Chicago, IL.

APPENDIX C: Results of Polymerization Experiments

The experimental conditions during the polymerization experiments with catalysts RBCT3, -4, -5 and –6 are shown in the following four figures. The top panel in each figure contains the total reactor pressure as a function of time; the partial pressures of nitrogen and ethylene are indicated in the panel. The rate of addition of ethylene, in cm^3 at STP per minute is indicated in the middle panel. This rate, except during the filling stage, is equal to the rate of polymerization. In the bottom panel, the temperatures at two locations inside the reactor (T3 and T4) and the temperature of the oil in the bath surrounding the reactor (T7) are plotted as a function of time.

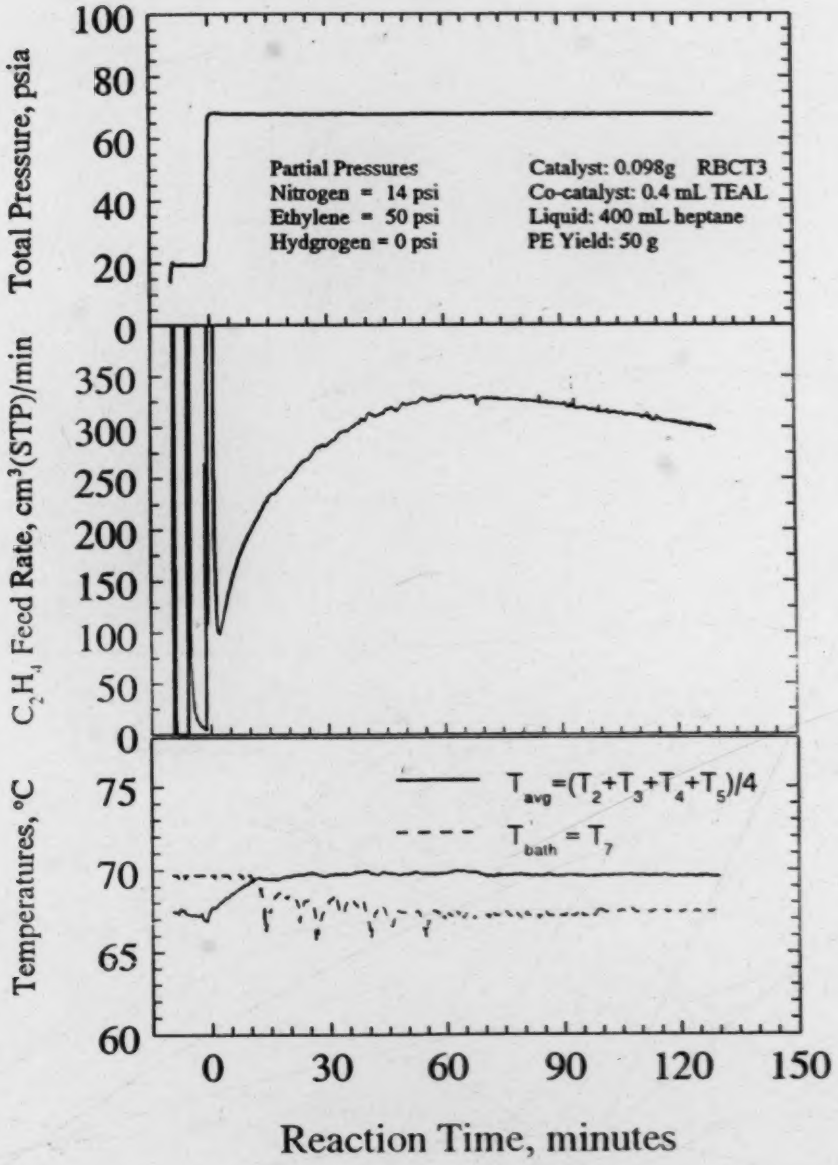

Figure C1. Run conditions and polymerization rate (Run SLROB03).

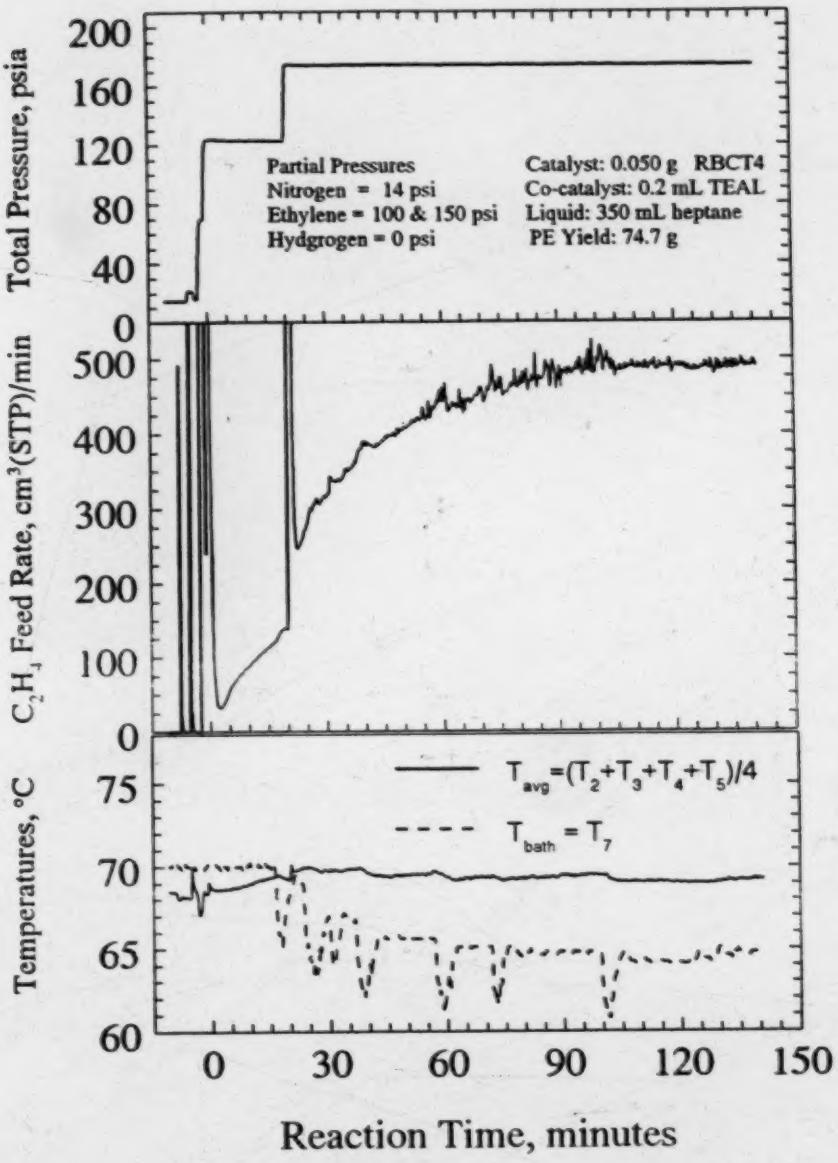

Figure C2. Run conditions and polymerization rate (Run SLROB04).

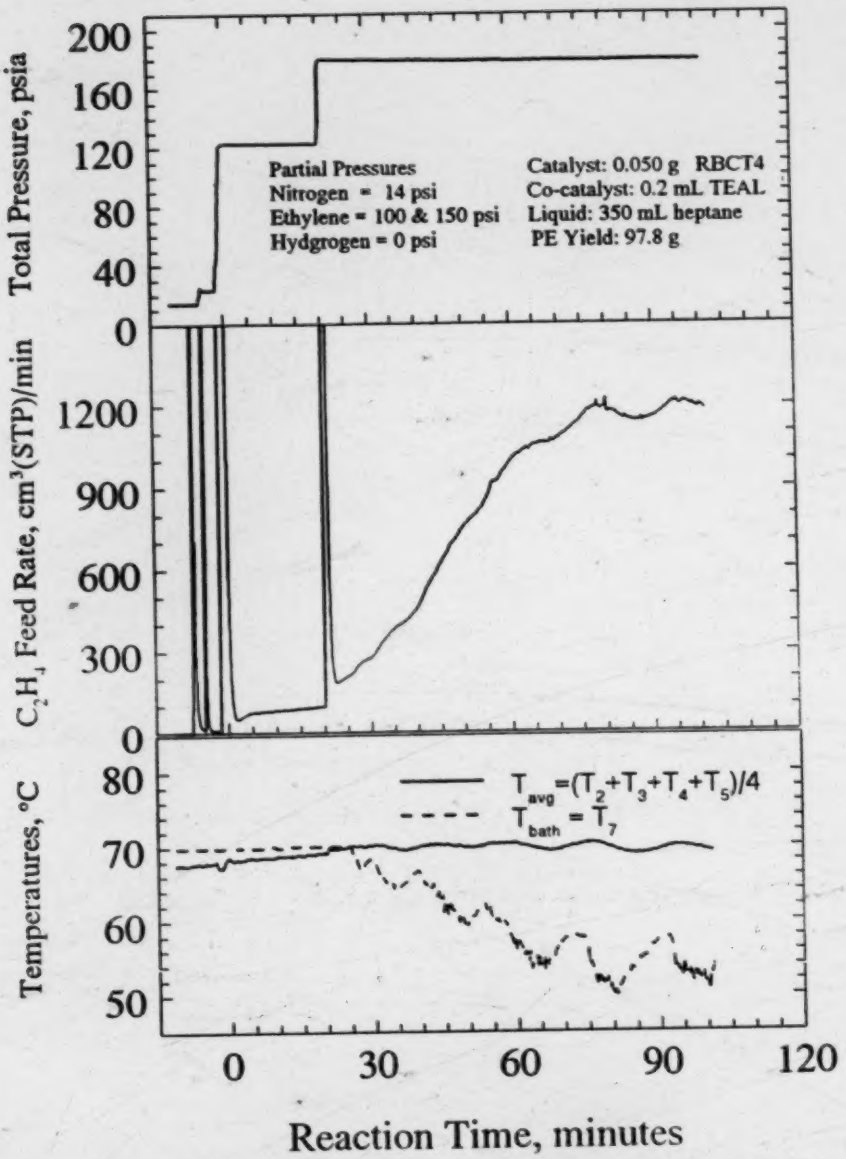

Figure C3. Run conditions and polymerization rate (Run SLROB05).

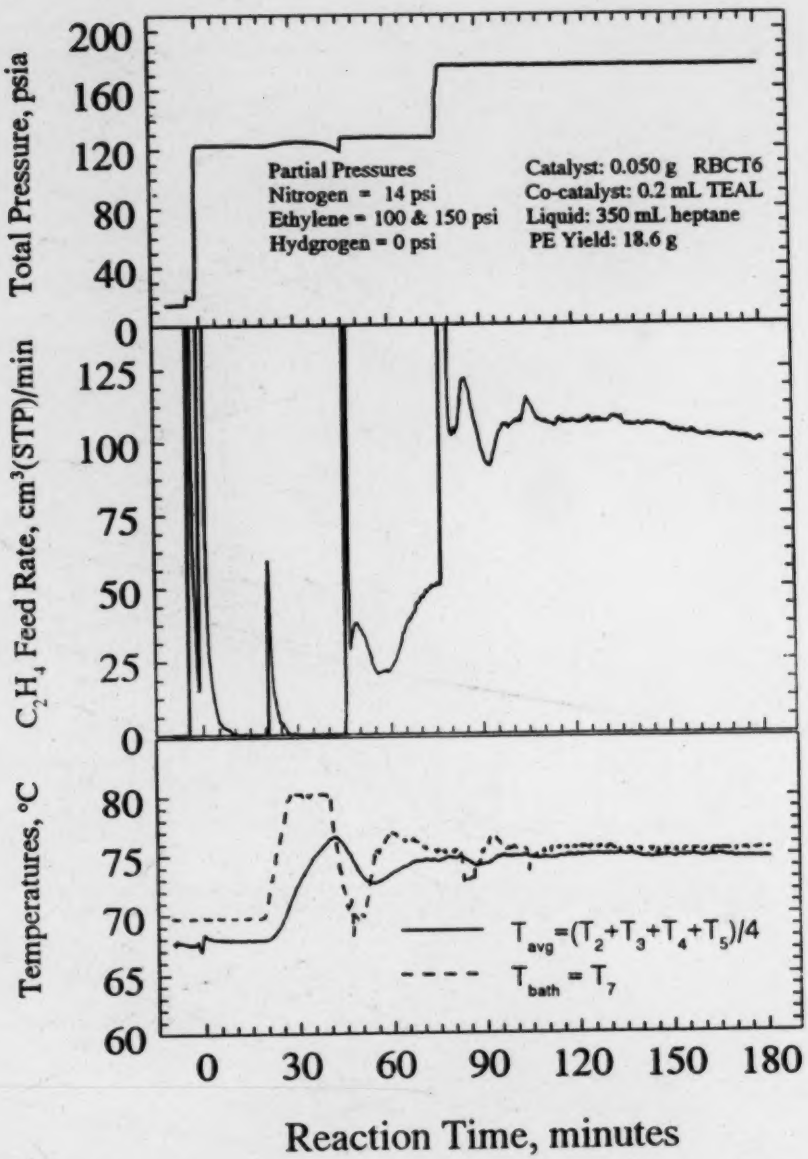

Figure C4. Run conditions and polymerization rate (Run SLROB06).